On Fast, Polarimetric Non-Reciprocal Calibration and Multipolarization Measurements on Weather Radars

von der Fakultät für Elektrotechnik und Informationstechnik
der Technischen Universität Chemnitz

genehmigte
Dissertation
zur Erlangung des akademischen Grades
Doktor-Ingenieur
Dr.-Ing.
vorgelegt

von Dipl.-Ing. Jens Reimann
geboren am 25. Juni 1984 in Lichtenstein

eingereicht am 24. Januar 2013

Gutachter: Prof. Dr. rer. nat. Madhukar Chandra
Prof. Dr.-Ing. Gerd Wanielik
Dr. rer. nat. Martin Hagen
Dr.-Ing. Mario Weber

Tag der Verleihung: 12. November 2013

Schnelle polarimetrische, nicht-reziproke Kalibrierung und Mehrpolarisationsmessungen an Wetterradaren

von der Fakultät für Elektrotechnik und Informationstechnik
der Technischen Universität Chemnitz

genehmigte
Dissertation
zur Erlangung des akademischen Grades
Doktor-Ingenieur
Dr.-Ing.
vorgelegt

von Dipl.-Ing. Jens Reimann
geboren am 25. Juni 1984 in Lichtenstein

eingereicht am 24. Januar 2013

Gutachter: Prof. Dr. rer. nat. Madhukar Chandra
Prof. Dr.-Ing. Gerd Wanielik
Dr. rer. nat. Martin Hagen
Dr.-Ing. Mario Weber

Tag der Verleihung: 12. November 2013

Reimann, Jens

On Fast, Polarimetric Non-Reciprocal Calibration and Multipolarization Measurements on Weather Radars

Dissertation, Fakultät für Elektrotechnik und Informationstechnik

Technische Universität Chemnitz, Januar 2012.

161 Seiten, 50 Abbildungen, 11 Tabellen, 64 Literaturquellen.

Abstract

In this study a calibration concept for a multi-polarimetric weather radar is developed. Several common calibration techniques are analysed, but many are insufficient due to the non-reciprocal behaviour of the employed radar. Hence, an electronic calibration device was developed, which was designed for fast polarization determination of any polarization (including elliptical ones). The non-reciprocal behaviour was overcome by splitting receive and transmit calibration, which virtually uses the radar as a communication system. Beside the calibration a new and flexible signal processing system was implemented on that radar which allows interleaved measurements using several polarimetric modes. This capability was used to analyse the STAR (hybrid basis with linear 45° transmit and horizontal/vertical receive) mode and the alternating H/V mode with respect to depolarization. Although it is known that depolarization causes errors in STAR mode, it is used in most commercial weather radars.

Keywords: weather radar, radar polarimetry, multi-polarization measurement, calibration, PARC, POLDIRAD

Referat

In dieser Arbeit wird ein Kalibrierkonzept für ein Multipolarisation-Radar entwickelt. Dazu wurden verschiedene gebräuchliche Techniken untersucht. Dabei stellte sich heraus, dass dieses Verfahren für das untersuche nichtreziproke Radar unzureichend sind. Deshalb wurde ein elektronisches Kalibriergerät entwickelt, welches speziell der schnellen Messung von beliebigen Polarisationen - einschließlich Elliptischer - dient. Das nichtreziproke Verhalten wurde durch die Aufteilung in eine Sende- und eine Empfangskalibrierung umgangen, wodurch das Radar praktisch als Kommunikationssystem verwendet wird. Des Wv eiteren wurde eine neue, flexible Signalverarbeitung an dem Radar entwickelt, welches gemischte Messungen mit mehreren Polarisationsmoden erlaubt. Diese neuartige Möglichkeit wurde benutzt um den STAR-Modus, welches eine hybride Polarisationsbasis (linear 45° senden, horizontal/vertikal empfangen) benutzt, mit dem alternierende H/V-Modus zu vergleichen. Dabei wurde speziell das Verhalten des STAR-Modus im Hinblick auf Depolarisation untersucht, da dies bekanntermaßen zu Fehlern in den Messgrößen führen kann. Dies ist von besonderem Interesse, da der STAR-Modus in den meisten kommerziellen Wetterradarsystemen eingesetzt wird.

Schlagwörter: Wetterradar, Radarpolarimetrie, Mehrpolarisationsmessung, Kalibrierung, PARC, POLDIRAD

Contents

List of Symbols **17**

List of Abbreviation **21**

1 Introduction **23**

2 Basics **25**

2.1 Electromagnetic Basics 25

2.2 Polarization Basics 26

2.2.1 Polarization Transformation 29

2.3 Scattering Matrix 30

2.4 Radar Basics 30

2.5 Radar Equation 32

3 System Description of the Radar POLDIRAD **35**

3.1 Transmitter 35

3.2 Polarization Network 37

3.3 Antenna 40

3.4 Receiver 41

3.5 Built-In Test Equipment 41

4 Radar Calibration **43**

4.1 Requirements 43

4.2 Uncertainty Requirements 44

4.3 Calibration Model 45

4.4 Standard Techniques 45

4.4.1 Internal calibration 46

4.4.2 Sphere 46

4.4.3 Rain 47

4.4.4 Astronomic Targets 48
4.5 Sun-Calibration for the POLDIRAD Radar 49

5 Preliminary Investigation of an External Calibration Device 59
5.1 Antenna Measurement Techniques 60
5.1.1 Near Field 60
5.1.2 Compact Range 60
5.1.3 Far Field 60
5.2 Polarization Measurement Techniques 61
5.2.1 Single Rotating Linear Polarized Antenna 62
5.2.2 Orthogonal Antenna Pair 62
5.2.3 Four-Antennas Power Measurement 62
5.3 Prior Systems 63
5.3.1 Single Antenna PARC 64
5.3.2 Automated Polarization Measurement Chamber 64
5.3.3 DLR PARC 64
5.3.4 Summary 65
5.4 Technology Evaluation 65

6 PARC 69
6.1 System Description 69
6.2 First RF Power Estimation 71
6.2.1 Trigger Generation 71
6.3 System Development 72
6.3.1 Hardware 72
6.3.2 PARC Server Software 74
6.4 Calibration Technology for PARC 79
6.4.1 Calibration Model 79
6.4.2 Determination of the Polarization Independent Loss 80
6.4.3 Radar PARC Synchronisation 81
6.5 Calibration modules 83
6.5.1 Time Plot 83
6.5.2 Radar Transmit Pulse Measurement 83
6.5.3 Defined PARC Transmit Signal 84
6.5.4 Radar Receive Signal Measurement 84

6.5.5 Automatic Radar Receive Polarization Optimization 85
6.5.6 Automatic Radar Transmit Polarization Optimization 86
6.5.7 Radar Transmit/Receive Data Plot 87
6.5.8 Polarization Phase Difference Measurement 87
6.6 PARC Measurements 88
6.6.1 Polarization Phase Calibration 90
6.6.2 PARC Power Measurements 92
6.7 Limitations 93

7 Radar Data Processing **95**
7.1 Introduction 95
7.2 Signal Processing for the POLDIRAD Radar 96
7.3 The New Realization of the Alternating H/V Mode 97
7.4 Alternating Right/Left-hand Circular Mode 104
7.5 Signal Processing for Multi-Polarization Scans 105
7.5.1 Practical Implementation 106
7.6 Polarimetric Data Analysis 108
7.6.1 Huynen Fork-Parameters 108
7.6.2 Additional Parameters 111

8 Multi-Polarization Measurements **113**
8.1 Influence of the Transmit Phase in Simultaneous H/V Mode and Comparison to the Alternating H/V Mode 113
8.1.1 Theoretical Predictions 113
8.1.2 Measurements of Copolar-Correlations-Coefficient 115
8.1.3 Measurement of Differential Reflectivity 117
8.2 Measurements of the Co-Cross-Correlation-Coefficient 119

9 Conclusions **123**

10 Outlook **125**

A PARC Specifications **127**
A.1 Antenna 127
A.2 PARC Circuits 129

B Best Practice in Weather Radar Calibration **131**

B.1 Introduction 131

B.2 Range 131

B.3 Antenna Pointing 132

B.4 Receiver Offset 132

B.5 Absolute Power Calibration 132

B.6 Polarimetric Calibration 133

C Sun Scan Plots **135**

Bibliography **142**

Inhaltsverzeichnis

Symbolverzeichnis **17**

Abkürzungsverzeichnis **21**

1 Einleitung **23**

2 Grundlagen **25**

2.1 Elektromagnetische Grundlagen 25

2.2 Grundlagen zur Polarisation 26

2.2.1 Transformation der Polarisationsbasis 29

2.3 Streumatrix 30

2.4 Radargrundlagen 30

2.5 Radargleichung 32

3 Systembeschreibung für das Radar POLDIRAD **35**

3.1 Radarsender 35

3.2 Polarisationsnetzwerk 37

3.3 Antenne 40

3.4 Empfänger 41

3.5 Radarinterne Testsysteme 41

4 Radarkalibrierung **43**

4.1 Anforderungen 43

4.2 Genauigkeitsanforderungen 44

4.3 Kalibriermodell 45

4.4 Standard Techniken 45

4.4.1 Interne Kalibrierung 46

4.4.2 Kugelkalibrierung 46

4.4.3 Regen 47

4.4.4 Astronomische Ziele 48
4.5 Sonnenkalibrierung am POLDIRAD Radar 49

5 Voruntersuchungen für ein externes Kalibriergerät 59
5.1 Antennenmessmethoden 60
5.1.1 Nahfeld 60
5.1.2 Compact Range 60
5.1.3 Fernfeld 60
5.2 Polarisationsmesstechniken 61
5.2.1 Rotierende linear-polarisierte Antenne 62
5.2.2 Orthogonales Antennenpaar 62
5.2.3 Vier-Antennen Leistungsmessung 62
5.3 Stand der Technik 63
5.3.1 Einzelantennen PARC 64
5.3.2 Automatische Polarisationsmesskammer 64
5.3.3 DLR PARC 64
5.3.4 Zusammenfassung 65
5.4 Technologiebewertung 65

6 PARC 69
6.1 Systembeschreibung 69
6.2 Erste HF-Leistungsschätzung 71
6.2.1 Trigger-Erzeugung 71
6.3 Systementwicklung 72
6.3.1 Hardware 72
6.3.2 PARC Server Software 74
6.4 Kalibriertechnologie des PARC 79
6.4.1 Kalibriermodell 79
6.4.2 Bestimmung des polarisationsunabhängigen Verlustes 80
6.4.3 Radar PARC Sychronisierung 81
6.5 Kalibriermodule 83
6.5.1 Zeitreihe 83
6.5.2 Radarpulsmessung 83
6.5.3 Bekanntes PARC Signal 84
6.5.4 Radar Empfangssignalmessung 84

6.5.5 Automatische Polarisationsoptimierung für den Radarempfang 85
6.5.6 Automatische Polarisationsoptimierung beim Senden des Radars 86
6.5.7 Radardatendarstellung 87
6.5.8 Messung des Polarisationsphasenversatzes 87
6.6 PARC-Messungen 88
6.6.1 Kalibrierung der Polarisationsphasen 90
6.6.2 Leistungsmessung mit dem PARC 92
6.7 Einschränkungen 93

7 Radardatenverarbeitung 95
7.1 Einleitung 95
7.2 Signalverarbeitung am POLDIRAD Radar 96
7.3 Die neue Realisierung des alternierenden H/V-Modus 97
7.4 Der alternierende rechts-/linkszirkulare Modus 104
7.5 Signalprozessierung für Mehrpolarisationsmessungen 105
7.5.1 Praktische Implementierung 106
7.6 Polarimetrische Datenanalyse 108
7.6.1 Huynen Fork-Parameter 108
7.6.2 Weitere Parameter 111

8 Mehrpolarisationsmessungen 113
8.1 Einfluss der Sendephase im simultanen H/V-Modus und Vergleich zum alternierenden H/V-Modus 113
8.1.1 Theoretische Vorhersagen 113
8.1.2 Messung des kopolaren Korrelationskoeffizienten 115
8.1.3 Messung der Differentiellen Reflektivität 117
8.2 Messung des Ko-Kreuz-Korrelationskoeffizienten 119

9 Zusammenfassung 123

10 Ausblick 125

A PARC Spezifikationen 127
A.1 Antenne 127
A.2 PARC Schaltpläne 129

B Tipps zur Wetterradarkalibrierung **131**

B.1 Einleitung 131

B.2 Messstrecke 131

B.3 Antennenausrichtung 132

B.4 Versatz in dem Radarempfängern 132

B.5 Absolute Leistungskalibrierung 132

B.6 Polarisationskalibrierung 133

C Plots der Sonnenmessungen **135**

Bibliografie **149**

List of Symbols

All symbol follow a certain regime. An underlined letter indicates a complex number, an arrow above means a vector. Bold letters represent matrices. A $\times$ means an outer or vector product, a $\cdot$ the inner of scalar product. Arrow brackets $\langle\cdot\rangle$ indicate an average.

The real part of a complex number x in written as $\Re\{x\}$ and the imaginary part as $\Im\{x\}$.

A	amplitude
A_e	effective radiation area
ALD	alignment parameter
Att	attenuation in dB
AV	axial ratio
$\vec{B}$	magnetic flux density
c	speed of light
C_{DR}	circular depolarization ratio
CAN	cancellation parameter
d	distance
D	diameter
$\vec{D}$	electric flux density
$\vec{E}$	electric field vector
$\vec{E}$	Jones vector
f	frequency
g	sphericity parameter
g	linear antenna gain
G	logarithmic antenna gain
H	entropy
$\vec{H}$	magnetic field vector

$\vec{j_t}$	electric current density
$\mathbf{J}$	Wolf's coherency matrix
$\underline{k}$	wave number
$\vec{\underline{k}}$	Cloude-Pottier feature vector
K	dielectricity factor
$\vec{k}$	direction of propagation
l	loss
L_{DR}	linear depolarization ratio
$\vec{M}$	magnetization vector
$\mathbf{M}$	Mueller matrix
N	number of samples
$ORTT$	orientation parameter
p	degree of polarization
P	power
$\vec{P}$	polarization vector
P_t	transmit power
P_r	receive power
$R(x)$	covariance with time lag x
Rx	receive
r	range
$R(n)_{XY}$	correlation coefficient time lag n for Tx polarization Y and Rx polarization X
S	power density
$\vec{S}$	Stokes' vector
$\mathbf{S}$	scattering matrix
S_{xy}	elements of the scattering matrix
t	time
$\mathbf{T}$	coherency matrix
$\mathbf{U}$	2×2 polarization transformation matrix
v	Doppler velocity
V	volume
W	spectral width
z	reflectivity factor
Z	logarithmic reflectivity factor

Z_{dr}	differential reflectivity
α	angle in Cloude/Pottier decomposition
δ	phase difference
ϵ	permittivity
θ	horizontal 3 dB antenna beamwidth
λ	wavelength
$\lambda_{1,2}$	eigenvalues
μ	permeability
ρ	free current density
ρ_{HV}	co-polar correlation coefficient
$\rho_{HV\|45}$	co-polar correlation coefficient for linear 45 ° polarization
$\rho_{HV\|L,R}$	co-polar correlation coefficient for circular polarization
$\underline{\rho_{xy}}$	complex polarization ratio
$\underline{\rho_{x_y}}$	co-cross correlation coefficient for polarization y
ρ_4	shape parameter
σ	standard deviation
σ	radar cross section
τ	polarization ellipticity angle
τ	radar pulse time
ϕ	polarization orientation angle
ϕ_{DP}	differential phase shift
ϕ_{sys}	system phase
Ψ	tilt angle
ψ	vertical 3 dB antenna beamwidth
ω	angular frequency

List of Abbreviation

1dB GCP 1 dB Gain Compression Point.

ADC Analogue Digital Converter.

BITE Built-In Test Equipment.

CPI coherent processing interval.

CPU central processing unit.

DAC Digital Analogue Converter.

DFT Discrete Fourier Transformation.

DLR Deutsches Zentrum für Luft- und Raumfahrt.

DSD Drop Size Distribution.

EM Electromagnetic.

FMCW Frequency-modulated Continuous-wave.

GPS Global Positioning System.

ICPR Integrated Cross-Polarization Ratio.

IF Intermediate Frequency.

IIR Infinite Impulse Response.

NWP Numeric Weather Prediction.

PARC Polarimetric Active Radar Calibrator.

PC Personal Computer.

PLC Programmable Logic Controller.

PLL Phase-Locked Loop.

POLDIRAD Polarization Diversity Doppler Radar.

PPI Planar Position Indicator.

PPRF Polarization Pattern Repetition Frequency.

PRF Pulse Repetition Frequency.

RADAR Radio Detection and Ranging.

RAM Random Access Memory.

RCS Radar Cross Section.

RF Radio Frequency.

RHI Range Height Indicator.

SAR Synthetic Aperture Radar.

SAT Site Acceptance Test.

SAW Surface Acoustic Wave.

SDR Software Defined Radio.

SNR Signal to Noise Ratio.

STAR Simultaneous Transmit and Receive.

TCP/IP Transmission Control Protocol/Internet Protocol.

TTL Transistor-Transistor-Logic.

UTC Universal Time Coordinated.

VNA Vector Network Analyser.

Chapter 1

Introduction

"How will be the weather tomorrow?"
"When is the right time for seeding/harvesting?"
These are questions mankind asking ever since. Weather forecasting has been made huge progress the last decades mainly due to a better understanding of the processes in the atmosphere of our Earth and due to available computing power for Numerical Weather Prediction (NWP) models. However, these models need high quality input about the current state of the atmosphere. One tool to provide these data is a weather radar. These systems scan the sky with high temporal and spatial resolution to provide three-dimensional information about the situation in the atmosphere. This information is not only relevant to forecasters. For many users it is sufficient to have warnings within minutes before weather hazards appear to react properly, e.g. airports or organizers of public events.

Other users are more interested in quantitative data, e.g. the amount of rain falling in a certain period. To derive this information, the electromagnetic quantities measured by radar have to be converted to meteorological ones. This can be very challenging as they cannot easily be connected. The scattering function of single hydrometeors (rain, hail, ice,...) has to be known as well as the number, size and shape of these particles. Modern weather radars can measure different parameters of the electromagnetic wave, which provide information to retrieve hydrometeor types and quantities.

The work tries helping to understand the processes of scattering for different hydrometeors by improving one of the most advanced weather radars to provide unique data sets for scattering analysis. One task will be the calibration of the

system to record high quality data. In a second step, the signal processing will be extended to enable new measurements using several polarizations. This will allow a comparison of different polarimetric measurement schemes, their advantages and disadvantages. There will also be a look at measurement quantities currently not used for weather radars.

Chapter 2

Basics

This chapter will show the basics on which this work will rely upon. First, the polarization properties of electromagnetic wave are derived starting from the Maxwell's equations. Afterwards common descriptions of the polarization state will be introduced. It will also be shown how to transfer these quantities between different polarization bases. Following the scattering matrix will be introduced. At the end, the technique of radar will be shown.

2.1 Electromagnetic Basics

It was already shown by Clerk Maxwell (Maxwell (1865)) in the 19^{th} century that all electromagnetic waves can be described by a set of equations nowadays commonly known as the Maxwell's equations:

$$\begin{aligned} \vec{\nabla} \times \vec{E}(\vec{r},t) &= -\frac{\partial \vec{B}(\vec{r},t)}{\partial t}; & \vec{\nabla} \times \vec{H}(\vec{r},t) &= \vec{j_t}(\vec{r},t) + \frac{\partial \vec{D}(\vec{r},t)}{\partial t} \\ \vec{\nabla} \cdot \vec{D}(\vec{r},t) &= \rho(\vec{r},t); & \vec{\nabla} \cdot \vec{B}(\vec{r},t) &= 0 \end{aligned} \tag{2.1}$$

where $\vec{E}(\vec{r},t)$ is the electric field, $\vec{H}(\vec{r},t)$ the magnetic field, $\vec{D}(\vec{r},t)$ the electric flux density, $\vec{B}(\vec{r},t)$ the magnetic flux density, $\vec{j_t}(\vec{r},t)$ the electric current density and $\rho(\vec{r},t)$ the free charge density.

If the media is isotropic and linear relationship between the field vectors and the flux density holds:

$$\begin{aligned} \vec{D}(\vec{r},t) &= \varepsilon \vec{E}(\vec{r},t) + \vec{P}(\vec{r},t) \\ \vec{B}(\vec{r},t) &= \mu \left(\vec{H}(\vec{r},t) + \vec{M}(\vec{r},t) \right) \end{aligned} \tag{2.2}$$

The polarization vector $\vec{P}(\vec{r},t)$ is caused by (temporary) shifts of charges within the media. The magnetization $\vec{M}(\vec{r},t)$ is provoked by the alignment of the magnetic dipoles in ferromagnetic materials. The constant ε is called the permittivity and μ the permeability.

For the case of linear, homogeneous and isotropic media, the Maxwell's equation (2.1) can be simplified to:

$$\triangle\vec{E}(\vec{r},t) - \mu\varepsilon\frac{\partial^2\vec{E}(\vec{r},t)}{\partial t^2} - \mu\sigma\frac{\partial\vec{E}(\vec{r},t)}{\partial t} = -\frac{1}{\varepsilon}\frac{\partial\nabla\rho(\vec{r},t)}{\partial t} \tag{2.3}$$

If there are no free charges, the term $\frac{\partial\vec{\nabla}\rho(\vec{r},t)}{\partial t}$ vanishes.

Further simplification can be achieved if the electric field can be described by a complex vector

$$\vec{E}(\vec{r},t) = \Re\left\{\underline{\vec{E}}(\vec{r})e^{j\omega t}\right\} \tag{2.4}$$

where j is the complex unit defined as $j\cdot j = -1$. Using this representation (2.3) can be rewritten to

$$\triangle\underline{\vec{E}}(\vec{r}) - \omega^2\mu\varepsilon\left(1 - j\frac{\sigma}{\varepsilon\omega}\right)\underline{\vec{E}}(\vec{r}) = \triangle\underline{\vec{E}}(\vec{r}) - \underline{k}^2\underline{\vec{E}}(\vec{r}) \tag{2.5}$$

$$\text{with } \underline{k} = \frac{\omega}{v}\sqrt{1 - j\frac{\sigma}{\varepsilon\omega}} \tag{2.6}$$

The factor $\underline{k}$ is known as the complex wave number.

2.2 Polarization Basics

As transversal waves electromagnetic waves are a two-dimensional phenomenon *on the oscillation plane* in a three-dimensional space. If radiated into the three-dimensional space there is still a degree of freedom, characterized by the polarization. From eq. (2.4) it can be seen that the electric field of a wave traveling into direction $\vec{k}$ can be described as:

$$\underline{\vec{E}}(\vec{r}) = \underline{\vec{E}}_0 e^{-j\vec{k}\cdot\vec{r}} = (\underline{E}_{0_x}\cdot\vec{e_x} + \underline{E}_{0_y}\cdot\vec{e_y})e^{-j\vec{k}\cdot\vec{r}} \tag{2.7}$$

For a plane wave the direction of propagation is $\vec{k} = \vec{e_x}\times\vec{e_y}$ and $\vec{e_x}$, $\vec{e_y}$ are unity vectors for the coordinate system in x/y direction.

$$\underline{\vec{E}}(\vec{r}) \;=\; (E_{0_x}e^{j\theta_x}\cdot\vec{e_x} + E_{0_y}e^{j\theta_y}\cdot\vec{e_y})e^{-j\vec{k}\cdot\vec{r}} \tag{2.8}$$

At a fixed point in space ($z = const.$) the electric field becomes:

$$\begin{aligned}\vec{E}(z = const., t) = \Re\left\{\underline{\vec{E}}(\vec{r})e^{j\omega t}\right\} &= \begin{bmatrix} E_{0_x}\Re\left\{e^{\omega t - kz}\cdot e^{\delta_x}\right\} \\ E_{0_y}\Re\left\{e^{\omega t - kz}\cdot e^{\delta_y}\right\} \\ 0 \end{bmatrix} \\ &= \begin{bmatrix} E_{0_x}\cos(\omega t - kz + \delta_x) \\ E_{0_y}\cos(\omega t - kz + \delta_y) \\ 0 \end{bmatrix} \end{aligned} \tag{2.9}$$

The Jones vector is defined by omitting the z-component, which is of no interest for the polarization in the far field:

$$\vec{E} = \begin{bmatrix} \underline{E_x} \\ \underline{E_y} \end{bmatrix} \tag{2.10}$$

The complex polarization ratio $\underline{\rho_{xy}}$ is defined as:

$$\underline{\rho_{xy}} = \frac{\underline{E_y}}{\underline{E_x}} = \frac{|E_y|}{|E_x|}e^{j(\theta_y - \theta_x)} = \tan(\epsilon)e^{j\delta} \tag{2.11}$$

with $\delta = \delta_y - \delta_x$ and $\epsilon = \frac{|E_y|}{|E_x|}$. The subscript generally denotes to the polarization basis which is used to calculate ρ. In general case, an arbitrary orthogonal basis X and Y (or A and B) is defined. Commonly use subscripts in the paper are listed in table 2.1.

H	linear horizontal
V	linear vertical
/	linear 45°
\	linear 135°
R	right hand circular
L	left hand circular

Table 2.1: Commonly used abbreviations for polarization states

There are several means to describe the polarization state beside the complex polarization ratio ρ and the Jones vector. One of them is the polarization ellipse (Fig. 2.1) which is formed by the rotating vector $\vec{E}$. The orientation angle ϕ and

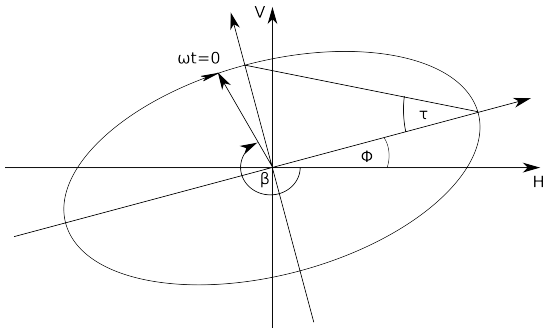

Figure 2.1: Polarization ellipse

the ellipticity angle τ of this ellipse are defined as:

$$\tau = 0.5 \cdot \arcsin\left(\frac{2 \cdot \Im\{\rho\}}{1 + \rho\rho^*}\right) \tag{2.12}$$

$$\phi = 0.5 \cdot \arctan\left(\frac{2 \cdot \Re\{\rho\}}{1 - \rho\rho^*}\right) \tag{2.13}$$

These geometric parameters as well as the complex polarization ratio ρ are only valid for fully polarized waves. For partially polarized wave the Stokes vector may be used:

$$\vec{S} = \begin{bmatrix} S_0 \\ S_1 \\ S_2 \\ S_3 \end{bmatrix} = \begin{bmatrix} I \\ Q \\ U \\ V \end{bmatrix} = \begin{bmatrix} |E_H|^2 + |E_V|^2 \\ |E_H|^2 - |E_V|^2 \\ 2\,|E_H|\,|E_V| \cos\phi \\ 2\,|E_H|\,|E_V| \sin\phi \end{bmatrix} = \begin{bmatrix} A^2 \\ A^2 \cos(2\phi)\cos(2\tau) \\ A^2 \cos(2\phi)\sin(2\tau) \\ A^2 \sin(2\tau) \end{bmatrix} \tag{2.14}$$

If the wave is fully polarized $S_0^2 = S_1^2 + S_2^2 + S_3^2$ holds.

The scattering of incoherent media can also be defined by its change of the Stokes vector ($\vec{S^i}$ incident Stokes vector and $\vec{S^s}$ scattered vector) using the Mueller matrix.

$$\vec{S^s} = \mathbf{M}\vec{S^i} \tag{2.15}$$

Yet another option to characterize the polarization state is the Poincaré sphere (Fig. 2.2). All fully polarized states are located on its surface, while partially polarized states are inside of the sphere. The center of the sphere marks completely unpolarized waves. Often the sphere is drawn with all linear polarization on the equator and left/right hand circular polarization at the poles.

The conversion between complex polarization ratio, Stokes vector, the parameters of the polarization ellipse and the Poincaré sphere are given in other sources. The interested reader will be referred to common literature (e.g. Boerner (2011)).

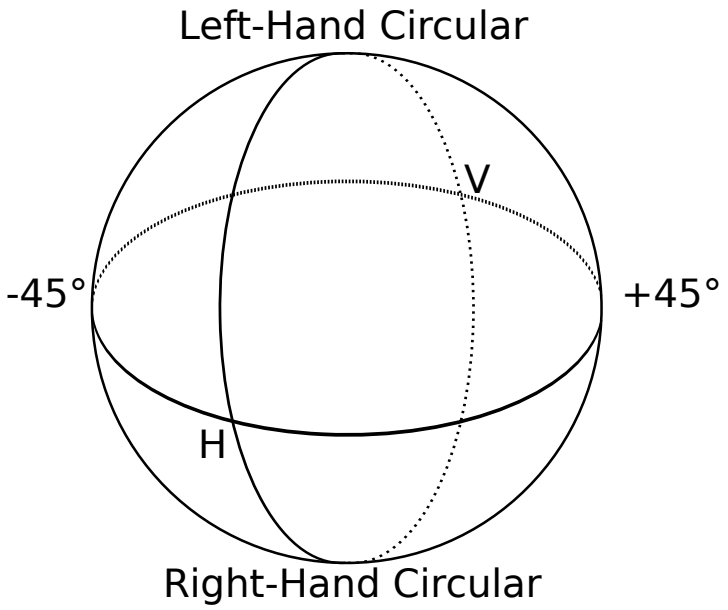

Figure 2.2: Illustration of the Poincaré sphere

2.2.1 Polarization Transformation

The polarization measured is bound to a polarization basis defined by $\vec{e_x}$ and $\vec{e_y}$. Any two orthogonal vectors xy or ab can be used to define this polarization basis. If the representation of a polarization in another basis is of interest, a transformation can be applied. This conversion is commonly defined by a transformation matrix U for the electric field vectors:

$$\vec{E}_{xy} = \mathbf{U} \cdot \vec{E}_{ab} \tag{2.16}$$

$$\begin{bmatrix} \underline{E_x} \\ \underline{E_y} \end{bmatrix} = \begin{bmatrix} \underline{U_{11}} & \underline{U_{12}} \\ \underline{U_{21}} & \underline{U_{22}} \end{bmatrix} \begin{bmatrix} \underline{E_a} \\ \underline{E_b} \end{bmatrix} \tag{2.17}$$

These equations can easily be modified to transform the complex polarization ratio:

$$\underline{\rho_{xy}} = \frac{\underline{U_{21}} + \underline{U_{22}}\underline{\rho_{ab}}}{\underline{U_{11}} + \underline{U_{12}}\underline{\rho_{ab}}} \tag{2.18}$$

The derivation to create U from ρ can be found e.g. in Agrawal and Boerner (1989):

$$U = \frac{1}{\sqrt{1 + |\underline{\rho}|^2}} \begin{bmatrix} 1 & -\underline{\rho}^* \\ \underline{\rho} & 1 \end{bmatrix} \begin{bmatrix} e^{-j\xi} & 0 \\ 0 & e^{j\xi} \end{bmatrix} \tag{2.19}$$

with $\xi = \arctan(\tan\phi \tan\tau)$

From eq. (2.18) and (2.19) the complex polarization ratio can be transformed into another by:

$$\underline{\rho_{new}} = f_T(\underline{\rho_{trans}}, \underline{\rho_{orig}}) = \frac{\underline{\rho_{trans}} e^{-j\xi} + \underline{\rho_{orig}} e^{j\xi}}{e^{-j\xi} - \underline{\rho_{trans}}^* \underline{\rho_{orig}} e^{j\xi}} \tag{2.20}$$

2.3 Scattering Matrix

The complex 2×2 scattering matrix $\mathbf{S}$ is used to describe the scattering problem of a plane wave by a single object by means of the change of the Jones vector ($\vec{E}^i$ incident wave, $\vec{E}^s$ scattered wave). In radar community the backward scattering alignment (BSA) is commonly used, which defines the electric field vector components in a right-handed system in direction of propagation ($\underline{E_x^i} = -\underline{E_x^s}$ and $\underline{E_y^i} = \underline{E_y^s}$ with $\vec{k}^i = \underline{E_x^i} \times \underline{E_y^i}$ and $\vec{k}^s = \underline{E_x^s} \times \underline{E_y^s}$, $\vec{k}$ is the direction of propagation). This construction leads to the fact that a scattered wave that travels in the opposite direction than its incident wave will in general have a different polarization than the original wave. On the other hand, this leads to reciprocity for single particles ($\underline{S_{xy}} = \underline{S_{yx}}$,Saxon (1955)).

$$\begin{bmatrix} \underline{E_x^s} \\ \underline{E_y^s} \end{bmatrix} = \begin{bmatrix} \underline{S_{xx}} & \underline{S_{xy}} \\ \underline{S_{yx}} & \underline{S_{yy}} \end{bmatrix} \begin{bmatrix} \underline{E_x^i} \\ \underline{E_y^i} \end{bmatrix} \cdot \frac{e^{-jkr}}{r} \tag{2.21}$$

2.4 Radar Basics

*Ra*dio *D*etection *A*nd *R*anging (RADAR) is an active remote sensing technique using electromagnetic (EM) waves. It is about radiating waves of known characteristics which is changed while traveling through media (forward scattering) and can be reflected by obstacles to return to the transmitter (backward scattering). Information about these processes can be extracted by comparing the signal received by the radar with the transmitted one.

A great range of radar devices has been developed, but most weather radars are either pulse radars or frequency modulated continuous wave (FMCW) systems. A monostatic Pulse-Doppler weather radar is used for the research presented in this

document and all statements will apply only to this kind of radar if not differently marked.

Pulse-Doppler weather radars are forming a short strong packet of EM energy that is radiated into a small solid angle defined by the antenna used. This free space pulse travels with (nearly) the speed of light and is influenced by the atmosphere of the Earth which needs to be considered in the estimation later on. The radar pulse will interact with hydrometeors making them radiate on their own (scattering). This effect is very strong for most hydrometeors in the direction of propagation (forward scattering) and the direction of radiation origin (backward scattering). This backward directed energy can be measured by the radar. The localization of the scatterer is known through the direction of radiation (position of the antenna) and the travel time of radar pulse (using the known velocity).

Several quantities can be extracted by the radar for each location (range gate):

- Amplitude or power of the EM wave
- Doppler velocity using the frequency/phase information
- Polarization of the EM field vector

Modern polarimetric Doppler radars as the Polarization Diversity Doppler Radar (POLDIRAD) (Schroth et al. (1988)) used in this work can measure all mentioned information and therefore are a valuable tool for atmospheric and propagation research.

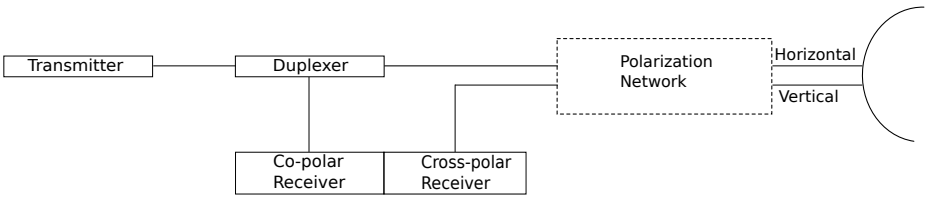

Figure 2.3: Simplified scheme of a monostatic polarimetric pulse radar

The basic hardware scheme is shown in Fig. 2.3. The transmitter creating the radar pulse is shown on the left side. The energy travels along waveguide, goes through an optional polarization network to the antenna where it is radiated. The received echo is divided into two orthogonal components (e.g. horizontal and vertical polarized) near the antenna. The cross-polar (orthogonal to the transmit polarization) signal is directly connected to its receiver, while the co-polar signal has to be

decoupled from the transmit path using a duplexer. At the receiver the signals are amplified, down converted and split into their in-phase (I) and quadrature-phase (Q) components. These voltages are digitalized and further processed in the radar signal processor, see Chapter 7.

The polarization network is optional and may be implemented differently. It is used to create a distinct polarization and is sometimes adjustable. Most operational weather radars in Europe are using a simple power divider to transmit simultaneously horizontal and vertical polarization. The American systems (NEXRAD) are using a mechanical phase shifter, a magic-Tee and a hybrid coupler to form a variable power divider (Walker (2009)). The polarization network of POLDIRAD is probably the most advanced one using electronic phase shifters to create (nearly) any polarization (see Section 3.2).

2.5 Radar Equation

When transmitting a given power P_t with an antenna having a gain g, a power density S at a distance r is given by:

$$S = \frac{P_t g}{4\pi r^2} \tag{2.22}$$

This power density S may be received by an object with an equivalent echo area A_σ and then partially reflected back towards the radar. The ratio of the back scattered to the incident power density is called the radar cross section (RCS) σ.

$$P_\sigma = \frac{P_t g \sigma}{4\pi r^2} \tag{2.23}$$

This scattered power is intercepted by the receiving antenna's effective area $A_e = \frac{g\lambda^2}{4\pi}$ which has again spherically spread ($\frac{P}{4\pi r^2}$). Hence the power received by the radar is

$$P_r = \frac{P_t g^2 \sigma \lambda^2}{64\pi^3 r^4} \tag{2.24}$$

for a single scatterer.

Weather targets consist of an ensemble of hydrometeors, which act as a volume scatterer. Hence, the Radar Cross Section (RCS) is the sum of all particles $\sigma_V = \sum_{Vol} \sigma_i$. The volume illuminated can be approximated as a cylinder having a length of half the pulse of time τ (length $h = \frac{c\tau}{2}$) with a diameter of the antenna

beamwidth θ times ψ as:

$$V = \pi \frac{r^2 \theta \phi \tau c}{8} \tag{2.25}$$

For a Gaussian shaped antenna pattern only $\frac{1}{2\ln 2} \approx 72\%$ of the energy is included in this volume. Combining these equations the total RCS for a volume scatterer can be found

$$\sigma_V = \frac{\pi r^2 \theta \phi \tau c}{16 \ln 2} \sum_{Vol} \sigma_i \tag{2.26}$$

The power a radar receives from a volume target becomes

$$P_r = \frac{P_t g^2 \lambda^2 \theta \phi \tau c}{1024 \ln 2 \pi^2 r^2} \sum_{Vol} \sigma_i \tag{2.27}$$

It should be stressed here that the range dependence is only r^2 for the volume target compared to r^4 for a point scatterer.

For small particles with diameter D the RCS can be found using the Rayleigh approximation

$$\sigma = \frac{\pi^5}{\lambda^4} |K|^2 D^6 \tag{2.28}$$

with a material dependent dielectric constant K. The radar reflectivity factor z is defined as

$$z = \sum_{Vol} D_i^6 \tag{2.29}$$

It can be calculated from the transmitted and received power of the radar (Batton, 1973, p. 42, eq (4.20))

$$z = \frac{\pi^5 |K|^2}{\lambda^4} \sum_{Vol} D_i^6 = \frac{1024 ln 2 \lambda^2}{P_t g^2 \pi^3 \theta \phi c \tau |K|} r^2 P_r \tag{2.30}$$

When using this equation in weather radars signal processing, path attenuation (e.g. from gas or hydrometeors) and system loss has to be taking into account, too.

Often the logarithmic values are used which are indicated by capital letters with the unit dBZ.

$$Z = 10 \log (z) \tag{2.31}$$

Chapter 3

System Description of the Radar POLDIRAD

The POLDIRAD was developed in the 1980's in a joined cooperation between the Microwaves and Radar Institute, the Institute for Physics of the Atmosphere of German Aerospace center (DLR) and Enterprise Electronics Corporation EEC. It is located in Oberpfaffenhofen, near Munich. Most of the electronics of the early years have been replaced. The signal processing for example is now performed by a modern GDRX© system (Selex (2009)) of Selex Systems Integration GmbH (SELEX-Gematronik). Many other hardware and software components of the radar are still internal developments of the DLR (either Institute of Atmospheric Physics or Microwave and Radar Institute). The current system characterisation and performance is listed in Table 3.1.

In this chapter the radar will be described briefly starting which the magnetron transmitter. Afterwards it will be stepped on to the unique polarization network, the antenna and the digital receiver.

3.1 Transmitter

The transmitter of POLDIRAD is a magnetron system with a solid-state pulse forming network developed by SELEX-Gematronik and Puls-Plasmatechnik GmbH. Ten parallel pulser boards create the pulse form with high current which is then transformed to a high voltage signal for the magnetron. The transmitter is triggered by the rising edge of a pulse created by the receiver. A Transistor-Transistor-Logic

System		**Antenna**	
Frequency	5.504 GHz	Gain	approx. 44 dB
Transmitter	Magnetron	3 dB Beamwidth	1 ° horizontal 1 ° vertical
Pulse width	0.5 μs,1 μs,2 μs		
Peak Power	approx. 400 kW	Sidelobe Level	−32 dB
PRF	160 Hz to 2400 Hz	Cross-polar Isolation	−28 dB (linear Polarization)
Coherency	on receive	Reflector Size	4.5 m
Max. Duty Cycle	0.12 %	Antenna Gear	continuous azimuth −5 ° to 95 ° elevation
Polarization	any fully polarized wave		
Receiver		Max.Rotation Speed	12 °s^{-1}
Channel	2 linear receivers 1 linear transmit sample	Radom	None
		Weight	3.7 t
Downconverter	digital	**Polarization Network**	
Range Resolution	15 m, 2000 Gates	Switching Time	max. 7 μs
Dynamic Range	−13 dBm to −114 dBm	Operation Temperature	nom.50 °
ADC	14-bit, 80 MHz 2 ADCs/Channel (high&low sensitive)	Number of States	2^{45}
		Isolation	>40 dB
		Power limit	450 kW peak 480 W average
IF	floating 60 MHz		
Signal Processing		Loss	2.1 dB to 2.7 dB
Operation Modes	STAR L_{DR} Alternating H/V Alternating R/L Covariance I/Q-Data	Return Loss	> −22 dB
		Location	
		Latitude	48.086 759 ° North
		Longitude	11.278 898 ° East
		Height	603 m
		Place	Oberpfaffenhofen-Weßling
Data Format	16-bit		

Table 3.1: System characteristic of POLDIRAD, 2012

(TTL) input circuit inside the transmitter creates the selected 2 µs, 1 µs or 0.5 µs pulse. It also locks the trigger input to meet the maximum duty cycle of the magnetron. The whole transmitter is internally controlled and monitored by a Siemens S5® Programmable Logic Controller (PLC) that also provides a Profibus® interface used by the control software of the radar.

3.2 Polarization Network

The polarization network of POLDIRAD is dedicated to define the polarization of the transmitted pulse and decodes the incoming wave into its co-polar (matching the selected polarization) and cross-polar (orthogonal) parts. It is a four-port device (Fig. 3.1): a horizontal and a vertical port to the antenna and a co-polar and cross-polar exit to the two receivers. The co-polar port waveguide includes the circulator to divide transmit and receive path.

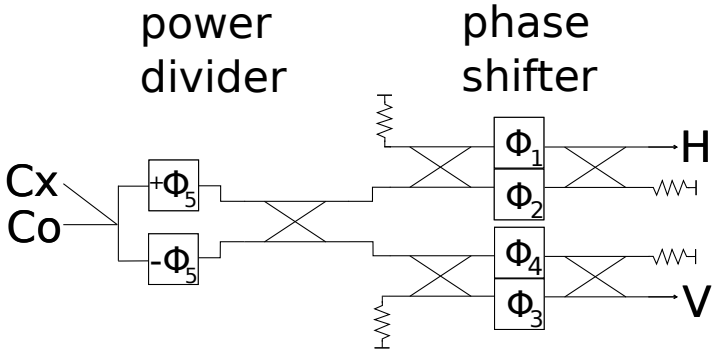

Figure 3.1: Schematic of the polarization network of POLDIRAD

The magic-Tee at the left side of Fig. 3.1 in combination with the phase-shifts Φ_5 and the 3 dB hybrid coupler are forming a variable power divider. These two phase-shifters are contrarily driven. The identical sections of two 3 dB hybrids and two phase-shifters for the H and V path are used for shifting phase only by setting the same phase shift to both parts. This section consists of two parallel devices for better power handling and for minimizing reflections within the network.

The whole polarization network consists of six phase-shifters. These components (Fig. 3.2) are latching high power ferrite phase-shifters (Ince and Stern (1967)). Each ferrite phase-shifter is composed of two anti-parallel ferrite toroids placed in the waveguide (Fig. 3.2) which are driven by one circuit board. The difference in

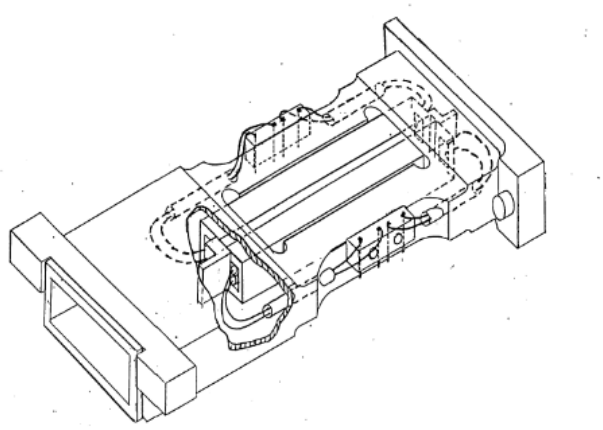

Figure 3.2: Drawing of a phase-shifter as used in the polarization network (from EMS (2004))

magnetization between the two toroids defines the phase-shift applied to the incident wave. This is a non-reciprocal effect. At high transmit power, spin waves (due to the coupling of the quantum spin in certain materials) appear in the ferrite material creating additional loss, which gives the devices a non-linear behaviour. Each circuit board is controlled by nine digital lines (one line to define the sign (or ferrite), eight for the level of magnetization) and a differential line to trigger the magnetization process.

For well-defined magnetization levels, the ferrites are first reset by driving them into magnetic saturation each time a switching process takes place. This whole process is monitored by the circuit board by measuring the current flow with a second wire. At saturation level the current flow will rise. In the next step, the given magnetization is created by applying a well-defined opposite current flow at a giving voltage through the selected toroid. The applied magnetization is again monitored by a feedback loop that uses the second wire. Using this feedback loop a Built-In Test Equipment (BITE) (Built-In Test Equipment) signal is created, which is low as long as the magnetization process is in progress. This needs $7\,\mu s$ at maximum, which defines the switching time of the device (see Sharon and Roberts (1984), Wallis et al. (1992)).

To provide fast switching behaviour while scanning, up to 32 polarizations configurations can be stored within RAMs (Random Access Memory) in the polarization network. These configurations are selected by four trigger lines controlled by the

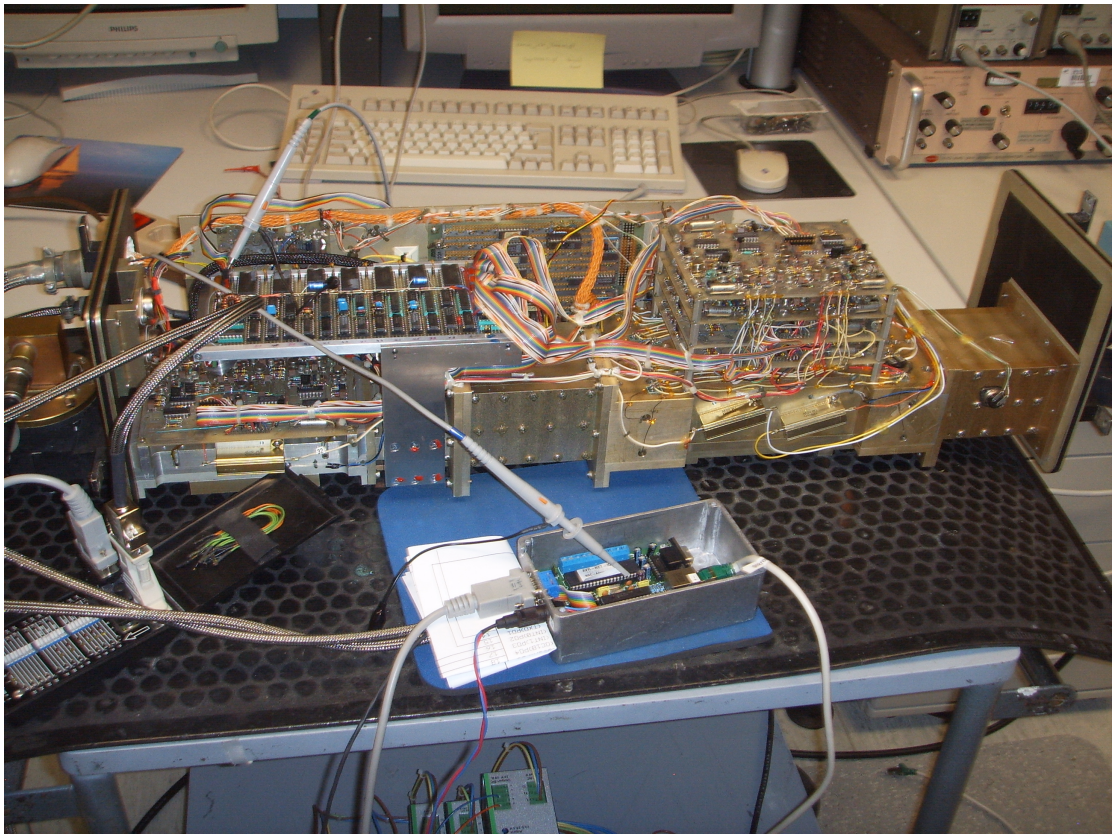

Figure 3.3: Picture of the polarization network. The dimensions are 208 × 203 × 1012 mm (height × depth × width) and the weight is approx. 32 kg

receiver hardware while measuring. The recorded data is tagged with this trigger pattern to allow a reconstruction of the polarization used for each radar pulse.

The polarization network has several temperature sensors that are needed as the ferrites are strongly temperature dependent. That is one reason for heating the polarization network. It is not only heated by the device loss from the transmit impulse (about 2.2 dB at 400 kW and duty cycle <0.11%) but also by an additional heating circuit. The temperature of the device is normally maintained within ±2 °C from its operational value of 51 °C.

It should also be noted here that the losses in the polarization network depend on the selected phase-shift. The electric parameters of the ferrites change with their magnetization level and so do loss and reflection factors (see Chapter 4) too.

3.3 Antenna

Figure 3.4: Polarization optimized offset antenna of POLDIRAD

The antenna of the POLDIRAD system is an offset design optimized (Fig. 3.4) for good polarization purity especially for horizontally and vertically polarized waves. The feed consists of an orthomode transducer and a tapered feed horn. The dish is a 15 ft $\approx$ 4.5 m parabolic shaped reflector providing about 44 dB gain. It has a large edge tapering (28 dB) for low side lobes ($<$ 32 dB) and a long focal length ($\sim$ 3.9 m). The weight of the rotating part is about 2.2 t and the whole antenna including the pedestal is approximately 3 t. The antenna can be stripped into smaller parts to be transportable. The rotation speed is software limited to 12 $^\circ s^{-1}$ in elevation and azimuth. The azimuth can be continuously rotated; the elevation is physically limited to $-5^\circ \ldots 95^\circ$ and software limited to $0^\circ \ldots 80^\circ$. The pedestal houses a combined waveguide and fibre optic rotary joint. Only the transmit pulse is transferred from the transmitter cabinet to the antenna. All other critical analogue parts of the radar

receiver including the polarization network are placed in two boxes mounted on the antenna. This guaranties short cable length. Only digitalized received samples are transferred back to the cabin using a standardized TCP/IP Ethernet link through the optical rotary joint.

3.4 Receiver

The current receiver and frontend is a commercial product of Selex Systems Integration GmbH Gematronik Weather Radar Systems named GDRX®. It is a full digital receiver sampling the radar Intermediate Frequency (IF). The sampling frequency is 80 MHz. Two approx. 30 dB separated ADCs channels (dynamic > 80 dB each) are used to give ≈ 110 dB linear dynamic range (Selex Sistemi Integrati (2010)). The floating 60 MHz IF is digitally down converted. An additional channel is sampling the magnetron transmit power and phase. The system becomes coherent (magnetron system, coherent on receive) through digital phase realignment of the received signal. The whole RF part is mounted on the antenna in one temperature controlled box. The signal processing is done on a standard Intel x86 compatible PC using a JAVA written software from Gematronik called Abacus©. The processing can be modified and extended by the DLR, which is extensively used (see Chapter 7).

3.5 Built-In Test Equipment

Test signals can be inserted into different components of the radar as shown in Fig. 3.5. A continuous wave (CW) signal which can be verified by a power meter is used for the receiver calibration (single point calibration) by applying it into the frontends. The same signal can also be injected into the waveguide near the antenna. Beside the CW signal a noise source can be used, too. The transmit power in the waveguide after the polarization network (and in front of the antenna) can be measured by switching the (peak) power meter to the corresponding test ports.

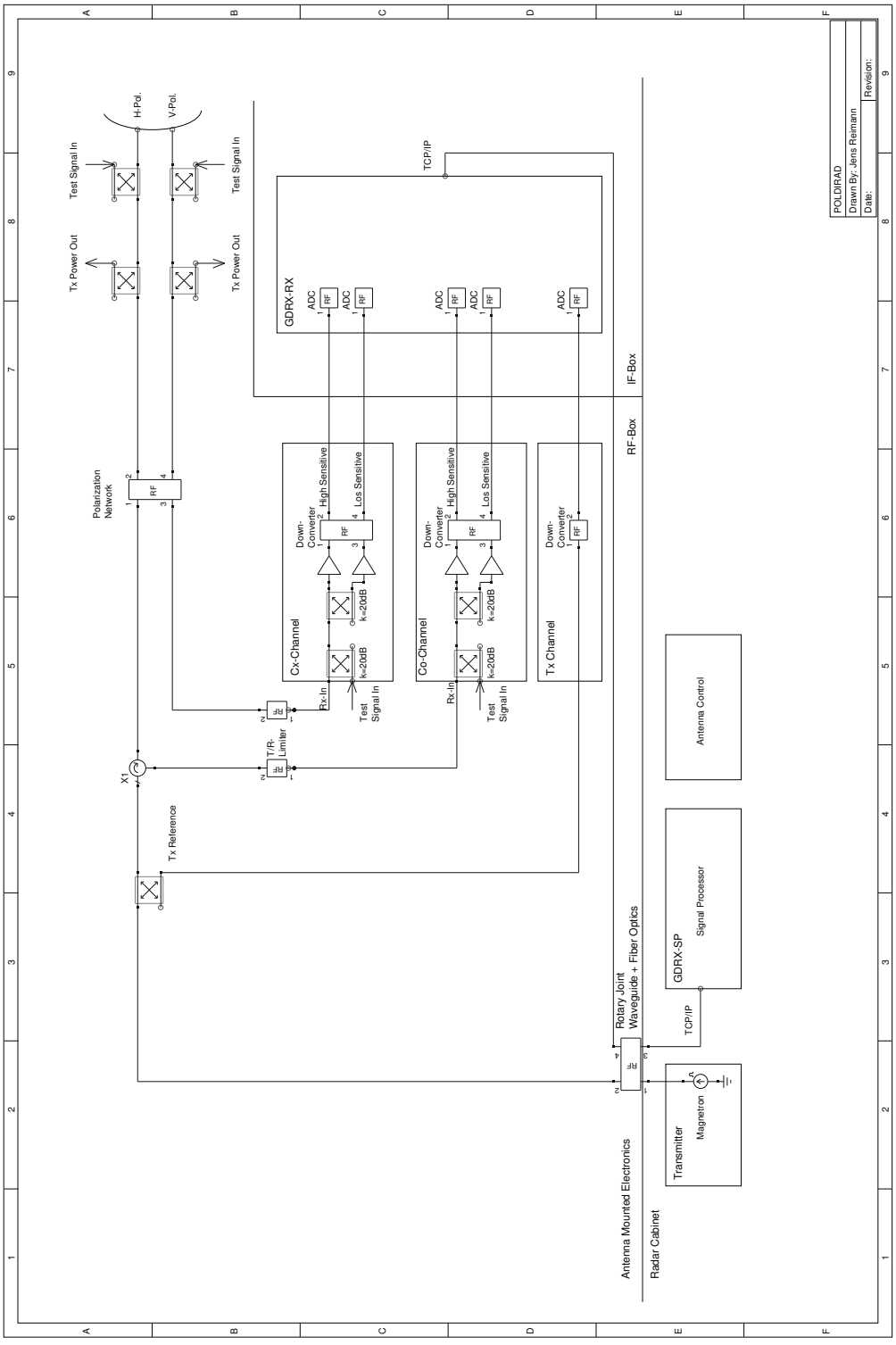

Figure 3.5: Simplified POLDIRAD Scheme

Chapter 4

Radar Calibration

In this chapter some calibration techniques used for weather radars will be introduced. It starts with some considerations about the requirements and the goal of radar calibration. There will be a deeper look into calibration using the sun. It will be shown, how this natural target is used for the characterization of POLDIRAD. The limitations will also be described. A new mathematical framework for plotting the sun scan data that is also valid for higher elevations will be presented. At the end, it will be shown how the polarization of the radar can be distinguished from the unpolarized signal radiated by the sun.

4.1 Requirements

There are three properties of the EM-wave that are measured by the POLDIRAD radar:

- Power
- Phase and Frequency
- Polarization

In principle, each of these items is a subject for calibration. In this work, we will not deal with the calibration of the phase and frequency, as the used time references are sufficiently precise ($< 10^{-10}$) and can be checked in a laboratory. The main part of the uncertainty in the derived Doppler velocity and spectral width comes from the statistical fluctuation of the distributed weather targets and the limited number of

samples recorded. Nevertheless, there are straightforward checks for phase stability of the radar (e.g. using ground clutter).

Power and polarization calibration may be combined as a polarization measurement includes relative power measurements. If a transformation to an absolute power level is possible, an absolute power calibration is also feasible.

The reflectivity can now be determined from the received power measurement by looking to the radar equation (2.30). Beside the transmit power, which has to be tracked, the antenna beamwidth and gain, the pulse length and the wavelength (frequency) are needed.

The polarization network of POLDIRAD creates the polarization using phase shifters (section 3.2). Unfortunately, each of these phase shifters behaves differently, depending on the production processes involved. Hence, it is not known which drive level creates a certain phase shift in the ferrite. This also implicates that the polarization created is unknown. The only way to find the settings for a certain polarization is measuring several configurations and optimize the settings for the different ferrites. As the search space is very large (9 bit and 5 independent shifters are $2^{9^5} = 2^{45} \approx 3.5 \cdot 10^{13}$), a fast measurement technique is needed.

Especially for the measurement of depolarization, it is important that received and transmitted polarization are matched well, which is not guaranteed due to the non-reciprocal behaviour. For the measurement of the scattering matrix, the set orthogonal polarization (receive and transmit) has to fit well too.

On the other hand, we assume relaxed requirements for the absolute polarization. The error introduced by a rotation of all polarizations by e.g. 2° is assumed to produce still meaningful measurements of weather targets. In other words a minimal orientation mismatch for horizontal polarization might be acceptable as long as both - received and transmitted polarization - are affected and both polarization are still orthogonal. For example: a 2° mismatch between receive and transmit will lead to large errors in depolarization estimation ($\sin(2°) \approx 0.0349 \approx -29.1\,\mathrm{dB}$ which is worse than the expected system limit of $\approx -35\,\mathrm{dB}$).

4.2 Uncertainty Requirements

The channel isolation of the polarization network is expected to be better than 35 dB (up to 60 dB were measured with a Vector Network Analyser (VNA), see Tracksdorf

(2010)). The worst-case cross-polarization of the antenna is about −28 dB Schroth et al. (1988). Theoretically, parts of the cross-polarization can be compensated by the polarization network by creating a 180° phase-shifted signal of same power. On the other hand, the polarization properties change also within the antenna pattern. The weather radar POLDIRAD is designed to measure random distributed targets. Therefore, the *Integrated Cross-Polarization Ratio* ICPR (Chandrasekar and Keeler (1993)) matters most. This ratio might be better than the antenna cross-polarization isolation for this antenna. Through the design of the POLDIRAD aerial, some cross-polar signals will cancel. This is caused by a 180° phase shift between the cross-polar maximums within the main beam. Therefore an ICPR of > 35 dB might be feasible.

An uncertainty level in the reflectivity estimation of about 1 dB is commonly assumed.

4.3 Calibration Model

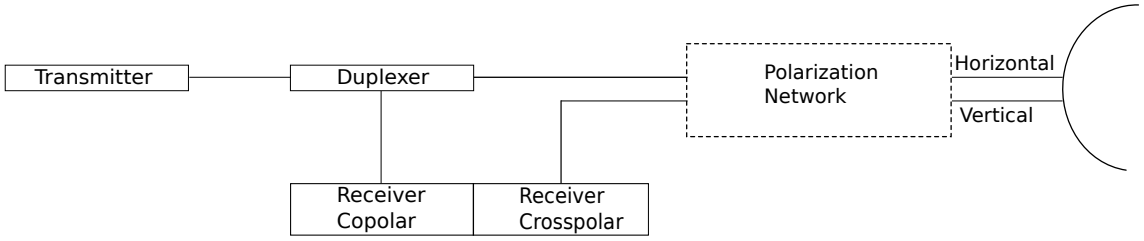

Figure 4.1: Simplified radar scheme for calibration as already shown in Fig. 2.3

In Fig. 4.1 the calibration model applied to POLDIRAD is shown. This model may also be - slightly modified - valid for other radars. This scheme is used to connect the measured voltage at the receiver with the electromagnetic field in front of the antenna. It is also used to characterize the system between the measurement point of the transmit power and the antenna. The wave-guide losses and length (phase), the behaviour of the polarization network, and the actual-value to digitalized receive power relation are assumed unknown.

4.4 Standard Techniques

A lot of different calibration techniques are available. It is not possible to name or even describe all of them. Only a small collection of commonly used techniques will be explained here briefly.

4.4.1 Internal calibration

The internal calibration includes a collection of different hardware built into the radar to characterize the system. It often includes a source of known power (generator or noise source) which can be injected at certain points into the receive path. If the signal is applied directly to the receiver frontend (low noise amplifier), it can be used to derive the relation between input power and the analogue-digital-converter output. The receive path (waveguides, couplers ...) can be characterized when the signal is injected near the antenna. In some configurations, these test signals can be used on-line by injecting the known reference at a defined range gate while the radar is measuring. POLDIRAD has also two power meters to measure the transmit signal at the two antenna ports. They can also be used to verify the reference signal for the receivers.

The main drawback of internal calibration devices is the impossibility to characterize the antenna. The precise electrical path length between transmitter/receiver and the antenna ports can also hardly be measured.

4.4.2 Sphere

An ideal metallic sphere is one of the targets for which the scattering properties can be analytical calculated, Scarchilli et al. (1995). Using the known scattering matrix and an ideal transmission matrix for the propagation path (good assumption for low frequencies and short range), the relation between transmitted and received electromagnetic wave can be calculated. This is probably the best technique in respect to uncertainty for power calibration. Although the polarimetric properties of the sphere are known, it is not sufficient for a full polarization calibration. This can easily be seen: a sphere will not depolarize any linear polarized wave no matter which orientation the wave has. Hence, the polarization orientation cannot be determined. A second or third (not reciprocal case) known target would be needed.

Some practical limitations apply: The sphere must be placed in the far field of the antenna, which is about 800 m for typical C-Band weather radars. The target has to produce a unique echo without any other targets like ground clutter. For a typical 1° weather radar antenna beam, the sphere has to be lifted more than 9 m above the ground (3 dB beamwidth). For precise measurements the sphere has to be lifted even higher. This is often done by a helium-filled balloon with the sphere connected

Figure 4.2: Sphere calibration performed in the 1990'th at POLDIRAD

by a nylon rope. Having the balloon outside the main beam of the antenna, a height of $> 18\,\mathrm{m}$ is needed. In practice, the balloon should be lifted much higher.

Another challenge is hitting the sphere directly. Therefore, the target must not move which requires a day without strong winds. On the other hand, the range resolution of the radar should be as high as possible to sample the maximum return. Hence, it is recommended performing several measurements, using the one with the strongest echo for calculations. A mean to measure the precise distance between radar and sphere is also required.

4.4.3 Rain

There are several calibration techniques using rain. Light rain consists of small, nearly round hydrometeors. This results in nearly no ($\sim -40\,\mathrm{dB}$) depolarization and can be used to check the channel isolation of the radar. The same can be done when pointing the radar vertical (if possible) and observing falling rain drops (having then a round shape). Events with low wind speed are to be preferred, to avoid canting of the particles.

Another approach is adjusting the radar against ground based rain gauges or distrometer measurements. The problem is the missing ground truth. Furthermore, the radar is measuring a volume in the atmosphere, while a gauge is a point measurement on the ground. The gauges also have statistical and systematic errors. It is also hard to determine which amount of hydrometeors measured by the radar

will reach the gauge. It can be shifted by wind, it will be time delayed and the hydrometeors may already been changed (melted, grown, evaporated). The drop size distribution (DSD) is not known when using rain gauges.

4.4.4 Astronomic Targets

Some astronomic targets have known properties, which can be used for calibration. These techniques have been used by radar astronomy for years now (e.g. Baars (1973)) and are well tested. In principle several astronomical objects can be used. In practice, strong emitters (or reflectors) are needed for weather radar calibration to get sufficient Signal-to-Noise-Ratio (SNR) values within reasonable integration time.

Sun

The sun is not only a source of visible light, but also radiates at microwave frequencies. Thus, it can be used for receiver verification. Besides that, it is probably one of the best targets to check the antenna alignment as the position is precisely known for a given time, Reda and Andreas (2008)

The sun is known to radiate unpolarized noise for common weather radar frequencies and antenna beamwidths. Hence, both receiver channels of a radar should measure the same power, Holleman et al. (2010). Both signals should be uncorrelated, too. Although the radiation of the sun is varying, it can be used for power calibration using external reference measurements, e.g. U.S. Dept. of Commerce (2012). A good description of sun scans can be found in Holleman and Beekhuis (2004). A detailed description of the measurements applied at the radar POLDIRAD can be found in Section 4.5.

Moon

The moon as a calibration target has been proposed by Gekat et al. (2011). In contrast to the sun, the complete radar hardware can be checked using the moon, since an echo can be recorded. The position and relative velocity is known, but the returned power might be low. Some additional efforts in data processing might be needed as the moon is far outside the normal ambiguous weather radar range (e.g. coherence in magnetron systems).

4.5 Sun-Calibration for the POLDIRAD Radar

A novel integrated computer program for sun measurements was developed for POLDIRAD. It calculates the sun position (using Reda and Andreas (2008)), sets up a radar scan and analyses the recorded data.

In preparation to the measurement, a complete calibration using built-in test equipment is carried out. For POLDIRAD this includes an internal calibration using the internal noise source, a zero check against clear sky and a receiver gain verification by injecting a known test signal into the receiver frontends.

To overcome the limited pointing accuracy of the antenna as well as getting a more complete picture of the sun, a raster scan using several Planar Position Indicator (PPI) is executed. This is more time consuming but allows extraction of beamwidth and potential side lobs from the data. As more data is recorded, the results become more stable. The scan time is no limiting factor for a non-operational radar.

Although radiation is switched on to keep stable (temperature and frequency) conditions during the sun scan, the radar operates as a radiometer. Obviously, there will be no echoes from the sun. The sampling is set up to avoid returns from weather targets, thus the near range is ignored. This is no limitation for higher elevation angles that should be used for sun scans because undesired echoes will probably appear only near the radar. High elevation angles are also to be preferred to avoid contamination from the *hot* ground ($\sim 300\,\mathrm{K}$) even through the side lobes. For low elevations, atmospheric attenuation and refraction ought to be considered. The receiver bandwidth is to be set to the highest possible value (or the smallest pulse width) to gather enough signal power.

Range	30 km to 90 km
Range Step	30 m
No. Range Gates	2000
No. Pulses	80
Rotation Speed	3 °/s
PRF	1000 Hz
Receiver Bandwidth	2.4 MHz

Table 4.1: Scan parameters for sun-calibration at POLDIRAD

The signal processing should be set up to gather the largest number of samples in the least time. Averaging along the radar ray should be performed, too. Data from several pulses can be combined from a higher number of samples, as long as the scan speed is low to keep good spatial resolution. Afterwards noise correction using a noise sample with the same characteristic (number samples, PRF, ...) is to be applied. The data plotting should take care of the sun movement during the scan by calculating the relative position of the sun for each point of the data set.

The sample size per data point and the receiver bandwidth are the most important quantities that define the SNR for the measurement. The SNR can be improved by a higher number of samples n by

$$SNR_{avg} = SNR_{raw} \cdot \sqrt{n} \tag{4.1}$$

at the expense of a longer scan time. E.g., 3 dB SNR improvement needs 4 times more data and hence 4 times longer scanning. This theoretical SNR improvement is only limited by the scan time and the slightly fluctuating noise seen by the radar for different antenna positions (e.g. due to different ground clutter seen by the side lobes). A separate noise scan sampling the same sky region at a time without the sun can further improve the measurement at the cost of even longer measurements. There is still a limitation due to changing indirect radiation from the sun. Using this technique the antenna pattern was measured down to ≈ -26 dB.

At POLDIRAD four data products are recorded:

- the combined power of both channels
- the channel power difference
- the absolute value of the cross correlation coefficient between both channels
- the phase of the cross correlation coefficient between both channels

The combined power is used for a two dimensional Gaussian fit of the sun with the parameters $(p_1 \dots p_6)$:

$$y = p_1 e^{-\frac{1}{2}\left(\frac{(x_1-p_2)^2}{p_3^2}+\frac{(x_2-p_4)^2}{p_5^2}\right)} + p_6 \tag{4.2}$$

This results in a much more stable estimation than by retrieving it from the raw data. From this equation the antenna alignment offset can also be found (p_2 and p_4)

and is found to be stable to a few hundredth of a degree. The estimated horizontal and vertical 3 dB beamwidth of the convolved antenna pattern and sun is derived.

$$beamWidth_{H/V} = 2\sqrt{-2\ln 0.5} \cdot p_{3/5} \tag{4.3}$$

and corrected using the formulas from Holleman and Beekhuis (2004)). The estimated power is automatically compared to a user given reference value (U.S. Dept. of Commerce (2012)) as described in Holleman and Beekhuis (2004).

The channel imbalance can be derived from the linear power samples of the two receiver channels using the gain of a linear fit between both data sets

$$ADC_h = \Delta_{gain} \cdot ADC_v + \Delta_{offset} \tag{4.4}$$

A SNR threshold (noise from eq. (4.2) parameter p_6) has to be applied to avoid the clear sky samples.

Data Plotting

In recent works Holleman and Beekhuis (2004) the sun data were plotted as the difference between the elevation and azimuth of sun and antenna. It will be shown that this is only a good approximation for low elevation angles. The azimuthal movement of most standard weather radar antenna (Fig. 4.3 Point A) at a certain elevation (circle C_3) is only a great circle on the sky half sphere for an elevation angle of 0°. For higher elevation angles this circle becomes smaller (e.g. circle C_4) and ends up as a point at 90° elevation. In this situation, although the antenna may rotate azimuthally, it points to a fixed position on the sky. It can be seen by this example that the relative elevation/azimuth angle between antenna and sun is not a proper description for the relative position between sun (point S) and antenna.

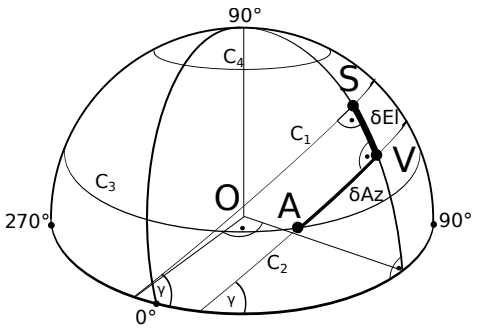

Figure 4.3: Sketch of the orthogonal coordinate system on the sphere

For correct data plotting an orthogonal coordinate system is needed. The x- and y-axis should be aligned along great circles. The origin of the coordinate system is the sun. The antenna position needs to be transformed to this coordinate system to get the new relative position (δEl and δAz). This can be done by equations similar to that used in astronomy to transform the coordinates of stars to the ecliptic. Fig. 4.4 illustrates the transformation. The sun (point S) on the right, the great circle (C_2) and the angle γ (which is the elevation angle $elSun$ of the sun) is defining a vertex. The antenna position (point A) is known in the original coordinate system by the elevation of the antenna ($elAnt$) and the difference in azimuth angle between antenna and sun (the bold lines, $azSun - azAnt$). The relative position δEl and δAz can be calculated using the triangle A-N-P. The sides A-N $= 90° - elAnt$ and N-P $= 90° - (elAnt - elSun)$ are known as well as the angle at point N $= 180° - (azSun - azAnt)$. The angle at point P (δAz) and the side A-P ($90° - \delta El$) are to be calculated. This can be done using the law of sines and the law of cosines for spherical triangles. The following equation for the transformation can be easily derived:

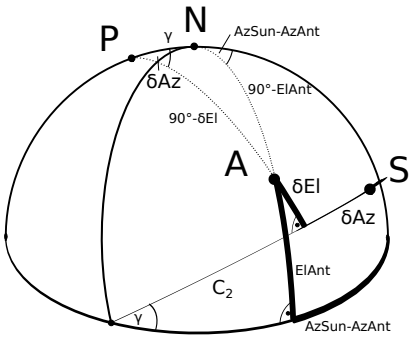

Figure 4.4: Illustration of the coordinate system transformation

$$\begin{aligned}
\cos(\delta El)\cos(\delta Az) &= \cos(elAnt)\cos(azSun - azAnt)\cos(elSun) + \\
&\quad \sin(elAnt) - sin(elSun) \\
\cos(\delta El)\sin(\delta Az) &= \cos(elAnt)\sin(azSun - azAnt) \\
\sin(\delta El) &= -\cos(elAnt)\cos(azSun - azAnt)\sin(elSun) + \\
&\quad \sin(elAnt)\cos(elSun)
\end{aligned} \tag{4.5}$$

Antenna Alignment Check

The antenna alignment check against the sun should be performed at different times of the day. This results in different azimuths and - dependent on the season - different elevations. On POLDIRAD the position offset was found azimuth/elevation dependent.

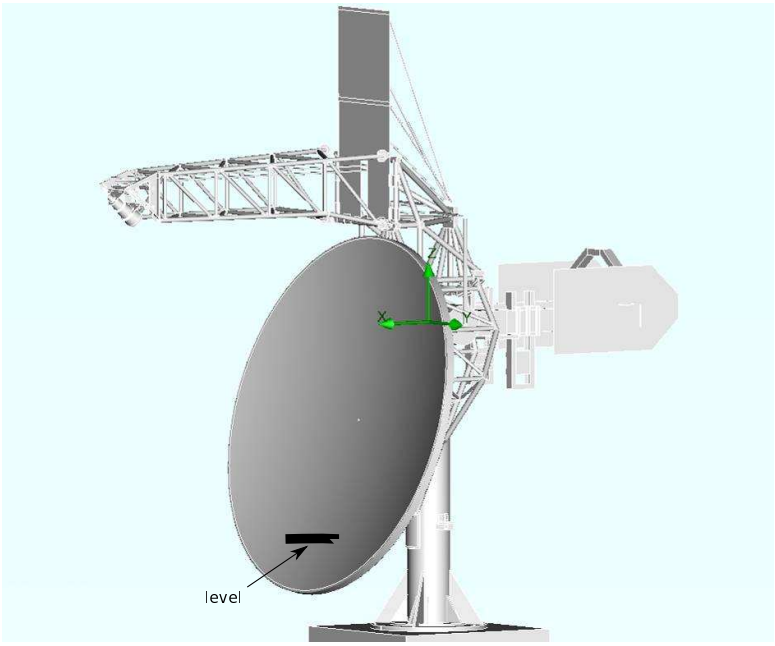

Figure 4.5: Mounting of the spirit level on the antenna, picture from Ceccarelli (2008)

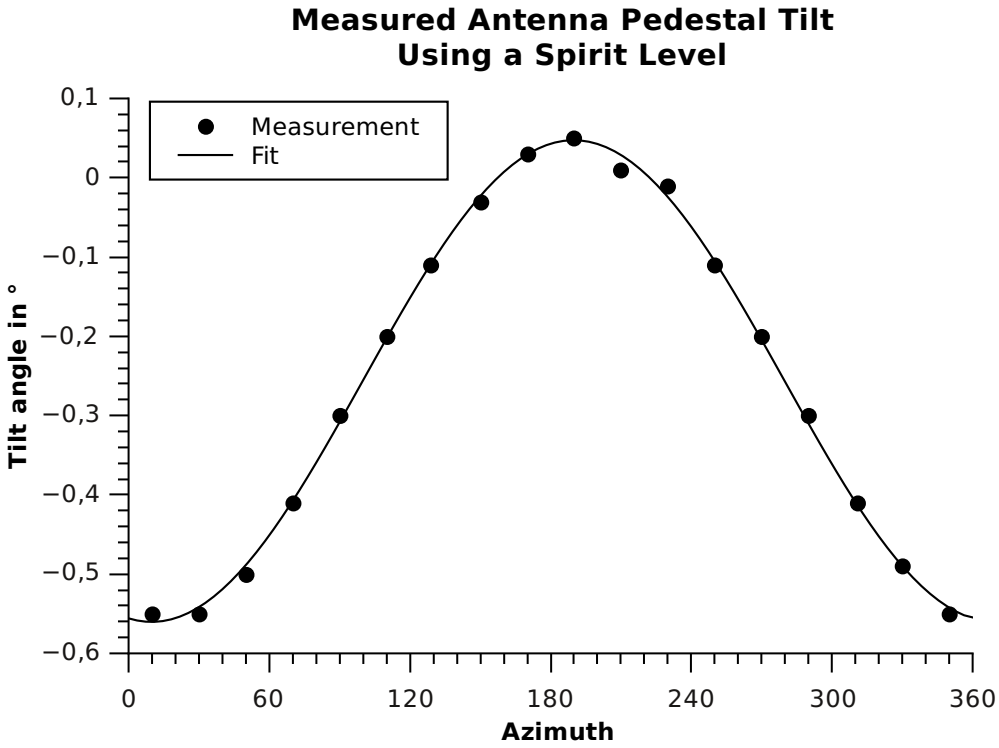

Figure 4.6: Antenna tilt measurement

Further analysis showed that the antenna pedestal was tilted. This was probably caused by the latest re-/assembling of the antenna for transport to the field campaign COPS. Using a spirit level the results were verified (Figure 4.5). The spirit level was attached parallelly to the dish, which causes a 90° the azimuth shift between gauge and tilt angle. The shown measurement setup benefits of being independent of the absolute angle of the mounting. The angle of the gauge is equal in direction of maximum tilt and 180° to it and maximum/minimum 90° from this position. From the data (Figure 4.5) the pedestal tilt was calculated to 0.3° at 100° azimuth.

The tilt was corrected afterwards and the reference measurements using the sun are now within 0.1° from the expected values. The sun measurements with its known position were the only clue for this pedestal tilt. It is not visible in normal radar scans.

Polarization determination

The sun is a very good noise source. Hence, if the system isolation between the channels would be ideal, the correlation between data of both channels tends to be zero.

$$\langle P_{channel1} \cdot P^*_{channel2} \rangle = 0 \tag{4.6}$$

For a limited, but large number of samples the absolute value of the correlation gives an estimation of the channel isolation. For POLDIRAD this value is strongly depended on the alignment of the antenna to the sun. This leads to the assumption that the antenna is the limiting factor for the system isolation, not the polarization network. This was also confirmed by measurements using a VNA giving an isolation between the H and V port of the polarization network of 40 dB or better Tracksdorf (2010).

The pattern of the correlation maxima was found to be similar to the shape of the cross-polar maxima. This is reasonable, as only in regions of low polarization isolation in the antenna, the correlation coefficient can rise. Furthermore there is a dependence of the correlation pattern with the receive polarization selected by the polarization network. This can be explained due to the offset configuration of the POLDIRAD antenna (Schroth et al. (1988)) and its polarization dependent radiation pattern.

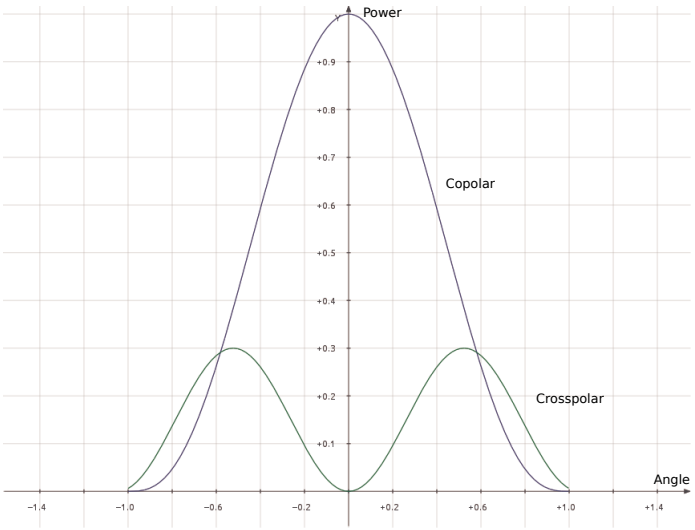

Figure 4.7: Modelled antenna pattern (not to scale)

For a deeper study of this effect, only an azimuth cut with equal sun and antenna elevation will be analysed. The co-polar power pattern is known to be $(1-x^2)^3$ and the cross-polar pattern is modelled as $a\sin(bx)^2$ (Fig. 4.7). The channel correlation analysed is a convolution of the antenna pattern with the radiation of the sun, which is uniformly distributed over the sun disk and consists of unpolarized noise. The uniform distribution will result in a spatial averaging.

For horizontally/vertically receiving polarization the modulus of the recorded correlation pattern will be this spatial averaged antenna pattern in the outer parts. In the centre ($\theta = 0°$) the 180° phase shifted cross-polar peaks causing a vanishing modulus (Fig. 4.8: 1^{st} and 2^{nd} row). The same correlation phase appears on the left and on the right. This phase is always 180° shifted between the left and the right.

It can be shown that for a linear 45°/135° basis the cross-polar peaks are in phase, Chu and Turrin (1973). The modulus of the correlation pattern is similar to the linear horizontal/vertical one without the minimum at $\theta = 0°$ (Fig. 4.8: 3^{rd} and 4^{th} row). The correlation phase is now swapped when comparing linear 45° and 135°.

For circular polarization, there will be no cross-polar peak for this kind of antenna, Fasold (2000), but the antenna pattern is no longer symmetrical, which leads to a squint. Due to the spatial averaging, there is only one central peak in the correlation modulus (Fig. 4.8: 5^{th} and 6^{th} row) that is also much lower than for linear polarization. The correlation phase is constant for both circular polarizations.

These differences in the correlation phase might be useful for roughly checking the

polarization. That might be of particular interested for linear 45°, linear 135° and circular polarization, as they only differ in relative phase in the H/V polarization basis of the radar.

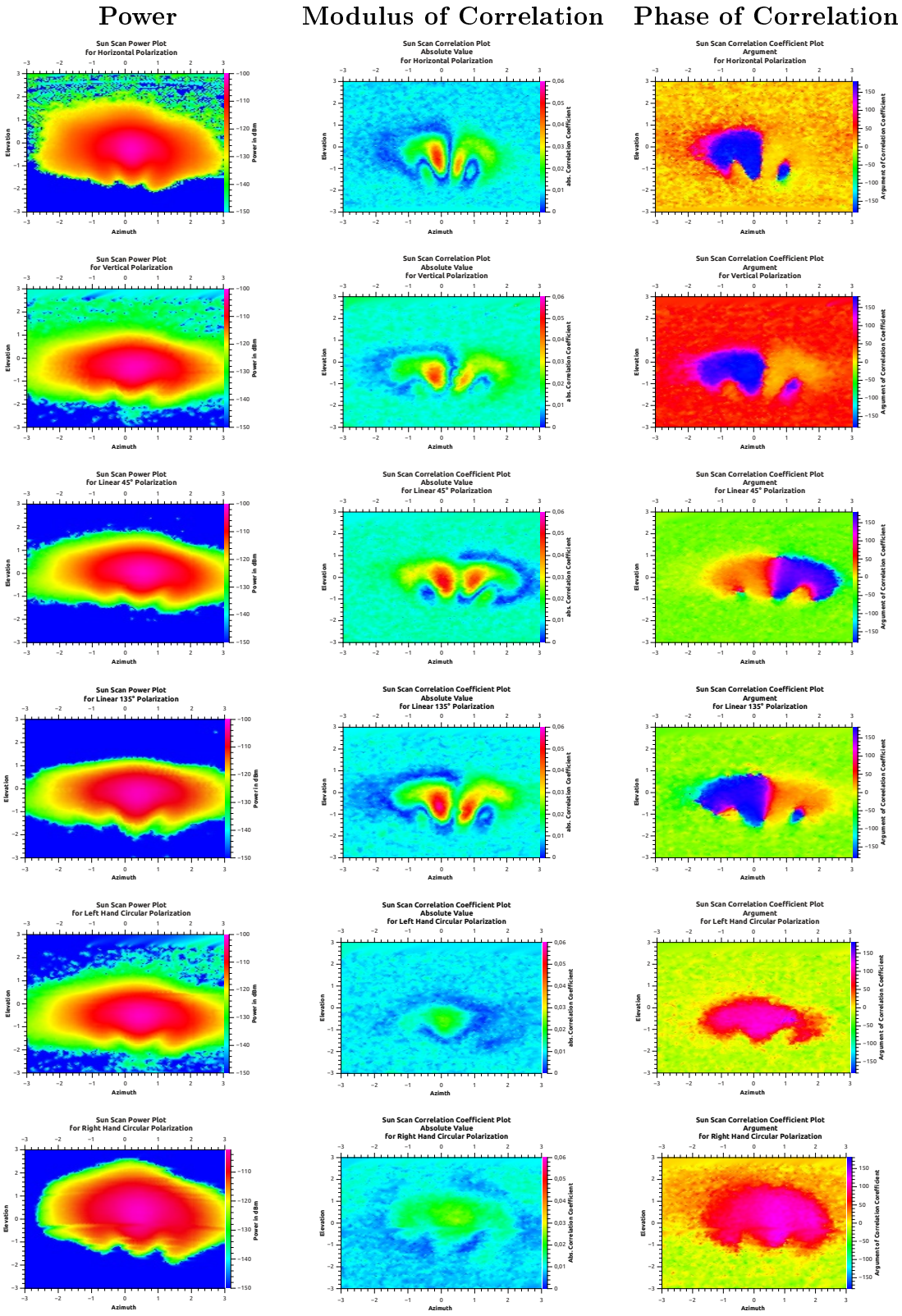

Figure 4.8: Antenna pattern for different polarization. Enlarged versions are found in Appendix C

Chapter 5

Preliminary Investigation of an External Calibration Device

Since the antenna plays an important role in creating the specified polarimetric properties it cannot be easily neglected (Gekat et al. (2010)). Therefore an end-to-end calibration is preferable when calibrating polarimetric radars. A characterization of the polarization network in a laboratory is very complicated if both low power measurements with a vector network analyser and high power tests would be performed. This is needed due to the non-reciprocal and non-linear behaviour. But this approach would still neglect environmental effects like the operational temperature of the device in the radar or mismatches in the system e.g. between the polarization network and the antenna ports. The phase shift of the two waveguides from the polarization network to the antenna and phase reference at the horn would be needed, too. On the other hand, a huge disadvantage of an external calibration approach is the lack of a controlled measurement environment. Most external measurement techniques are weather dependent and sensitive to interference, some are additionally very sensitive to undesired echoes from obstacles near the radar or other sources of reflection.

Nevertheless, an external calibration is the more versatile approach as it is easier to perform and leads to low uncertainty in phase measurements which is essential for the polarization creation as performed by POLDIRAD.

5.1 Antenna Measurement Techniques

The POLDIRAD is located at DLR in Oberpfaffenhofen-Wessling. The radar is built on top of the Institute of Atmospheric Physics, but is surrounded by other buildings, smaller hills and woods. Finding a good measurement technique suitable for the site and the measurement demands is challenging. Some limitations are unavoidable, although several options were considered. First part will be the selection of the measurement range.

5.1.1 Near Field

Modern processing techniques make near field antenna measurements feasible. A probe scans the radiation very close to the antenna (Balanis (2008)). From this measurement, the far field pattern can be derived.

The main drawback of this approach is the demand for a complete time consuming coating measurement to get the polarization characteristic for the main beam. This makes determination of the polarization inefficient. Optimization of the polarization settings of the polarization network would be nearly impossible. Therefore, this technique is of limited interest for POLDIRAD calibration.

5.1.2 Compact Range

For the technical point of view, a compact range measurement might be preferred. A shaped reflector is used to create a plane wave front, which would otherwise only appear at a much longer distance (Balanis (2008)). It is fairly precise and fast, but there is a need of reflectors. These reflectors would be very large for POLDIRAD. As they are to be outside of a building, the wind load could become a big issue. Furthermore, a suitable location for the construction was not found. Additionally, there were safety concerns due to potential reflection into office rooms.

5.1.3 Far Field

Far field setups are the ones commonly used. The drawback of this approach is the large range of nearly one kilometre needed to get into the far field and the problem of the ground reflections.

The condition for the far field is (from IEEE Std. 145-1983 IEEE (1993)):

$$R > \frac{2D^2}{\lambda} \tag{5.1}$$

with $D = 15\,\text{ft} \approx 4.57\,\text{m}$ and $\lambda = 0.0545\,\text{m}$ the minimum distance is about 766 m.

A first test site was found about 2 km from the radar (Fig. 5.1). The radar beam had to cross only an airport and flat fields. Only one building is situated near the radar but much lower than to be present in the first Fresnel zone (volume of energy transport). Unfortunately, this site was found to be heavily contaminated by ground reflection.

Therefore, the measurements were performed on a building only $\approx 227\,\text{m}$ away (Fig. 5.2). The distance to the new site is known not to be below the far field criteria, but was considered a better option than the first one. For lack of alternatives, all measurements were carried out at this location.

Figure 5.1: First approach measurement range (distance approx. 2 km)

Figure 5.2: Second approach measurement range (distance approx. 227 m)

5.2 Polarization Measurement Techniques

A suitable technique needs to be evaluated for measuring the polarization of the radar POLDIRAD. Its polarization network is able to produce nearly any polarization state. Therefore, the employed measurement technique should be also able to characterise every fully polarized wave. In addition, it should to be fast enough to make tuning of the polarization network feasible.

5.2.1 Single Rotating Linear Polarized Antenna

The polarization of a wave can be distinguished by rotating a linear polarized probe around the axis defined by the propagation direction of the wave (Sahler et al. (1968)). There will be a specific angle where the received power becomes minimal and one where it becomes maximal. The angle of the maximum is equal to the orientation angle, while the difference between maximum and minimum gives the aspect ratio. This technique cannot easily distinguish between left and right hand circular polarization. This can only be achieved by a fast rotating antenna, which would create some kind of frequency shift between the rotating electrical field vector and the antenna rotation. The rotation speed might be impractically high.

5.2.2 Orthogonal Antenna Pair

Measuring the two powers and the phase difference of two non-collinear antenna probes is sufficient for the determination of the polarization (Sahler et al. (1968)). It is convenient to use orthogonal probes. The orientation is then given by

$$\tan 2\phi = \frac{2\vec{E_1} \cdot \vec{E_2}}{\left|\vec{E_1}\right| - \left|\vec{E_2}\right|} \tag{5.2}$$

The ellipticity can be calculated from

$$\tan 2\tau = \frac{2\left|\vec{E_1} \times \vec{E_2}\right|}{\left|\vec{E_1}\right| + \left|\vec{E_2}\right|} \tag{5.3}$$

This leads to instantaneous measurement of the polarization. If the properties of an (imperfect) antenna are known, the corrected polarization can be calculated as shown by Lyakhovskii et al. (1996).

5.2.3 Four-Antennas Power Measurement

To avoid phase measurements, the four-antennas measurement using linear and circular polarized antennas was developed. There are three groups of probes:

- linear horizontal and vertical
- linear 135° and 45°

- left and right hand circular

For the measurement, four power samples are needed including at least one item of every group.

The polarization can be calculated by solving a set of equations.

$$E_x^2 = a_1^2 \tag{5.4}$$

$$E_y^2 = a_2^2 \tag{5.5}$$

$$E_{45}^2 = \frac{1}{2}\left(a_1^2 + a_2^2 + 2a_1a_2 \cdot \cos\delta\right) \tag{5.6}$$

$$E_{135}^2 = \frac{1}{2}\left(a_1^2 - a_2^2 + 2a_1a_2 \cdot \cos\delta\right) \tag{5.7}$$

$$E_L^2 = \frac{1}{4}\left(a_1^2 + a_2^2 + 2a_1a_2 \cdot \sin\delta\right) \tag{5.8}$$

$$E_R^2 = \frac{1}{4}\left(a_1^2 - a_2^2 + 2a_1a_2 \cdot \sin\delta\right) \tag{5.9}$$

$$E_x^2 + E_y^2 = E_{45}^2 + E_{135}^2 = 2(E_L^2 + E_R^2) \tag{5.10}$$

The axial ratio e.g. becomes

$$AV = \frac{||E_L| - |E_R||}{|E_L| + |E_R|} \tag{5.11}$$

and the tilt angle

$$\tan\Psi = \frac{E_{45}^2 - E_{135}^2}{E_x^2 - E_y^2} = \frac{2a_1a_2 \cdot \cos\delta}{a_1^2 - a_2^2} \tag{5.12}$$

A detailed description of polarization measurement can be found in Sahler et al. (1968). The advantage is that no phase measurement is involved. Drawbacks might be mutual cross coupling between the antennas, no defined phase centre, a heavy antenna construction and the problem of precisely manufactured antennas (and the errors introduced by them). Imperfect antenna cannot be corrected as easily as for the orthogonal antenna case.

5.3 Prior Systems

There have been already several efforts for calibration using remote stations. Some of them will be shown here. None of them met the requirements formulated in Section 4.1. Nevertheless, it gives an overview of the techniques used and their advantages and disadvantages.

5.3.1 Single Antenna PARC

Sarabandi, Ulaby et al. (Sarabandi et al. (1990) and Ahne et al. (1989)) developed a PARC concept for an airborne and a space-borne mission (AIRSAR and SIR-C). The concept included a delay line to separate the calibration signal from undesired ground clutter. The Polarimetric Active Radar Calibrator (PARC) was designed to provide a known constant RCS and scattering matrix. Reciprocity was assumed for the radar. There was no internal calibration loop for a self-check of the PARC.

The authors found huge stability issues coming from the delay line (for $\Delta T = 30\,°\mathrm{C}$ $\Delta G = 3\,\mathrm{dB}$). Hence, complex temperature stabilization was needed.

5.3.2 Automated Polarization Measurement Chamber

An automated polarization measurement chamber for antennas was introduced by Lyakhovskii et al. (1996). It utilizes a dual polarized antenna and a $\Phi K2-33$ microwave network analyser(soviet model) for polarization measurements in a chamber. A model for both polarization channels, the polarization divider and the antenna was developed to correct the data. Thus, an imperfect antenna could be used for measurements.

5.3.3 DLR PARC

Very early after POLDIRAD become operational, there was the demand for an end-to-end calibration. The concept of a first PARC was given by (Ziegler and Clemens (1993)). It was using a single linear polarized horn to record the power for several orientation angles. From the plot recorded this way, the polarization can be derived (Section 5.2.1). The PARC was placed on a tower located about 800 m from the radar. Unfortunately, this mast is not usable any longer, due to new buildings blocking the beam in that direction.

The drawback of this approach was the long time needed for calibration. There was one person placed at the tower rotating the measurement antenna and recording the data and one person at the radar. The mechanical rotation of the antenna was time consuming. It was advanced by an automatic rotation and recording system. Nevertheless, the measurement of one polarization still took minutes.

From this experience, a new design was created using a four antenna power measurement technique, which was shown in Section 5.2.3. The three dual polarized

antennas needed were already built (Wanninger (1994)), but the device was never completely finished.

5.3.4 Summary

Sarabandi et al. had an easy PARC concept but stability issues could not easily be overcome. The old DLR PARC improved this issue by using a SAW (surface acoustic wave) delay line. Although the old DLR PARC was a successful device, it was not any longer in shape for further usage. A disadvantage was the slow calibration speed. Unfortunately, the used location (a tower) is not any longer available. The concept of Lyakhowskii includes a technique for correcting the measurements by characterizing the imperfect hardware. Because building antennas with a very high cross-polar isolation ($> 40\,\mathrm{dB}$) can be difficult, using this technique as a fall back sounds promising.

5.4 Technology Evaluation

The polarization network is known to be not reciprocal. The phase shift introduced by the ferrites is depending on the direction of wave propagation. Furthermore the high power transmit pulse creates spin waves in the ferrites with raises the loss (see Section 3.2). This non-reciprocal behaviour increases the complexity for calibration. To overcome complexity it was decided to separate transmit and receive calibration, which unfortunately results in higher uncertainty. The transmitted radar pulse will be measured and an artificial echo signal created is used to calibrate the system. A smart calibration device able to perform an automatic calibration amounts to be state-of-the-art.

Considering the available techniques and methods mentioned above, a compromise has to be found which matches the demands for the calibration of POLDIRAD. The selection will be different for other radar systems with other demands and/or other emphasis of the designer.

Starting with the requirements as stated in Section 4.1 and 4.2. A good solution had to be found: For the required fast polarization measurement, only a far field setup seems worthwhile. Performing a near field to far field transformation is only possible if the whole or at least a sufficient large part of the near field pattern is

known. This would be a time consuming operation and has to be repeated for each setting of the polarization network.

A compact range measurement could be exact but also has some huge drawbacks: Placing the reflector on roof of the radar building would expose it to weather, which declines the performance. Safety concerning the radiation would arise in the radar building and the area surrounding.

Placing the antenna into an anechoic chamber would be another option. Unfortunately this would be an expensive task and not easy to repeat. Furthermore most parts of the radar would have to be moved to the measurement site too, as high power tests ($\sim 400\,\mathrm{kW}$) are mandatory.

Fortunately, only the far field pattern of the main beam is needed for weather radar measurements. Naturally far field measurements fit well. However, there are drawbacks, too: no controlled environment is available. Especially ground effects will have an impact on the measurements. In view of the arguments, this option seems to be the best compromise.

Besides the measurement range, the polarization determination technique needs to be evaluated. The rotating probe, as used in the old DLR PARC concept, limits the measurement speed to a mechanical boundary and was not considered any longer. Using one dual polarized antenna involves phase measurements that could become tricky. Furthermore it is hardly possible to purchase or build a dual polarized antenna having sufficient channel isolation better than the radar (about $-35\,\mathrm{dB}$). But this can be overcome by a precise determination of the real antenna parameters and a mathematical compensation (Lyakhovskii et al. (1996)).

The same antenna performance problem arises with the four component power measurement when using three dual polarized aerials. The usage of four single polarized antennas would be favourable. Unfortunately, there is no defined phase centre as several probes are involved. There might be a coupling between the antennas which has to be taken into account when designing the array. Errors in the polarization properties are hard to compensate. The main disadvantage is the physical dimension. Four horn antennas with polarisers and a mechanical construction to fix the position of the aerials may become heavy (estimated 60 kg to 70 kg). Another constrain are limited resources for building antennas. Keeping these aspects in mind, the dual polarized antenna using power and phase measurements was chosen.

Learning from the previously used systems, a delay line should be avoided. To

overcome the non-reciprocal properties of the radar, the calibration should be split into a radar transmit pulse measurement and an independent receive calibration. The receive part of the calibration can be easily performed by creating a continuous wave having a defined polarization which is to be recorded by the radar. This signal can easily be generated by a proper signal generator.

It turned out that measuring the transmit pulse in amplitude and phase is the difficult part. Standard equipment unfortunately fails. Oscilloscopes can measure the phase, but have a limited dynamic range of about $5 \ldots 6$ effective bits $\approx$ 30 dB to 36 dB. Spectrum analysers on the other hand have the proper dynamic range, but cannot retrieve the phase of the signal. Network analysers are expensive devices and the setup would be complicated because the internal signal sources cannot be used. The hardly controllable radar magnetron transmitter is needed for high power tests.

Having in mind the computer technology available today, a solution comes up using software-defined radio (SDR) or high speed sampling cards. The signal can be analysed in software with the computation power available today. This leads to a system design having a simple and robust analogue frontend and a fast digitalizer. This concept seems to be sober, but powerful.

Chapter 6

PARC

The constrains for a calibration device were developed in Chapter 5. Now the PARC system hardware will be shown. All the ideas from Section 5.4 will now be taken in consideration to develop the hardware design. Afterwards the software part of the calibration will be in focus. There are several software modules for the different calibration tasks. They will be introduced and their main purpose will be stated along with their principle of operation. At the end of this chapter, the measurement results will be shown and discussed.

6.1 System Description

The best solution for the calibration of POLDIRAD was found to be a system that uses a single dual-polarized antenna to measure power and phase as shown in Section 5.4. The developed concept includes a simple frontend with two bidirectional channels for transmit and receive, a calibration channel and a computer with a SDR (software defined radio) card to record and generate signals (Fig. 6.1). In addition there is a WiFi connection to the radar to control the system remotely, a 10 MHz GPS locked signal for frequency reference to the radar, from which *all* other signals are derived. This way, both, the POLDIRAD and the PARC can be synchronized and are made pseudo-coherent.

One main design goal is the avoidance of active devices in the signal paths to minimize stability issues as seen in other PARC systems. Unfortunately, this limits the options in the frontend as the signals can only be attenuated. This is not a limitation for the radar transmit case as the signal is very strong, but might be an

issue for creating a sufficiently strong signal for the radar receiver. From the selected components (max. mixer IF power of 0 dBm and approx. 5 dB conversion loss) a maximum output signal of only −5 dBm can be achieved which is sufficient as it will be shown later in Section 6.2.

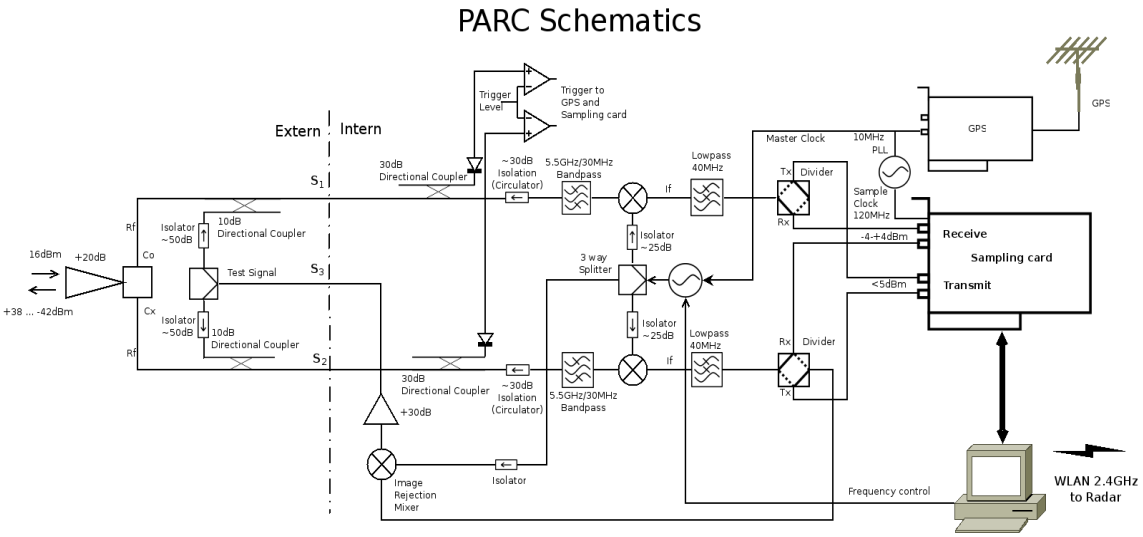

Figure 6.1: PARC schematics

For receive calibration only *two signals* with a defined polarization are needed. The radar can calculate the expected input signal at the receivers from the known polarization transmitted by the PARC, and the polarization basis chosen for the polarization network. Then it can optimize its polarization settings to match the expected signal at both receivers. The second signal is needed to segregate (differentiate) receive path losses from the polarization state at the antenna.

The radar pulse is to be analysed for radar transmit calibration. Therefore, the 5.504 GHz pulse from the radar is down converted to a floating intermediate frequency (IF) using a stable oscillator and then directly sampled. Signal processing is used to retrieve the exact radar frequency (the magnetron frequency of the transmitter is slightly varies e.g. versus temperature), the amplitude/power and the phase of both channels. From this information the radar transmit power, frequency, Pulse Repetition Frequency (PRF) and polarization can be calculated.

6.2 First RF Power Estimation

Some rough estimation of the expected power at the measurement site is needed. There are fixed values for the radar transmit power (400 kW), the radar antenna gain (43 dB) and the PARC antenna gain (approx. 18 dB). The distance between measurement site and the radar is 227 m.

The power received by the PARC (P_{RxParc}) is estimated using logarithmic values as:

$$\begin{aligned} P_{RxParc} &= P_{TxRadar} + G_{RadarAntenna} - Att + G_{ParcAntenna} && (6.1)\\ &= 86\,\text{dBm} + 43\,\text{dB} - 94.4\,\text{dB} + 18\,\text{dB} && (6.2)\\ &= 52.6\,\text{dBm} && (6.3) \end{aligned}$$

The free space attenuation for a path of length r is evaluated using the expression

$$Att = 20 \log \frac{4\pi r}{\lambda} \tag{6.4}$$

while the gas attenuation is neglected at this short distance.

For the radar receive case the minimum power which the PARC at least has to transmit will be calculated as:

$$P_{TxParc} = P_{RxRadar} - G_{RadarAntenna} + Att - G_{ParcAntenna} \tag{6.5}$$

The minimum discernible signal at the radar found at the site acceptance test (SAT) is better than −114 dBm and the 1 dB Gain Compression Point (1dB GCP) is approx. −10 dBm (Selex Sistemi Integrati (2010)). Using these values the PARC has to transmit a signal power of −80.6 dBm to 23.4 dBm. Keeping in mind, that a cross-polar signal of −40 dB should still be detectable the appropriate transmit power range shrinks to −40.6 dBm to 23.4 dBm.

6.2.1 Trigger Generation

The duty cycle (ratio between transmit pulse duration and receive time) is typical in the range of 1 : 1000. Hence, it is favourable to limit the recording interval to a range near the expected radar pulse. The simplest solution is the use of the pulse itself. Two detector diodes - one for each channel - can be used to trigger the recording system. This regime will, of course, not guarantee coherent sampling.

To overcome this drawback a separate trigger generator is used. It consists of a fixed and a variable divider, implemented as counters, to create a local PRF from the 10 MHz reference. A strobe signal from the GPS card is used to reset both counter and synchronize the PRF start to the expected radar pulse (see Appendix A.2).

If the PARC software detects missing pulses, it switches into a synchronization mode with a very long sampling time. These data are used to calculate the radar PRF and the start time of the pulses. The PRF generated is set to the new value and a proper strobe signal is generated in software to synchronize the system to the radar.

6.3 System Development

6.3.1 Hardware

The radio frequency parts of the PARC system is shown in Fig. 6.1. The antenna chosen is a dual polarized circular tapered horn with a T-Junction polariser built for an older version of the original DLR PARC. The used polarization divider has a very narrow bandwidth and was only designed to match the POLDIRAD frequency. A precise characterization of the aerial was performed on the compact range antenna measurement site of the DLR Microwaves and Radar Institute. The antenna gain was determined to be 18.6 dB with a 3 dB beamwidth of nearly 20° (see Appendix A.1).

A test signal circuit has been plugged directly onto the antenna ports, which was included into the antenna measurements. It consists of a power splitter and some isolators to mitigate coupling between the antenna ports, which have to be better than 40 dB. A signal inserted into this periphery will create a known phase shift and power difference at the antenna port. This acts as a reference to characterize the frontend during the internal calibration procedure. While the absolute power level fed into the reference port may not be precisely known (for an absolute power calibration), the relative signal behaviour between the both channels stays constant and was calibrated using a VNA. Hence, it can be used as a relative power and phase reference. This signal can also be interpreted as a known polarization reference being inserted at the antenna.

Two measurement cables and a test signal cable are connecting the antenna with the electronics stored in a closed metallic box. Two racks are placed in this bin: one for the Radio Frequency (RF) components, one for the computer, power supply, WiFi access point etc. This assembly allows easy maintenance and transport while minimizing interference between the components.

The RF parts in the rack are identical for both channels, only the electronics of the calibration path differ. Each measurement channel includes a coupler and a diode to detect the radar pulse. A combination of both signals is routed to the GPS cards event input to get the precise time stamp of the pulse (see circuits in Appendix A.2). Beside the radar pulse itself, an internal PRF source can be selected to generate the trigger for data recording. The internal source is to be selected for phase coherent measurements.

It can be seen from Section 6.2 that the power received from the radar is still very high and needs to be limited to protect the following hardware stages. Since the PARC transmit signal must not be attenuated, a reversely installed isolator is selected for this task. The precise, and practically limited, isolation value is characterized and corrected using the internal calibration procedure.

This isolator is followed by a band-pass filter to select the radar frequency. This is of less importance for the receive case as the radar pulse should be by far the most powerful signal the PARC antenna receives (which acts itself as a broad band-pass filter). While the PARC is transmitting, this filter is used to remove the unwanted side band generated due to the mixer stage. The local oscillator frequency for the mixer is selected to convert between the radio frequency of 5.504 GHz(for POLDIRAD) and an intermediate frequency of approx. 60 MHz. This is a floating IF through the varying frequency of the magnetron transmitter of the radar. The precise frequency determination is done in software.

Two switching matrices are used to connect both receive/transmit channels to the receive and transmit port of the sampling card (Pentek 7841). One channel also acts as test signal source while in receive state. This calibration channel employs an image rejection mixer for up-conversion and needs an amplifier to generate a sufficient strong signal to be inserted at the antenna calibration input.

6.3.2 PARC Server Software

The control software of the PARC is written in C++ using the Qt™ software library. It was designed as a network transparent client/server application. While a server is working on the PARC host computer controlling the hardware, a client with a user friendly interface can connect to that service to control the system through a Transmission Control Protocol/Internet Protocol (TCP/IP) connection. The software was designed modularly to allow code reuse and hardware abstraction while leaving space for future improvements and calibration tasks.

There are several low-level operation modes defined in the PARC software which set up the hardware properly for the given task:

- Transmit Mode
- Time Series Mode
- Polarization Measurement Mode
- Internal Calibration Mode

Transmit Mode

Using the transmit mode the PARC transmits a signal with a defined polarization. Currently only a continuous wave signal is specified, but it might be extended to (nearly) any modulated signal. The polarization $\underline{\rho_{xy}}$ is generated by two sines of a given frequency (the radar IF) with the desired amplitude and phase shift according eq. (6.6). These signals are stored in the memory of the sampling card and are repeatedly transmitted using the card's DACs. Special care was taken to create a smooth transition between the end and the restart of the sequence stored in the sampling card's buffer.

$$\begin{pmatrix} \underline{E_x} \\ \underline{E_y} \end{pmatrix} = \frac{E}{\sqrt{1 + \left|\underline{\rho_{xy}}\right|^2}} \begin{pmatrix} 1 \\ \underline{\rho_{xy}} \end{pmatrix} \tag{6.6}$$

Time Series Mode

The time series mode is used to provide the raw sampling data to the client. It can be used to extract shape parameters like raise and fall time, overshoot from the

radar pulse. Due to the limited bandwidth of the network connection, only a limited number of pulses recorded are sent to the client. For performance reasons these time series data is not corrected for channel imbalance or other hardware effects and may therefore not be used for quantitative measurements.

Internal Calibration Mode

The internal calibration is a two-step procedure. In a first step, noise is sampled for ADC offset compensation and noise correction of the recorded signals. Secondly a test signal is generated which is injected into the receiver paths at the antenna port (see Section 6.3.1). The calibration is going to stop when reaching a user defined uncertainty limit. This limit is defined by the remaining estimated error derived from the standard derivation for a number n samples:

$$s = \sqrt{\frac{1}{n-1}\left[\sum_{i=1}^{n} x_i^2 - \frac{1}{n}\left(\sum_{i=1}^{n} x_i\right)^2\right]} \tag{6.7}$$

The remaining error can also be estimated by

$$s = \frac{\sigma}{\sqrt{n}} \tag{6.8}$$

Using the recorded phase and power difference of the receiver channels, correction factors for the down converter path are calculated.

$$\underline{Correction_{Chx}} = \frac{Power(dBm)_{calib} \cdot \underline{S_{3X_{TestCoupler}}(dB)}}{Sample(adu)_{calib}} \tag{6.9}$$

where $Sample(adu)_{calib}$ is the ADC output for a power $Power(dBm)_{calib}$ injected into the calibration circuit and $\underline{S_{3X_{TestCoupler}}(dB)}$ the known transmission loss and phase between calibration input and the antenna port X for the test circuit at the antenna.

An extended internal calibration can be performed by changing the test signal in frequency. This allows a precise characterization of the receiver path versus frequency. A third order polynomial is used to interpolate the calibration to the actual radar frequency. Other internal check could be performed e.g. characteristics versus power or for different IFs.

Polarization Measurement Mode

One main objective of the PARC system is the polarization measurement of the radar pulse. Hence the signal processing has to extract the pulse parameters power and phase from the two channel sampled data. Only a limited number of pulses can be written into the sampling card memory. After this coherent sampling sequence the data is transferred into the main memory of the computer. The processing of the recordings is done asynchronously on several threads of the central processing unit (CPU). Only the coherently recorded sequence is guaranteed to be self-consistent and include all pulses. A limited number of pulses may be missed between consecutive recording intervals.

A number of processing steps are applied to extract the pulse quantities from the sampled data:

1. Pulse detection through a threshold
2. Determination of the stable pulse region by further shrinking the measured time interval from both sides
3. Extraction of amplitude, frequency and phase for both sampling channels independently
4. Plausibility/Sanity checks
5. Calculation of the combined power, the polarization and signal phase from both channel parameters
6. Apply system correction using calibration data
7. Data packaging

The extraction of amplitude, frequency and phase from a radar pulse is a crucial step. It has a huge impact on the precision of the whole measurement. This is especially true as only a limited number of data points are available. Care has to be taken in view of the limited processing power. Several hundred of pulses per second have to be analysed.

Several extraction techniques were investigated:

- Discrete Fourier Transformation (DFT): A simple approach is the application of a discrete Fourier transformation. The peak of the power spectrogram indicates the main frequency component. Due to the limited length of a radar pulse, the frequency resolution is quite modest. A flat-top window function should be applied to the time domain data for good power estimation Cerna and Harvey (2000). Also power leakage to frequency components nearby will inevitably occur. However, this fact can also be used to reconstruct the real frequency and power with higher resolution by using an interpolation. Due to the wrapping of the phase information and the high slope of the phase at the peak power, a reconstruction of the phase component is difficult and tends to be unstable.

- Direct sine fitting: Fitting a sine function to the data using a non-linear algorithm is a brute force approach. Due to the nature of a sine wave, the algorithm tends to change the frequency and not the phase to fit the curve leading to fits of n-times the original frequency. As a matter of fact, this will be successful for any multiple of the original frequency. Only a constrained fitting algorithm would be able to handle this, but would be much more time consuming.

- Harmonic Inversion: Ready to use algorithms are available to extract frequency components from a sampled signal. One of them is HarmInv by Mandelshtam and Taylor (1997). It uses a filter diagonalization method to extract frequencies with a higher precision than a normal DFT can perform. Unfortunately, the algorithm is hard to tune to produce reliable results.

- Hilbert Transformation: The Hilbert transformation can be used to create an analytic representation of a real signal. This complex signal can be interpreted as a rotating pointer. The frequency is to be derived from the rotation speed using a time lag-one correlation. The amplitude is represented by the pointer length. The phase difference between the receiver channels can be extracted from the phase of the cross correlation coefficient. Unfortunately, the realization of a good Hilbert transformation is complicated. This is especially true for a small sampling size. Neither a DFT nor an Infinite Impulse Response (IIR) filter realization could provide reasonable results.

- Down Conversion: Good results were achieved by a two step approach and learning from the drawbacks of the other approaches. A DFT is used to extract frequency of the radar pulse. Averaging over several pulses was used to get a stable and more reliable frequency estimation. The recorded samples are than mixed to the base-band:

$$\begin{aligned} f(t) &= \cos(\omega_{mix} \cdot t) \cdot A\cos(\omega_{signal} \cdot t + \phi) && (6.10)\\ &= \frac{A}{2}\left(\cos((\omega_{mix} - \omega_{signal}) + \phi) + \cos((\omega_{mix} + \omega_{signal}) + \phi)\right) && (6.11)\\ &\quad with \quad \omega_{mix} = \omega_{signal} = \omega && (6.12)\\ &= \frac{A}{2}\left(\cos(\phi) + \cos(2 \cdot \omega + \phi)\right) && (6.13) \end{aligned}$$

  after low-pass filtering it becomes:

$$\frac{A}{2}\cos(\phi) \tag{6.14}$$

  Performing the same with an orthogonal (90° phase shifted) mixing frequency results in

$$\frac{A}{2}\sin(\phi) \tag{6.15}$$

  From equation (6.14) and (6.15) the amplitude and phase can be directly estimated (e.g. treating it like real and imaginary part of a complex number).

After the extraction of phase and amplitude the channel correction, found using the internal calibration is applied. This corrects the influence of the two independent down converter paths and cables. In fact, it transfers the calibrated reference plane to the antenna input ports.

In the next step, the antenna correction model is applied as specified in Lyakhovskii et al. (1996). Well-known antenna properties are needed to remove the imperfect behaviour of the polarization divider of the antenna. These measurements were carried out by the DLR Microwaves and Radar Institute (Appendix A.1). The antenna gain is also applied to the data, now.

The data are valid after a polarization basis transformation from the antenna basis (knowing the mechanical alignment) to the commonly used H/V basis using equation (2.20). This way, the data become independent of the PARC antenna setup.

The data is further enriched with a unique sequence, pulse number and the GPS time stamp before sending them to the radar for further analysis.

6.4 Calibration Technology for PARC

The PARC is a tool to measure the radar pulse and to radiate defined signals. For the different calibration tasks to be performed at POLDIRAD, different algorithms have to be used. Some of them are straightforward like power and polarization measurements for receive and/or transmit case at the radar. Other duties are more complex e.g. the automatic polarization optimization of the POLDIRAD's polarization network. The calibration methods that the PARC client provides at the radar are described in the following. Nevertheless, the starting point will be the calibration model and used mathematical model used.

6.4.1 Calibration Model

A transformation matrix $\mathbf{U}$ can be defined, which describes the change of the electric field in the measurement

$$\vec{E}_{h,v} = \mathbf{U} \cdot \vec{E}_{e1,e2} \tag{6.16}$$

$$\begin{bmatrix} \underline{E_h} \\ \underline{E_v} \end{bmatrix} = \begin{bmatrix} \underline{U_{11}} & \underline{U_{12}} \\ \underline{U_{21}} & \underline{U_{22}} \end{bmatrix} \cdot \begin{bmatrix} \underline{E_{e1}} \\ \underline{E_{e2}} \end{bmatrix} \tag{6.17}$$

where $\vec{E}_{h,v}$ is the electric field as received at the radar and $\vec{E}_{e1,e2}$ the field as radiated at the PARC. This transformation matrix is modelled as a polarization transformation (compare eq. (2.19)) and a complex system loss ($\Delta loss$) within the radar:

$$\Delta loss = \frac{loss_H}{loss_V} \tag{6.18}$$

$$\mathbf{U} = \begin{bmatrix} \underline{loss_H} & 0 \\ 0 & \underline{loss_V} \end{bmatrix} \cdot \frac{1}{\sqrt{1 + |\underline{\rho}|^2}} \begin{bmatrix} 1 & -\underline{\rho}^* \\ \underline{\rho} & 1 \end{bmatrix} \tag{6.19}$$

$$= \frac{1}{\sqrt{1 + |\underline{\rho}|^2}} \begin{bmatrix} \underline{loss_H} & -\underline{\rho}^* \cdot \underline{loss_H} \\ \underline{\rho} \cdot \underline{loss_V} & \underline{loss_V} \end{bmatrix} \tag{6.20}$$

The matrix $\mathbf{U}$ can be calculated from a set of two measurements with different transmit polarization states at the PARC.

The loss term can be calculated from

$$\underline{\Delta loss} = \frac{\underline{U_{11}}}{\underline{U_{22}}} \tag{6.21}$$

$$\underline{\rho} = \frac{\underline{U_{21}}}{\underline{U_{22}}} = -\frac{\underline{U_{12}}^*}{\underline{U_{11}}^*} \tag{6.22}$$

Unfortunately, it is not guaranteed that a measured **U** can be represented by eq. (6.19). The constrain from eq. (6.22) may not be satisfied e.g. due to noise (limited SNR). A carefully designed setup will limit these problems. There are several means to find the best parameter. One simple approach is the calculation of two solutions (e.g. $-\underline{U_{12}}^*/\underline{U_{22}}^*$ and $\underline{U_{12}}/\underline{U_{22}}$). The difference of both solutions can then be treated as a merit of uncertainty for the whole measurement.

For all polarization which have half-power splitting in the H/V basis (45°/135° linear, left/right hand circular) the phase difference in system loss become collinear with the polarization phase. Hence, both components cannot be separated. For that reason, the (constant) system loss was determined independently.

6.4.2 Determination of the Polarization Independent Loss

For this measurement the PARC antenna was setup in a H/V-basis which is the same as the radar is using. For both, horizontal (ρ_{xy}) and vertical (ρ_{ab}) PARC transmit the received signals at the radar was recorded for different polarization network settings. In these special cases, there are only signals in either the horizontal or vertical waveguide and the phase-shifter section idle. Thus, only the loss/phase-shift between the power-divider section of the polarization network up to the receivers is measured.

The data is listed in Table 6.1. Two orthogonal polarizations are defined by

$$\underline{\rho}_{\perp} = -\frac{1}{\underline{\rho}^*_{=}} \tag{6.23}$$

Therefore, the phase-shift should be 180° and the logarithmic power should change sign. Any discrepancies can be related to internal channel differences.

In detail, the first polarization measurement is

$$\frac{\underline{P_2}}{\underline{P_1}} = \left(\underline{\rho}_{xy}\right)^2 \cdot \frac{\underline{loss_2}}{\underline{loss_1}} = \left(\frac{\underline{E_V}}{\underline{E_H}}\right)^2 \cdot \frac{\underline{loss_2}}{\underline{loss_1}} \tag{6.24}$$

. For the orthogonal polarization the incoming signal changes but the system loss stays constant:

$$\frac{\underline{\underline{P_2}}}{\underline{P_1}} = \left(\underline{\underline{\rho}}_{ab}\right)^2 \cdot \frac{\underline{\underline{loss_2}}}{\underline{loss_1}} = \left(\frac{1}{\underline{\underline{\rho}}^*_{xy}}\right)^2 \cdot \frac{\underline{\underline{loss_2}}}{\underline{loss_1}} = \left(\frac{\underline{\underline{E_H}}^*}{\underline{\underline{E_V}}^*}\right)^2 \cdot \frac{\underline{\underline{loss_2}}}{\underline{loss_1}} \tag{6.25}$$

. Thus,

$$\left|\left(\frac{\underline{\underline{E_V}}}{\underline{\underline{E_H}}}\right)^2 \cdot \frac{\underline{\underline{loss_2}}}{\underline{loss_1}}\right| \cdot \left|\left(\frac{\underline{\underline{E_H}}^*}{\underline{\underline{E_V}}^*}\right)^2 \cdot \frac{\underline{\underline{loss_2}}}{\underline{loss_1}}\right| = \left|\left(\frac{\underline{\underline{loss_2}}}{\underline{loss_1}}\right)^2\right| \tag{6.26}$$

from which the loss can be determined.

	PARC Transmit		
	H	V	$\frac{P_{Tx_H}+P_{Tx_V}}{2}$
linear 45°	−1.49 dB; 1.43 rad	4.08 dB; −1.71 rad	1.3 dB
*linear*135°	0.52 dB; 1.46 rad	2.12 dB; −1.71 rad	1.32 dB
right hand circular	2.03 dB; 1.44 rad	0.77 dB; −1.70 rad	1.4 dB
left hand circular	−0.65 dB; 1.45 rad	3.00 dB; −1.71 rad	1.17 dB
	1.44 rad	−1.71 rad	1.3 dB

Table 6.1: Differential power and phase recorded at the radar for H and V illumination (14/06/2012).

From that, the system characteristic was determined to 1.3 dB and 1.43 rad = −1.71 rad + $\pi \approx 82°$. These values are saved and used for the polarization settings optimization.

6.4.3 Radar PARC Synchronisation

For some measurements a precise synchronization between radar and PARC is mandatory. It has to be known which radar pulse transmitted corresponds to a pulse measured at the PARC. Although, the PARC adds a GPS time stamp to each received pulse, the radar does not. Therefore, time synchronization is not possible. A novel technique for synchronizing a device with a radar was used.

The absolute phase of each radar pulse is random for magnetron transmitters. Hence, the series of transmit phases recorded at the radar and measured at the PARC have in general a low correlation coefficient. Only for exact matches of the phases the coefficient raises to approx. 1. Thus, the pulse characteristic as measured at the

PARC and the POLDIRAD can be put into correspondence. Further improvement can be achieved by using the differences (derivation) of the pulse phases for the correlation. This improves the robustness against small frequency drifts between the radar and PARC frequency reference (e.g. due to imperfect GPS synchronization). Even with a small number of samples (e.g. 128) a sufficient precise discrimination between low (mismatch) and high (match) correlation coefficient is possible.

6.5 Calibration modules

6.5.1 Time Plot

The time plot module is one of the simpler modules. The uncorrected sampled data as recorded at the PARC is plotted. This is of great interest to check the proper operation of the transmission channel between radar and PARC. Furthermore, the plot could be used to extract pulse envelope parameters like raise and fall time, pulse length etcetera. Several plotting options are available: time series, x-y plot (polarization ellipse), spectra and pulse envelope.

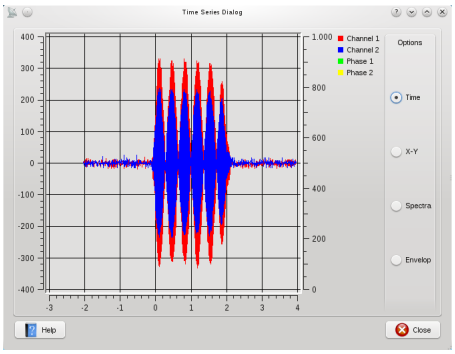

Figure 6.2: Dialog to display the raw radar pulse

6.5.2 Radar Transmit Pulse Measurement

The PARC is put into receive mode for the radar pulse measurement. The sampled and analysed pulses are averaged and displayed. The absolute power and the polarization properties of the radar pulses are shown as well as the calculated uncertainty (see eq. (6.7)). The data are shown as measured at the PARC site. No path losses or attenuation is included here. This module can be used at any radar, as it does not depend on special features of POLDIRAD or on a network connection to the radar.

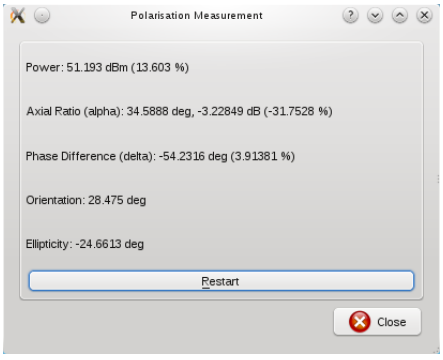

Figure 6.3: Frontend showing the averaged radar pulse parameters as received on the PARC

6.5.3 Defined PARC Transmit Signal

This module is designed to allow the user to manually control the transmit settings of the PARC. The power and polarization properties of the transmit signal can be defined by the user. Both hardware channels are used to transmit the specified signal and the system is no longer able to receive pulses from a radar. This module is also independent from any POLDIRAD features. Using this setup the PARC can provide a test signal with known polarization for any radar.

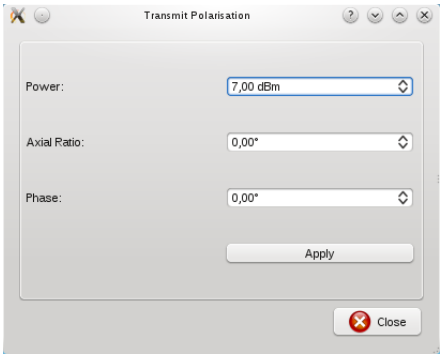

Figure 6.4: Window to setup PARC transmit signal

6.5.4 Radar Receive Signal Measurement

The *Radar Receive Signal Measurement* module is designed to measure the PARC signal as received on the radar. It sets up the PARC hardware to transmit a defined signal. Furthermore, it controls the radar signal processor to record that signal. These raw data can be displayed or they can be transformed with respect to the PARC antenna rotation into a H/V polarization basis (see eq. (2.20)). The polarization network can be controlled manually to see the effect on the received polarization. Hence, it can be used to analyse the polarization transformation performed by the polarization network.

An additional feature is the test signal measurement. A continuous wave signal can be inserted into the radar receiver near the antenna. Knowing the properties of this reference an internal re-calibration of the radar can be performed by reproducing the earlier measured values. It can also be used to track drifts of the radar hardware without the need for a more time consuming PARC measurement, but neglecting the antenna as an error source.

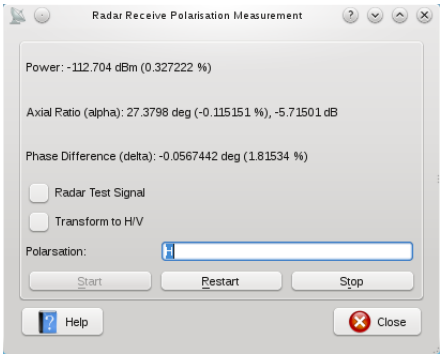

Figure 6.5: Dialog for radar receive signal measurement

6.5.5 Automatic Radar Receive Polarization Optimization

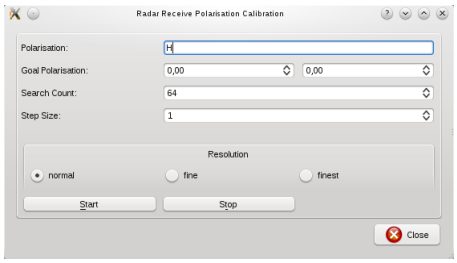

Figure 6.6: Calibration dialog for radar receive polarization

The main subject of the PARC design was creating a tool to perform an automatic polarization settings optimization for POLDIRAD. This module is dedicated for the automatic calibration of the radar receive part. It is an extension of the above-mentioned modules.

All polarization setting storages of the polarization network are used to measure 16 polarizations at once. Through the signal processing all data is tagged with the according polarization setting. These calculations are performed in real-time and independently for the different polarizations. Hence, the measurement is carried out for 16 hardware settings at once. New polarization data is loaded into the polarization network until all selected settings are measured. In a second pass, the same configuration is measured with a second polarization.

Thus, the data can be separated into a polarization change performed by the polarization network and systems loss as shown in Section 6.4.1. The polarization change is compared with the user supplied optimization goal to find the best match, which can be stored as the new settings for the desired polarization. The best polarization is found by calculating the distance of two polarizations on the Poincaré sphere:

$$\begin{aligned} \text{diff} = &\arccos\left[\sin(2\cdot\tau_{measured})\cdot\sin(2\cdot\tau_{goal})+\right.\\ &\left.\cos(2\cdot\tau_{measured})\cdot\cos(2\cdot\tau_{goal})\cdot\cos(2\cdot\phi_{measured}-2\cdot\phi_{goal})\right] \end{aligned} \tag{6.27}$$

where τ is the ellipticity and ϕ is the orientation as defined in eq. (2.12) and (2.13).

Beside the polarization, the differential receiver path losses as well as absolute losses are estimated and stored. These parameters are directly applied to the radar signal processing (Chapter 7).

6.5.6 Automatic Radar Transmit Polarization Optimization

The transmit polarization optimization is probably the most challenging task. The power, polarization and phase is to be extracted from a short radar pulse. Additionally, these data have to be matched with the pulse information only available at the radar like state of the polarization network the actual power and phase.

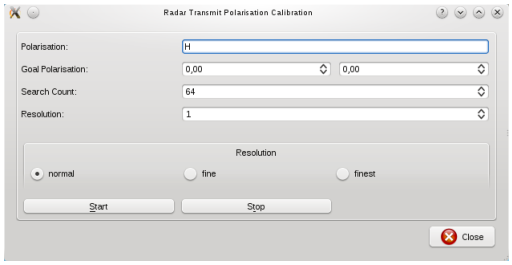

Figure 6.7: Calibration dialog for radar transmit polarization

There are two main differences to the receive optimization: Only one measurement has to be carried out to extract all hardware information. Obviously, there is no need to determine distortions within the radar, but only characterize the pulse as transmitted. Only this polarization is of further interest. On the other hand, the radar pulse needs to be measured not only at the PARC but also at the radar. This is because the magnetron transmitter used by POLDIRAD changes output power and phase for every pulse.

Unfortunately, there is no precise time stamp for the radar transmit pulses. Hence, the pulses transmitted by the radar and the data recorded at the PARC have to be matched. This is done by a newly developed correlation method as described in Section 6.4.3. Using this algorithm the power and polarization transmitted at the radar can be combined with the information received at the PARC. This still works in the fast switching mode when all 16 polarization storages of the polarization network are used.

Having the combined data, determining the optimal settings is straightforward. The absolute transmit path loss in the radar can simply be found from the free space attenuation, the transmit power as measured by the radar and the power received by the PARC.

6.5.7 Radar Transmit/Receive Data Plot

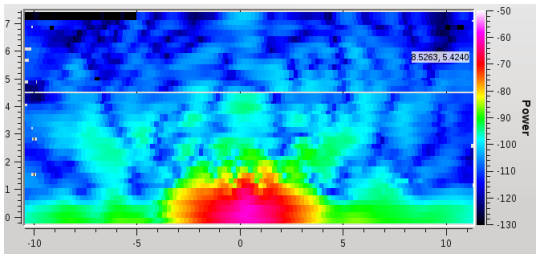

Figure 6.8: Plotted power as received by the PARC

As stated before, the PARC hardware can also be used to record the polarimetric antenna pattern by using a fixed polarization, but a scanning antenna. This can be performed for both, the radar transmit and the radar receive case. Due to the good dynamic range of the radar and PARC, also the side lobes of the antenna can be analysed. But it has to be kept in mind, that ground reflection may affect the measurements of the side lobs as they are typically several magnitudes (e.g. 30 dB) lower than the main lobe.

6.5.8 Polarization Phase Difference Measurement

When performing multi-polarization measurements e.g. using the alternating H/V mode the phase difference between the polarization bases has to be known. This phase is introduced by the radar hardware due to the phase shifters involved. For example: when transmitting linear 45° and alternating receiving in a H/V and V/H basis a phase shift might appear related to the switching performed by the polarization network. There is no mathematical reason for this phase shift. The same applies to both columns of the scattering matrix when measure in alternating H/V mode.

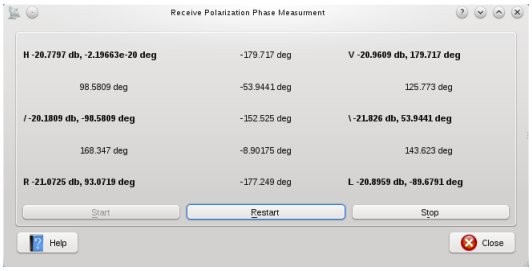

Figure 6.9: Phase difference between different polarization bases

The *Polarization Phase Difference Measurement* module measures this phase difference for the radar receive case. This is done by alternating the receive polarization basis on a per pulse basis and recording the absolute phase and power of the signals. The data is displayed in a matrix representation (bold values) with phase difference between the polarizations calculated. The results are presented in Section 6.6.1.

6.6 PARC Measurements

Finally the measurements were carried out on a building near the radar (Figure 6.10). Unfortunately it is not in the antenna far field region, but was the best site available. Hence, some artefact may be in the data.

Figure 6.10: Measurement setup for calibration (the POLDIRAD antenna is the white, most left one)

The PARC was used several times to perform a precise receive and transmit calibration. The simple deployment of the system was a huge benefit as no permanent site could be found. The horizontal and vertical polarization was of highest demand, but right/left hand circular and 45°/135° were also optimized. This way the research on the transmit phase could be carried out (Section 8.1).

For horizontal and vertical transmit a special configuration was used (Fig. 6.11). The phase shifter section is 'abused' to transfer the energy to the dummy load. For horizontal transmit the vertical channel is routed to the load, for vertical transmit the horizontal one. This increases the transmit channel isolation to the measurement limit of the internal power meters.

The calibration was independently checked using weather targets. From mea-

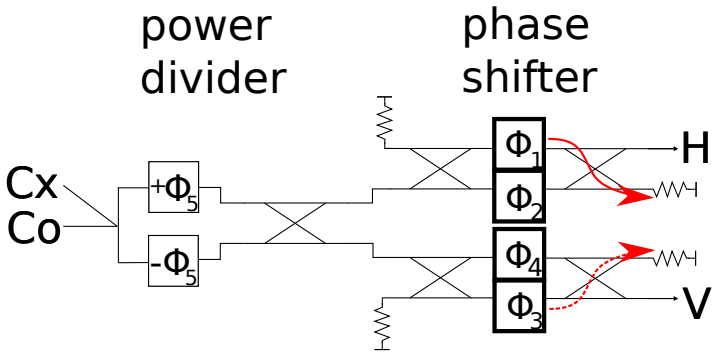

Figure 6.11: Configuration of the polarization network for better performance

surements using alternating 45° and circular polarization the transmit phase can for example be checked using ϕ_{DP}. The ϕ_{DP} difference between linear and circular transmit polarization should become 90° if the receive polarization is both times horizontal/vertical.

The horizontal/vertical polarization basis was checked using light rain and the depolarization parameter L_{DR}. This parameter is very sensitive to small mismatches in the orientation angle of the polarization. A histogram from a case study (volume scan from 12/06/2012, 14:36 UTC) is shown in Fig. 6.12. There is a histogram peak at −18 dB which is related to the bright band at that day and another peak at about −37 dB. This is well at the level expected for rain. There is a limited number of samples even below −37 dB, which may indicate a much better ICPR for the antenna. The lowest sample is nearly −50 dB. Similar values are seen in several recordings. A third mode, which is not so pronounced in the histogram, can be found at approx. −28 dB and can be attributed to ice above the bright band.

As stated before, the PARC can be used for polarimetric antenna pattern measurements. A 2D pattern is shown in Figure 6.13. An azimuth and an elevation cut are shown in Figure 6.14 and 6.15. While the elevation cut is similar to the original pattern (published in Schroth et al. (1988)), there is a degeneration in azimuth pattern. The beamwidth was enlarged from 1° to about 2° and there is some artefact in the central upper part of the pattern (Figure 6.13 - azimuth 0°, elevation 1°). This artefact might be related to a small gap (about 5 mm) between the two central panels of the antenna reflector. The larger azimuth beamwidth might be a result of a deformation in the support structure of the reflector. The event causing this degeneration can only be roughly estimated. A sun scan from 16. March 1993

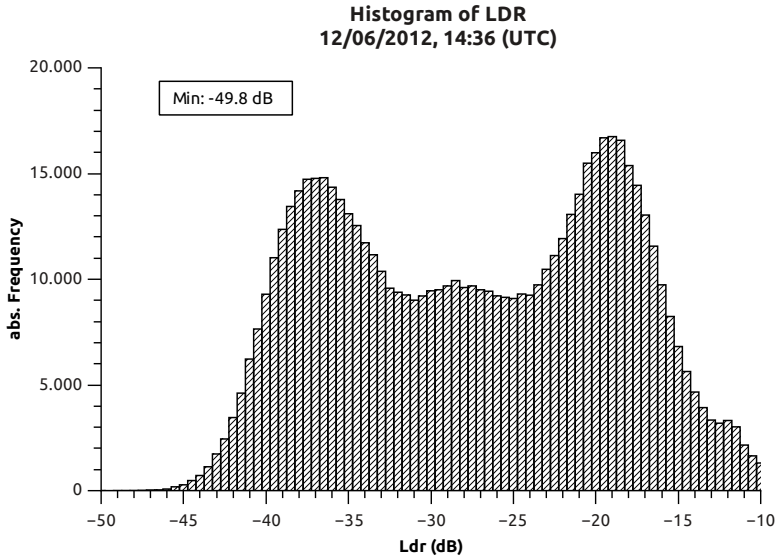

Figure 6.12: Measured Linear Depolarization Ratio in rain

does not show the larger azimuth beamwidth, while a series of sun scan starting from April 2005 are already affected. The position of the feed horn is most likely not the reason for the changed beamwidth. There are no indications of changes in the mounting of the feed and the elevation pattern seems to be right, too. Also the cross-polar pattern like reasonable okay, beside the difference in the main peaks in the azimuth cut, which might be caused by a small misalignment in the roll angle of the PARC antenna. Some more research is needed to verify the reflector and to find a practical solution reshape the dish.

The PARC uses a general design, which allows a usage with different radars and frequencies. The measurement antenna was characterized for 3.9 GHz to 5.9 GHz. The synthesizer for the mixer frequency can operate between 5.45 GHz to 5.7 GHz and both - upper and lower mixer side-bands can be used. To prove this flexibility the PARC was successfully deployed to the German Weather Service (DWD) radar at Hohenpeissenberg where the antenna radiation pattern as well as the polarization was recorded.

6.6.1 Polarization Phase Calibration

As stated in Section 6.5.8 the system introduced phase shift between the difference polarization bases has to be known and corrected. The presented value are measured

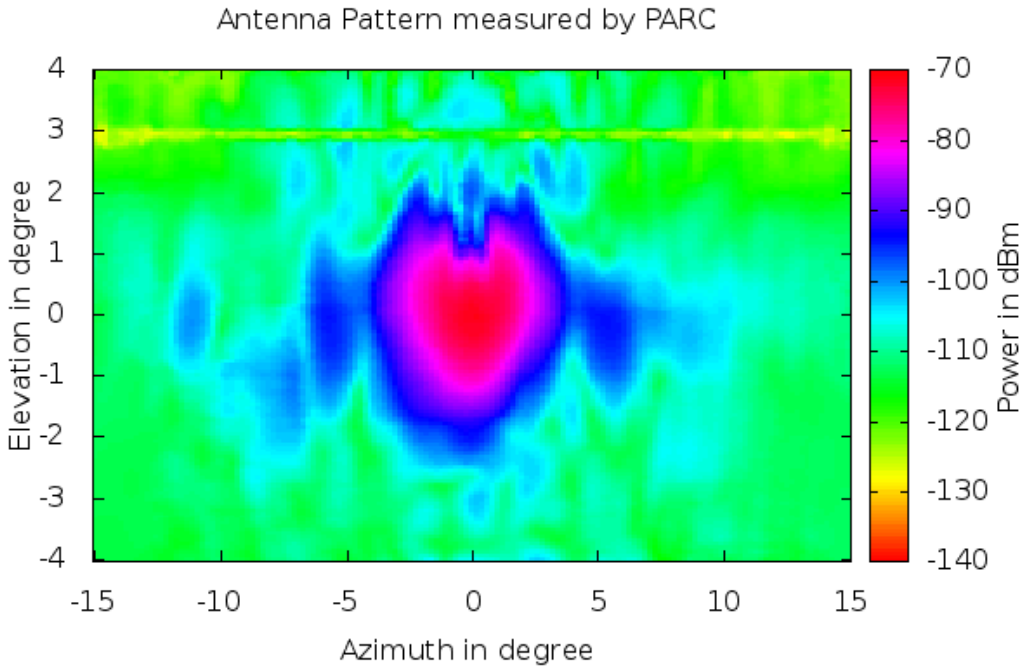

Figure 6.13: Two dimensional antenna radiation pattern of POLDIRAD

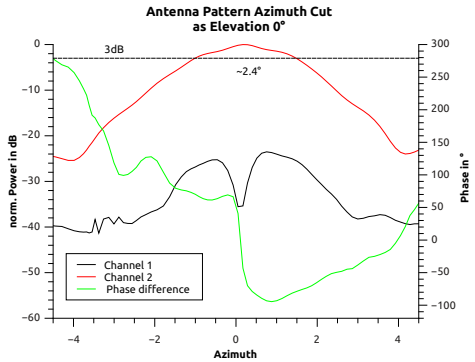

Figure 6.14: POLDIRAD antenna radiation pattern azimuth cut at 0°

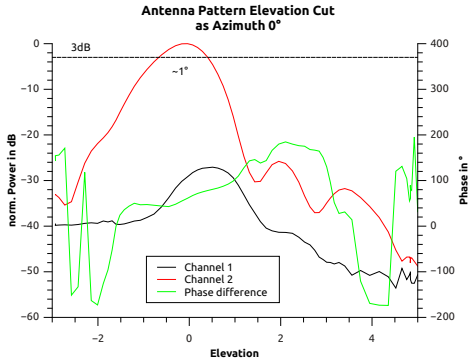

Figure 6.15: POLDIRAD antenna radiation pattern elevation cut at 0°

illuminating the radar with linear 45° polarization. Using horizontal as reference, vertical polarization has 179.7° phase shift, when 180° would be expected. Right hand circular has −89.6° and left hand circular 93.0° in contrast to the ±90° assumed. The phase difference for linear 45° and 135° were unstable due to the low SNR in one of the channels.

When the radar is radiated by horizontal polarization, the V and linear 135° phase difference was 9°, linear 135° 76°, left-hand circular −87° and right-hand circular −15°. It has to stressed, that these values are quiet unstable as they rely on absolute phase stability between POLDIRAD and PARC, which is poor. Nevertheless, it shows that the phase relation is meaningful.

6.6.2 PARC Power Measurements

Although the PARC is optimized for fast polarization measurements, also absolute power calibration is feasible with less precision. This inaccuracy has several reasons: The splitting of receive and transmit calibration for example increases uncertainty. Beside this, the reference signal for the internal PARC calibration might be less precise due to the mandatory amplifier. Furthermore the PARC antenna gain has an uncertainty of about 0.5 dB. Nevertheless, meaningful calibration could be performed.

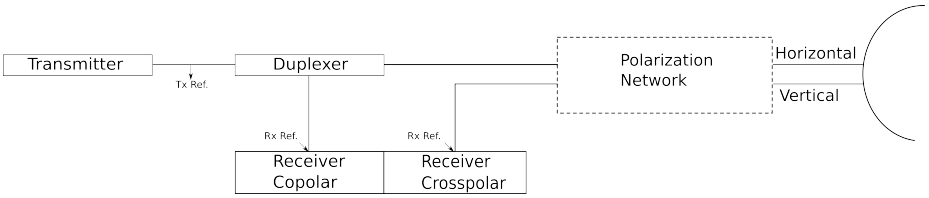

Figure 6.16: Reference points for POLDIRAD calibration. Losses for duplexer, polarization network and antenna were estimated from manufacture data

Before on-site calibration, estimated losses were applied to characterize the hardware behind the technical reference points(Fig. 6.16). The polarization network loss estimation was taken from VNA measurements (Tracksdorf (2010)) and the antenna gain was found from the manufacture acceptance test far field measurements in 1984.

For the radar transmit case using horizontal polarization a discrepancy of 6.0 dB between the expected and the measured value was found. It is known that the

polarization network has a low power loss of about 2.6 dB. For the high power transmit pulse a higher loss can be assumed as a result of the spin waves created in the ferrites. Additionally, the antenna azimuth beamwidth was found higher than expected (see above). The doubled beamwidth will lower the antenna gain by roughly 3 dB. The losses created by both effects are in good agreement with the loss found.

For the radar receive case the difference between the measured and the expected value is $\sim$ 7.3 dB. Again the reduced antenna gain and polarization network loss can explain about 5.6 dB of the divergence. But still $\sim$ 1.7 dB are missing. This value was supported by sun measurements (see Section 4.5) which found a power mismatch of about 7 dB.

In result, although the PARC was not designed for absolute power calibration, reasonable system losses were found. The transmit power differs some tenth of a dB from the used calculated calibration. The unknown high power losses of the polarization network might be the reason for that. The receive calibration differs about 1.5 dB from the expected one, but was verified by two independent techniques which have about 0.3 dB difference. This is well within the uncertainty limits of the both - sun and PARC - calibration technique. The reason for the missing 1.5 dB is not known, but might by related to wave guide and cable losses or the T/R limiter.

6.7 Limitations

While the PARC technology is working well, there are still some issues: First of all, radar measurement near the surface may always distorted by ground reflections. This can be mitigated by high gain antenna and a suitable measurement site (no obstacles, measurement on buildings/towers).

The PARC antenna is a critical part in the absolute calibration. Because the antenna is used for receive and transmit, the uncertainty of the antenna counts twice for the absolute RCS calibration. The reference antenna used for calibration has an uncertainty of $\pm$0.37 dB (Calibration Certificate Böttcher et al. (2011)). Hence the absolute gain uncertainty has to be estimate worse than 0.5 dB.

A PARC calibration using a defined reference (e.g. a sphere) is difficult as the PARC is designed for high input and medium output power. A passive reflector would require an unpractical high RCS. Nevertheless, the PARC's main design goal

was good and fast polarization calibration, while absolute power calibration is still possible.

Another point is the different signal processing chain used by radar and PARC. The PARC for example does not use a matched filter (although it could be added). It has a higher sampling rate and algorithms designed to extract precisely the polarimetric properties. On the other hand, the polarization of the echoes as measured by the radar is of interest. That might be a problem if different measurement techniques produce different outcomes (e.g. the matched filter does not agree to the transmitted pulse). From this prospective, the PARC ought to imitate the radar's signal processing.

A weather radar normally samples distributed targets. This implicates that the whole radar beam is homogeneously filled with scatterers. The calibration of a weather radar should therefore either also employ a huge distributed target of known characteristics or measure the full (main) beam pattern to calculate the equivalent result. While the PARC system is capable to scan the antenna pattern, the regime is not used from the optimization of the polarization settings as it is very time consuming. Only the bore-sight direction is used for polarization characterization.

Chapter 7

Radar Data Processing

7.1 Introduction

In the first stage a weather radar records voltages (in-phase and quadrature component, I/Q) at its receivers. Complex signal processing is applied to transform these raw I/Q data to quantities usable to meteorologists. During this process models are applied to extract and reduce information of the signals. These models applied include several assumptions. For weather radars e.g. the target is treated as an ensemble of small scatterers forming a Gaussian shaped frequency spectrum (Bringi and Chandrasekar (2001)). The parameters reflectivity (maximum peak), velocity (mean frequency) and spectral width (3 dB frequency span) are extracted from this Gaussian spectrum.

Beside the model based information extraction, quality enhancement methods are applied. Second trip recovery, velocity unfolding, speckle filtering and signal thresholding are commonly used.

A simple processing chain using frequency domain clutter filtering can be sketched as following:

1. Recording of I/Q data
2. Fourier transformation
3. Clutter filtering
4. Back transformation of the power spectrum into time domain to calculate covariances
5. Calculation of radar moments from these covariances

7.2 Signal Processing for the POLDIRAD Radar

The POLDIRAD has a unique polarization switching capability. Up to sixteen receive and transmit polarization can be stored in a polarization network device which can be selected by the radar system while scanning. A repeating pattern of polarizations can be defined for each scan in the radar hardware. The recorded data is tagged with the current pattern enabling the reconstruction of the polarization for each sample. This very flexible design allows the radar to record data using different polarization in one scan. The signal processing of mixed polarization data can become very cumbersome. Each polarization has to be processed independently to be meaningful. Unfortunately, spectrum estimation is difficult for unevenly sampled data. Therefore it is beneficial to confirm that data of the same polarization is equally spaced in time.

Depending on the polarizations used, the data processing is different and other (polarimetric) moments can be calculated. There are several polarimetric measurement schemes found in literature which are made available through the new advanced signal processing chains. These are:

- STAR mode (hybrid polarization basis): the horizontal and vertical polarization components are transmitted simultaneously and are independently received to measure the major axis elements of the scattering matrix.

- L_{DR} mode: horizontal (rarely vertical) polarization is transmitted. Horizontal and vertical echoes are received to measure one column of the scattering matrix.

- Alternating H/V mode (Section 7.3): horizontal and vertical polarization is alternating transmitted. Horizontal and vertical echoes are received to measure the full scattering matrix in the H/V polarization basis.

- Alternating R/L mode (Section 7.4): left and right hand circular polarization is alternating transmitted. Left and right hand circular echoes are received to measure the full scattering matrix in the R/L polarization basis.

The first two modes are commercially available. They do not need a fast high power switch for the transmit pulse, which reduces system complexity. In the STAR mode horizontal and vertical polarization is simultaneously transmitted and the echo

of both polarization is received. This mode is used in most operational polarimetric weather radars. In the L_{DR} mode, only horizontal polarization is transmitted and the horizontal and vertical return is received. Hence, the depolarization can be measured.

The last two modes listed were newly implemented by the author and are special features of POLDIRAD. Beside these basic modes, combinations of them are possible. To the author's knowledge, this is the first system to process mixed polarization data to meteorological quantities in real-time (Section 7.5). Using this functionality a direct comparison of the extracted data becomes feasible. Example measurements will be shown in Section 7.6.

Additionally to the named mode, there is a covariance matrix mode created by the author. The data is only processed up to the covariances. This leads to much smaller files than recording the I/Q samples. Up to eight polarization pairs, can be recorded this way. Up to this step, there is no need for a physical interpretation which would need knowledge about the used polarization. Thus, a very flexible processing scheme for research is available.

In the following only the new alternating H/V and alternating R/L mode will be treated in detail. For calculations in the other modes the author refers to standard literature (e.g. Bringi and Chandrasekar (2001)).

7.3 The New Realization of the Alternating H/V Mode

Most time of the last 25 years POLDIRAD was operating in the alternating H/V mode. A good reference for the algorithms can be found in Chapter 5 of the *RVP7 User's Manual* from Sigmet, now Vaisala Sigmet (2003). The algorithms found there, are the same as they were found in the very first signal processor for POLDIRAD. A short description can also be found in the author's master thesis Reimann (2009)

The scattering matrix is recorded by an alternating transmission of horizontally and vertically polarized radar pulses. Both - the horizontal and vertical echoes of the target - are recorded for each pulse. Obviously, there is a small time gap between the two transmit pulses. Hence the two columns of the scattering matrix will also have a time lag and the matrix is not an instantaneous measurement. An estimation of the real scattering matrix can be calculated by moving both columns to a common

time base e.g. by using an estimated Doppler velocity to correct the phase shift introduced due to the particle movement.

Formula	**Description**	**Covariance Object**	**Data**
$S_{HH}(0) \cdot S^*_{HH}(0)$	Power HH	Covariance 1	$R(0)$ co-polar
$S_{VH}(0) \cdot S^*_{VH}(0)$	Power VH	Covariance 1	$R(0)$ cross-polar
$S_{VV}(0) \cdot S^*_{VV}(0)$	Power VV	Covariance 2	$R(0)$ co-polar
$S_{HV}(0) \cdot S^*_{HV}(0)$	Power HV	Covariance 2	$R(0)$ cross-polar
$S_{HH}(0) \cdot S^*_{VH}(0)$	Co-Cross-Correlation	Covariance 1	$R_{HV}(0)$
$S_{VV}(0) \cdot S^*_{HV}(0)$	Co-Cross-Correlation	Covariance 2	$R_{HV}(0)$
$S_{HH}(0) \cdot S^*_{HH}(1)$	Doppler Velocity lag 1	Covariance 1	R(1) co-polar
$S_{VH}(0) \cdot S^*_{VH}(1)$	Doppler Velocity lag 1	Covariance 1	R(1) cross-polar
$S_{VV}(0) \cdot S^*_{VV}(1)$	Doppler Velocity lag 1	Covariance 2	R(1) co-polar
$S_{HV}(0) \cdot S^*_{HV}(1)$	Doppler Velocity lag 1	Covariance 2	R(1) cross-polar
$S_{HH}(0) \cdot S^*_{HH}(2)$	Spectral Width	Covariance 1	R(2) co-polar
$S_{VH}(0) \cdot S^*_{VH}(2)$	Spectral Width	Covariance 1	R(2) cross-polar
$S_{VV}(0) \cdot S^*_{VV}(2)$	Spectral Width	Covariance 2	R(2) co-polar
$S_{HV}(0) \cdot S^*_{HV}(2)$	Spectral Width	Covariance 2	R(2) cross-polar
$S_{HH}(0) \cdot S^*_{VV}(0)$	Doppler Velocity lag 0.5	Covariance 3	R(0.5) co-polar
$S_{HV}(0) \cdot S^*_{VH}(0)$	Doppler Velocity lag 0.5	Covariance 3	R(0.5) cross-polar
$S_{HH}(0) \cdot S^*_{HV}(0)$	Doppler Velocity lag 0.5	Covariance 3	R(0.5) mixed
$S_{VV}(0) \cdot S^*_{VH}(0)$	Doppler Velocity lag 0.5	Covariance 3	R(0.5) mixed

Table 7.1: List of calculated covariances

The new version of the alternating H/V mode is to be included into Abacus® signal processing software from Selex SI Gematronik, which is used for POLDIRAD. This software implements the whole signal processing by a chain of small modules, only performing a single transformation step each. This allows extensive code reuse and flexibility. To preserve these advantages the newly developed processing mode

should be as similar as possible to reuse available code. The main obstacle was found by the missing representation for the whole scattering matrix in the software design. This is owed to the fact that none of the supported weather radars has fast polarization switching yet and therefore no way to record the full matrix. This design issue was overcome using several data structures to represent the whole information (Table 7.1). Due to this trick it is still possible to use the powerful processing modules, which already exist.

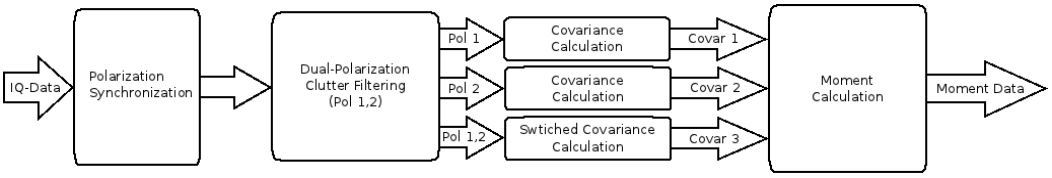

Figure 7.1: Alternating H/V Mode processing chain

The new version of the alternating H/V mode is shown in Figure 7.1 in a simplified way. It should be stressed that there are three covariance sets needed for the moment calculation due to the missing representation of the whole scattering matrix.

The *Polarization Synchronization Module* ensures that every coherent processing interval (CPI) starts at the beginning of a new polarization sequence. For the alternating H/V mode this means that the resulting data starts always with a horizontal pulse. This greatly simplifies further processing. For more complex polarization switching schemes (see below) this synchronization becomes even more important. This module also ensures that no incomplete polarization sequences are processed.

The new *Clutter Filter Module* is polarization sensitive and operates in frequency domain. Obviously, the clutter can be polarization dependent and has to be corrected for each polarization separately. The module selects the desired polarization from the data stream and applies the clutter filtering. The outputs are two streams containing a single polarization (H or V). The data is enriched by important information, like the new, resulting PRF for this stream and information to restore the original composition.

From the clutter filtered as well as the unfiltered data, sets of covariance are calculated. This is done by an inverse DFT of the power spectrum. From the horizontal and vertical transmit polarization data two covariances are processed. There is a special module for the calculation of mixed-polarization covariances, too. These data have to be treated carefully as they contain information of different

polarimetric *views*. The information store in the covariance objects are listed in Table 7.1.

From this set of three covariance objects, which include all important covariances, the radar product in H/V mode can be calculated:

- *Reflectivity Factor* is calculated from the elements on the main axis of the covariance matrix, namely $R(0)_{HH}$, $R(0)_{VH}$, $R(0)_{HV}$ and $R(0)_{VV}$ by

$$Z_{XY} = 10 \log_{10} \left(\frac{1024 \ln 2 \cdot \lambda^2}{P_t \cdot g^2 \cdot \pi^3 \cdot \theta \cdot \psi \cdot c \cdot \tau \cdot |K|^2} \cdot r^2 \cdot R(0)_{XY} \cdot l_{tx_Y} \cdot l_{rx_X} \right) \tag{7.1}$$

  This is the radar equation as introduced in Section 2.5. Here Y is the transmitted and X the received polarization. The variable λ is the wavelength, P_t the transmit power, g the linear antenna gain, θ and ψ the horizontal and vertical 3 dB beamwidth, K the dielectric constant of the hydrometeors, r the range between the radar and the target and $R(0)_{XY}$ the corresponding covariance. The losses l_{tx} and l_{rx} are defined by the calibration and are polarization dependent. These values are taken directly from the latest calibration. For sake of simplicity only the loss is made polarization dependent and accounts also the difference in antenna gain for the polarization. This is valid as there is no distinction possibility whether there is possibly higher loss or lower antenna gain.

- *Differential Reflectivity* is calculated from the logarithmic horizontal and vertical reflectivity factor by

$$Z_{DR} = 10 \log_{10} \left(\frac{z_{hh}}{z_{vv}} \right) = Z_{HH} - Z_{VV} \tag{7.2}$$

  This can be done for clutter filtered or unfiltered data. Z_{DR} should be treated with care on clutter contaminated range gates. In general, the clutter power is polarization dependent and must be filtered independently (see clutter filtering above). Inaccuracy in clutter removal can easily lead to high discrepancies.

- There are two *Linear Depolarization Ratios*. It can be calculated either from the horizontal or the vertical pulses. For single scattering, the value is expected to be equal (Bringi and Chandrasekar (2001)). For the horizontal case it becomes $L_{DR_H} = Z_{VH} - Z_{HH}$. The definition for the vertical case is similar and up to the user.

- The *Doppler Velocity* can be easily derived for time lag 1 by

$$v_{XX} = -\frac{\lambda \cdot PRF}{4\pi} \arg\left(\underline{R(1)_{XX}}\right) \tag{7.3}$$

  Obviously there are four Doppler velocities for the four possible time lag 1 covariances. With respect to the data quality and coverage, the covariances calculated from the co-polar channels should be used. This is either $\underline{R(1)_{HH}}$ or $\underline{R(1)_{VV}}$.

- The *Spectral Width* can be estimated using different quantities. To prevent problems with noise estimation the time lag 0 should be avoided as the noise term will not cancel in this case. Large time lags should not be used due to the smaller and more unstable covariance value

  The spectral width can be estimated as $W = \frac{\lambda \cdot PRF}{4\pi} \cdot \sqrt{\sigma^2}$ where σ^2 can generally be described by

$$\sigma^2 = \frac{2}{m^2 - n^2} \ln \frac{\left|\underline{R(n)}\right|}{\left|\underline{R(m)}\right|} \tag{7.4}$$

  which is derived from the well known Gaussian function. The variables n and m define the time lags used.

- The *Co-polar Correlation Coefficient* ρ_{HV} at time lag 0 cannot be directly measured due to the time difference between horizontal and vertical pulse. An estimator (eq. 7.5) using the directly measurable $\rho_{HV}(0.5)$ (first term) and the expected temporal decorrelation (second term) can be used (Liu et al. (1994)):

$$\rho_{HV}(0) = \frac{\left|\underline{R(n)_{HV}}\right|}{\sqrt{R(0)_{HH} \cdot R(0)_{VV}}} \cdot \left(\frac{1}{2} \cdot \left(\frac{R(0)_{HH}}{\left|\underline{R(m)_{HH}}\right|} + \frac{R(0)_{VV}}{\left|\underline{R(m)_{VV}}\right|}\right)\right)^{\left(\frac{n}{m}\right)^2} \tag{7.5}$$

  with $n = 0.5$ and $m = 1$.

- The *Co-Cross-Correlation Coefficient* can be directly measured for horizontal and vertical polarization and is defined (for horizontal polarization) as

$$\rho_{xH} = -\frac{\left|\underline{R(0)_{VH}}\right|}{\sqrt{R(0)_{HH} \cdot R(0)_{VH}}} \tag{7.6}$$

POLDIRAD has become one of the first weather radar which also extracts the phase of the Co-Cross-Correlation Coefficient. Older systems can either not measure the depolarized signal or use logarithmic receiver without phase information.

- The Differential Phase Shift describes the phase delay between horizontal and vertical polarization due to the oblate shape of the rain drop. A new algorithm is proposed for the extraction of ϕ_{DP} in alternating H/V mode:

  Problems arise due to the time lag between the H and V pulse in switching mode causing a Doppler shift and an unknown fixed system introduced phase shift. Furthermore the phase is in general only valid in a range of $0° \leq \phi < 360°$ and this maximum range should be preserved as much as possible. The presented new algorithm uses a rough estimation of the system phase and assumes a constant phase shift due to the Doppler velocity between all pulses of a CPI. The model

  $$\arg\left\{\left(\underline{R(t_{VH})_{VH}}\right)^n\right\} + \phi_{sys} + \phi_{DP} = \arg\left\{\underline{R(t_{HH})_H}\right\} \tag{7.7}$$

  is used, where ϕ_{sys} is the system phase shift, ϕ_{DP} the differential phase shift and $n = \frac{t_{HH}}{t_{VH}}$. Here t_{HH} is the time between two pulses of same polarization (e.g. two horizontal polarized pulses) and t_{HV} is the time between the horizontal and vertical pulse. For the alternating H/V mode $n = 2$, but can be higher for multi-polarization scans (Section 7.5). In other words, equation (7.7) states that the phase shift due to the Doppler velocity for time lag t_{HH} is n times higher than for lag t_{VH} except for the differential phase and a constant system phase. The phase $\arg\left\{\left(\underline{R(t_{VH})_{VH}}\right)^n\right\} = n \cdot \arg\left\{\left(\underline{R(t_{VH})_{VH}}\right)\right\}$ measured may be folded several times.

  From eq. (7.7), the estimation

  $$\phi_{sys} + \phi_{DP} \approx \arg\left\{\underline{R(t_{HH})_{HH}}^{\frac{1}{n}}\right\} - \arg\left\{\underline{R(t_{VH})_{HV}}\right\} \tag{7.8}$$

  can be calculated. This value is now only valid in a range of $0 \ldots \frac{360°}{n}$. With the roughly known system phase and the assumption that ϕ_{DP} is small, a new ϕ_{DP} can be calculated. ϕ_{DP} can also only be derived in the range of $0 \ldots \frac{360°}{n}$ and has therefore to be folded accordingly (e.g. to $-10°$ to $170°$ for $n = 2$ including small negative values for ϕ_{DP} for stability). This scheme mitigates

the ambiguous range of the phase and uses only a roughly known system phase to distinguish between the n possible ϕ_{DP} values. The algorithm will fail if ϕ_{DP} accumulates to value outside its ambiguous range. This could be fixed by unfolding ϕ_{DP} using algorithms similar to the Doppler velocity.

- The *Doppler velocity at time lag 0.5* is hard to estimate as the phase shift between a horizontal and vertical transmit pulse includes not only the Doppler velocity (as from lag 1 which is the same polarization), but also the differential phase shift ϕ_{DP} and a system phase (like seen in the ϕ_{DP} computation). Using the knowledge from the ϕ_{DP} estimation an inversion is possible.

$$v_{HV} = \frac{\lambda \cdot PRF}{4\pi} \cdot (\arg\left\{\underline{R(0.5)_{HV}}\right\} - \phi_{sys} - \phi_{DP}) \tag{7.9}$$

  can give a estimated velocity as long as the ϕ_{DP} calculation was correct (e.g. ϕ_{DP} folding).

- The *Degree Of Polarization* is one of the new non-standard weather radar observables added. It was, for example, analysed by Galletti et al. (2008). As it is calculated for all scans a huge data archive for different weather situations is available for further investigation of this parameter.

$$p = \sqrt{1 - \frac{4 \cdot \det(\mathbf{J})}{trace\,(\mathbf{J})^2}} \tag{7.10}$$

  The Wolf's coherence matrix $\mathbf{J}$ is defined by $\mathbf{J} = \left\langle \vec{E}\vec{E}^t \right\rangle$, where $\vec{E}$ is the Jones vector.

- *Entropy and Alpha* are used in the Cloude-Pottier classification (Cloude and Pottier (1996)) often used by the Synthetic Aperture Radar (SAR) community. It was probably first time implemented in a real-time signal processing for weather radars.

  A target feature vector $\underline{\vec{k}} = \frac{1}{\sqrt{2}} \left[\underline{S_{xx}} + \underline{S_{yy}} \quad \underline{S_{xx}} - \underline{S_{yy}} \quad 2\underline{S_{xy}}\right]^T$ is defined from the elements of the scattering matrix. The averaged coherence matrix $\mathbf{T}$ is calculated from this vector by

$$\langle \mathbf{T} \rangle = \frac{1}{N} \sum_{i=1}^{N} \underline{\vec{k_i}} \cdot \underline{\vec{k_i}}^{*T} \tag{7.11}$$

Now the three eigenvalues (λ_i) of $\mathbf{T}$ have to be determined from which the entropy is calculated:

$$H = -\sum_{i=1}^{3} P_i \log_3(P_i) \tag{7.12}$$

with $P_i = \frac{\lambda_i}{\sum \lambda_i}$.

The angle alpha is determined from the normalized eigenvectors of $\mathbf{T}$.

$$\vec{e_i} = e^{i\phi_i} \begin{bmatrix} \cos\alpha_i \\ \sin\alpha_i \cos\beta_i e^{i\delta_i} \\ \sin\alpha_i \sin\beta_i e^{i\gamma_i} \end{bmatrix} \tag{7.13}$$

The compound angle alpha is now evaluated as $\alpha = P_1\alpha_2 + P_2\alpha_1 + P_3\alpha_3$.

- Sample Averaged Differential Reflectivity is different version of Z_{DR} processing:

$$Z_{DR} = 10\log_{10}\left(\left\langle \frac{|\underline{S_{hh}}|}{|\underline{S_{vv}}|} \right\rangle\right) \tag{7.14}$$

While the standard Z_{DR} is calculated from the averaged reflectivities (see eq. (7.2)), it can also be evaluated by averaging the differences of co-polar horizontal and vertical echoes for each single scattering matrix recorded.

7.4 Alternating Right/Left-hand Circular Mode

Circular polarization is used for weather radar for a long time (McCormick and Hendry (1972)). As rain drops are nearly round shaped this polarization has advantage in the discrimination of weather and non-weather targets. Consequently, it was used very early in research. It has been shown that certain hydrometeors properties can be easily derived using this configuration e.g. measuring electric fields in the atmosphere Krehbiel et al. (1996). The extracted radar products are named differently and contain different target properties, but the calculation is quiet similar to the alternation H/V mode.

It has to be stressed that the scattering matrix in an R/L basis could also be calculated from the H/V data as the scattering matrix includes all information and can be transformed into any other polarization basis.

- *Reflectivity Factor* can be calculated as for any other polarization. For the equation see alternating H/V mode (see eq. (7.1)).

- *Circular Depolarization Ratio* is similar to the H/V L_{DR}. It is also available for right-hand and left-hand circular polarization. It is an estimation for the shape of the particles. One advantage of C_{DR} over L_{DR} is its independence from orientation (Bringi and Chandrasekar, 2001, ch. 3.5.3).

$$C_{DR_R} = \frac{|Z_{RR}|^2}{|Z_{LR}|^2} \tag{7.15}$$

- *Cancellation* parameter CAN. Similar to Z_{DR} in the H/V basis, the difference of the co-polar echoes the cancellation CAN can be calculated:

$$CAN = \frac{Z_{RR}}{Z_{LL}} \tag{7.16}$$

- *Orientation parameter ORTT* is a correlation defined as:

$$ORTT_R = \frac{\left|\underline{R(0)_{LR}}\right|}{\sqrt{R(0)_{RR} \cdot R(0)_{LR}}} \tag{7.17}$$

  It includes knowledge about the orientation and the shape. Both quantities can be separated as shown in (Bringi and Chandrasekar, 2001, ch. 3.13.4).

- *Shape parameter* ρ_4 which is related to the orientation of the particles about the propagation direction:

$$\rho_4 = \frac{\left|\underline{R(1)_{RL}}\right|}{\sqrt{R(0)_{RR} \cdot R(0)_{LL}}} \tag{7.18}$$

- *Alignment direction ALD is a measurement for the arrangement of the particles in the volume towards the radar*

$$ALD = \frac{1}{2} \arctan \left(\frac{\Im\left\{\underline{R(0)_{LR}}\right\} - \Im\left\{\underline{R(0)_{RL}}\right\}}{\Re\left\{\underline{R(0)_{RL}}\right\} + \Re\left\{\underline{R(0)_{LR}}\right\}} \right) \tag{7.19}$$

7.5 Signal Processing for Multi-Polarization Scans

The signal processing using an arbitrary sequence of polarization can become difficult and has not yet been widely used. Each polarization has to be separately transformed into frequency domain. Sorely, arbitrary polarization sequences will in

general lead to non-uniformly sampled data, for which the frequency representation is hard to find. The problem is avoided for the presented work by using only fixed, repeating polarization pattern. For sake of consistency a polarization pattern repetition frequency PPRF will be introduced, which refers to the repeating frequency of the whole polarization sequence or equally the repetition frequency of a certain pulse within this pattern.

Moment calculation also becomes more difficult: The time lags are in general non-uniformly spaced and are defined by the polarization pattern used. For Doppler velocity estimation the correct time lag has to be used (see alternating H/V signal processing, Section 7.3). For spectral width estimation the generalized form of the estimator as written in eq. (7.4) has to be applied, which can handle different time lags.

7.5.1 Practical Implementation

To (re-)use the normal signal processing chains, a new module is inserted at the beginning of the processing chain. It splits the recorded I/Q data into its polarization and adjusts the PRF according to the removed samples (Figure 7.2). Additional tags are stored to reconstruct the original data. For switched polarization (e.g. full scattering matrix) modes, like the H/V switching mode, the time difference between the two consecutive measurements for the matrix is completely uncoupled from the repetition time. This implies that the time between a horizontal and a vertical pulse is in general different from the time between V and H. This case is already considered in the algorithms presented in Section 7.3.

All data processing modes can be used as usual (as long as they can handle the non-uniform time lags). At the end of the data processing chain the independently calculated observables are combined into one output stream. This design allows a simple, but even flexible processing for radar data containing different polarization. Possible radar moment calculation modules can be found in Table 7.2. It has to be stressed, that any combination of these modes can be used (even employing one mode twice, see Section 8.1).

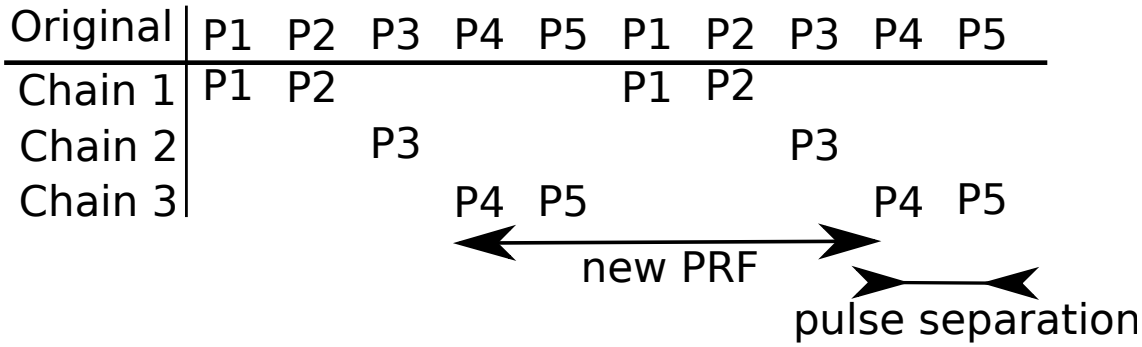

Figure 7.2: Polarization splitting regime: $P1 \ldots P5$ name the pulses with polarization $1 \ldots 5$. They are split into three chains, which are independently processed. There is a new PRF (polarization PRF, PPRF) between the pulses of same polarization

Module	**Description**
H/V switching	Signal processing for alternating H/V polarization
R/L switching	Signal processing for alternating R/L polarization
Hybrid Basis	Signal processing for simultaneous transmit alternating receive (STAR) mode
L_{DR} Mode	Signal processing for horizontal transmit alternating receive mode
Covariance	Processing of the (polarization independent) covariance matrix
I/Q recording	Recording of the I/Q data of the complete stream

Table 7.2: Available processing modes on POLDIRAD

7.6 Polarimetric Data Analysis

7.6.1 Huynen Fork-Parameters

The S-matrix includes all information about the scattering of a particle. For the end-user (e.g. meteorologist) these data are not of particular interest. The distribution of size, shape and orientation is to be derived for easy interpretation. Several decompositions have been developed (e.g. by Krogager (1990), Cloude and Pottier (1996)) over the last decades. One of them was derived by J. R. Huynen in his thesis (Huynen (1970)).

It is based on an eigenvalue calculation of a scattering matrix ($\mathbf{S}(\mathbf{HV})$) in the HV-basis. We will follow the solution as presented in (Xi and Boerner (1992)). A new polarization basis AB is defined for which the minor axes elements of the scattering matrix $\mathbf{S}(\mathbf{AB})$ and $\mathbf{S}(\mathbf{BA})$ vanish. A polarization basis transformation ($\mathbf{U}$, see eq. (2.19)) to convert $\mathbf{S}(\mathbf{HV})$ into $\mathbf{S}(\mathbf{AB})$ is to be found:

$$\mathbf{S}(\mathbf{AB}) = \mathbf{U}^{\mathbf{T}}\mathbf{S}(\mathbf{HV})\mathbf{U} \tag{7.20}$$

The condition for the zero minor axis elements can be found from the elements of $\mathbf{S}(\mathbf{HV})$ as:

$$\rho\underline{S_{HV}} + (1 - \rho\rho^*)\underline{S_{HV}} - \rho^*\underline{S_{HH}} = 0 \tag{7.21}$$

And ρ can be solved:

$$\rho_{1,2} = \frac{-B \pm (B^2 - 4AC)^{\frac{1}{2}}}{2A} \tag{7.22}$$

with $A = \underline{S_{HH}}^*\underline{S_{HV}} + \underline{S_{HV}}^*\underline{S_{VV}}$, $B = \left|\underline{S_{HH}}\right|^2 - \left|\underline{S_{VV}}\right|^2$ and $C = -A^*$. The eigenvalue λ_1 and λ_2 can be calculated for both solutions of ρ:

$$\lambda_1 = \underline{S_{AA}} = \frac{1}{1 + \rho\rho^*}\left(\underline{S_{HH}} + 2\rho\underline{S_{HV}} + \rho^2\underline{S_{VV}}\right)e^{2j\psi_1} \tag{7.23}$$

$$\lambda_2 = \underline{S_{BB}} = \frac{1}{1 + \rho\rho^*}\left(\rho^{*2}\underline{S_{HH}} - 2\rho^*\underline{S_{HV}} + \underline{S_{VV}}\right)^{2j\psi_4} \tag{7.24}$$

The phase parameters ψ_1 and ψ_4 are still to be determined:

$$\psi_1 = -\frac{\delta_2}{2} - \frac{\pi}{4} \tag{7.25}$$

$$\psi_4 = \frac{\delta_2}{2} - \frac{\pi}{4} \tag{7.26}$$

where $\delta_2 = \arg(\rho_2)$.

Target Size S_{AA}

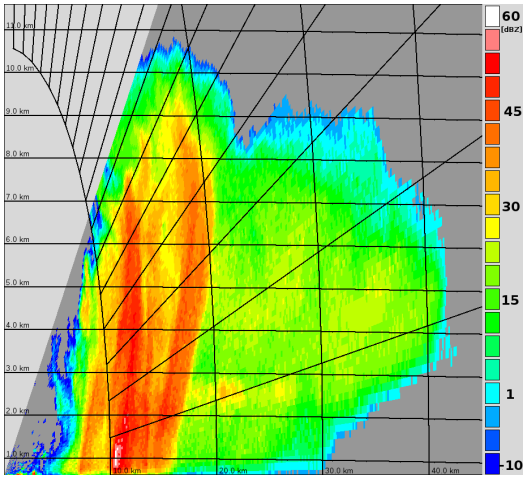

Differential Reflectivity Z_{DR}

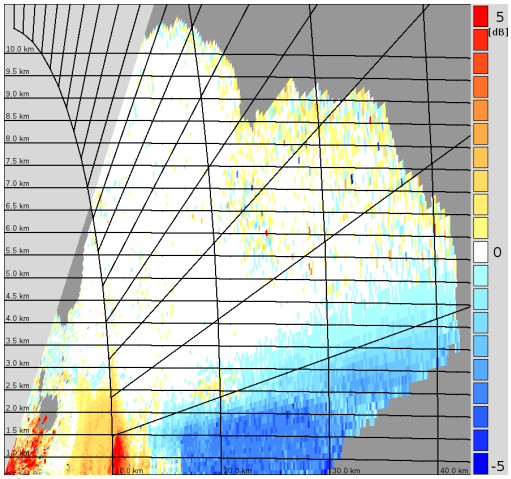

Orientation ϕ

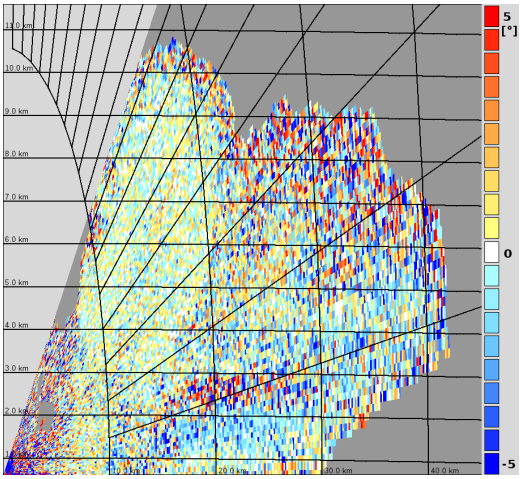

Ellipticity τ

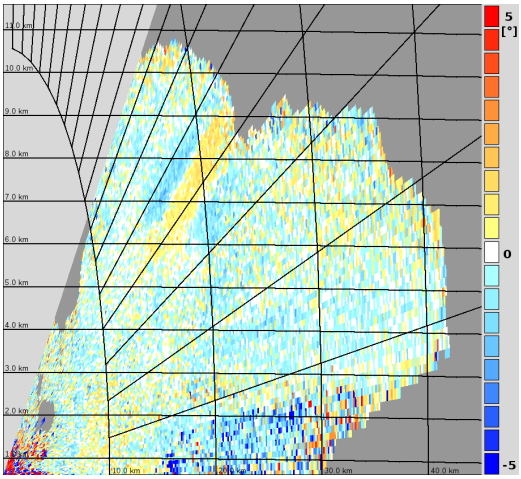

Characteristic Angle γ

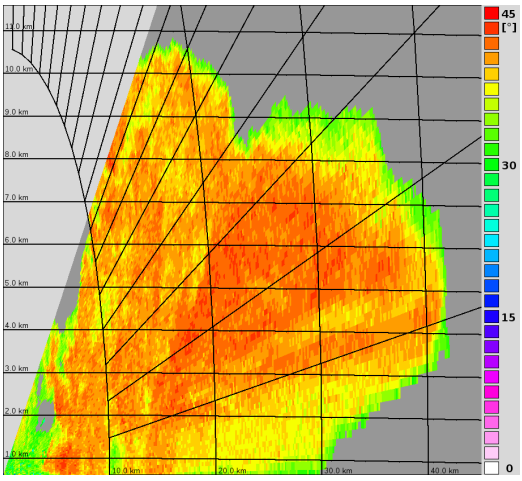

Skip Angle ν

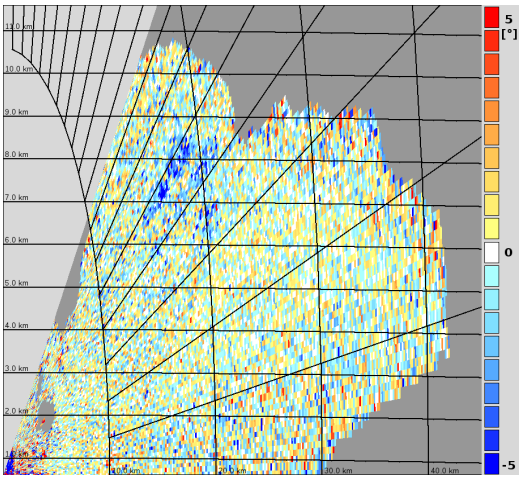

Table 7.3: Huynen fork parameters calculated for a thunderstorm from 30/05/2012, 12:58 UTC, azimuth: 217°.

The reference, the signal processing algorithm implemented was cross checked to the value reported in Schroth et al. (1988).

The calculated Huynen fork parameters for a thunderstorm case will be shown in Figure 7.3. The standard polarimetric moments can be found in Figure 8.4, where the same case is analysed.

The target size is very similar to the commonly used reflectivity, but is polarization independent. The hydrometeors are mostly 0° oriented, but the data becomes noisier at low reflectivity areas and the melting layer. The ellipticity parameters show a significant change in one strip starting at 6 km. This feature will be further analysed in Section 8.2. Only in this region, the skip angle shows significant changes, which should be related to a phase-shift upon scattering (Schroth et al. (1988)). The characteristic or fork angle shows most details. It is comparable to the differential reflectivity Z_{DR} but shows more information in this case. Especially, there are many features in the convective region.

7.6.2 Additional Parameters

Figure 7.4 shows both, the standard formulation Z_{DR} and the sample averaged Z_{DR}. A calibration offset was not adjusted in the samples averaged case. Besides that, both variants behave similar. The standard deviation is a bit smaller for the standard Z_{DR} algorithm (5.91 dB and 6.15 dB)

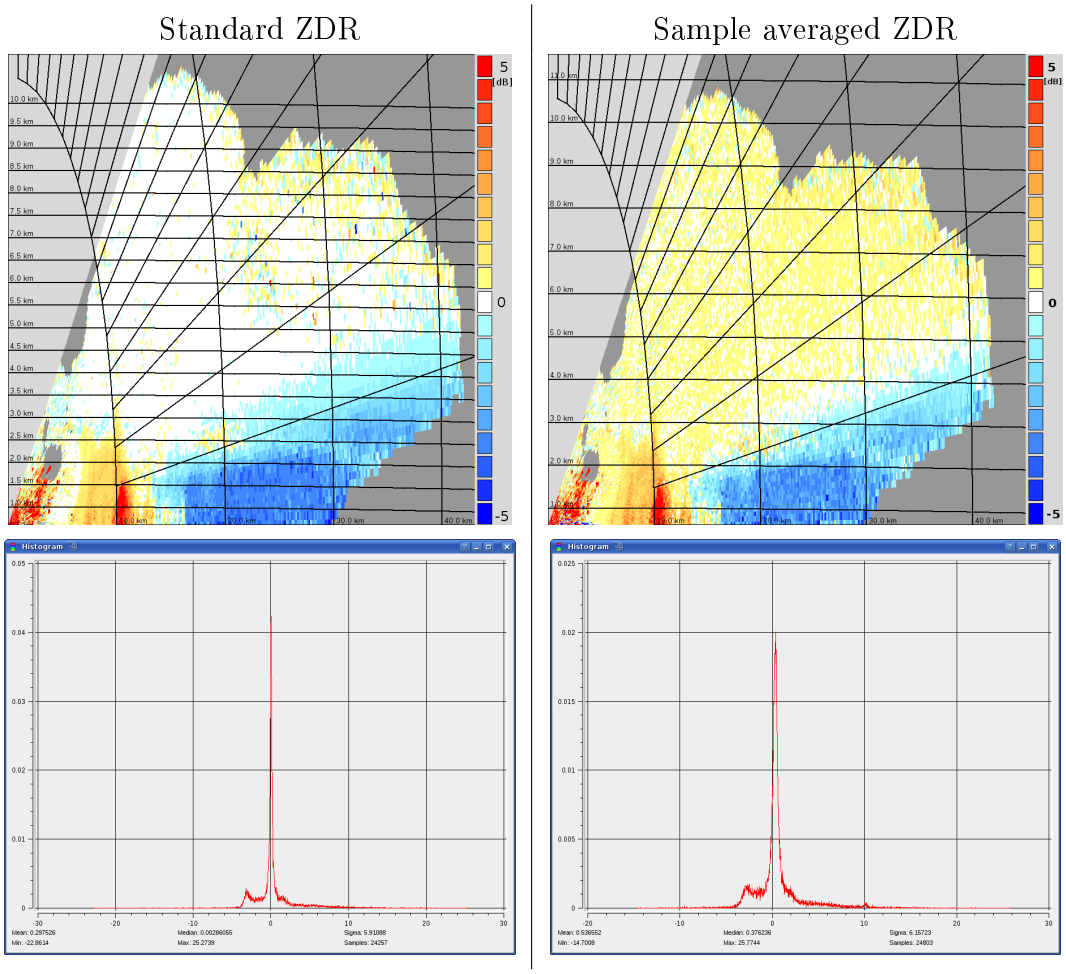

Table 7.4: Standard and alternative Differential Reflectivity data for a thunderstorm from 30/05/2012, 12:58 UTC, azimuth: 217°.

The degree of polarization is proposed as an additional parameter, similar to the copolar-correlation-coefficient ρ_{HV}. Figure 7.5 shows both parameters. In the case shown, the degree of polarization is much higher than the copolar-correlation-coefficient. While ρ_{HV} is dropping, especially in the convective region, the degree of polarization stays high there. Only in the melting layer, both parameters are lowered. A detailed description of the parameters properties can be found in Galletti et al. (2008).

Degree of Polarization

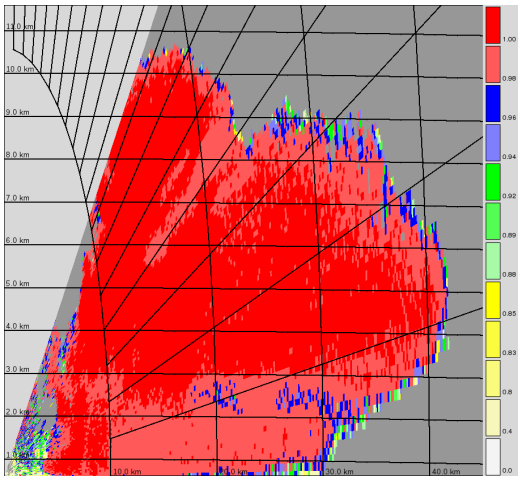

Copolar-Correlation-Coefficient ρ_{HV}

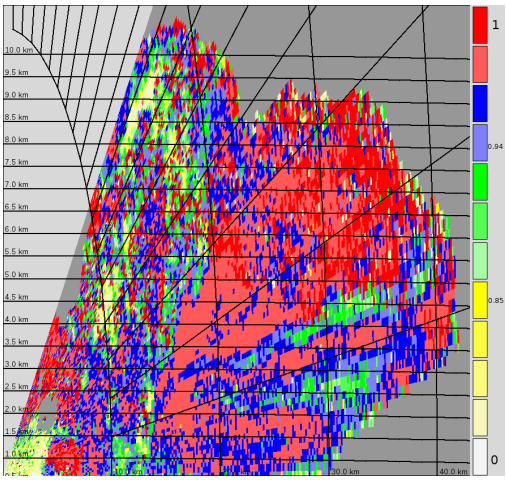

Table 7.5: Degree of Polarization for a thunderstorm from 30/05/2012, 12:58 UTC, azimuth: 217 °.

Chapter 8

Multi-Polarization Measurements

8.1 Influence of the Transmit Phase in Simultaneous H/V Mode and Comparison to the Alternating H/V Mode

8.1.1 Theoretical Predictions

The influence of the transmit phase in hybrid mode measurements has been analysed for a long time. There are several papers from Hubbert et al (Hubbert et al. (2010a), Hubbert et al. (2010b) and Hubbert and Bringi (2003)) as well as from Scott et al. (2001) and Wang and Chandrasekar (2006) analysing this problem.

On radars using a hybrid polarization basis (STAR mode) the pulse is created by a simultaneous transmit of horizontal and vertical polarization. The transmit phase is defined as the phase between the horizontal and vertical component. It is easy to see that a change in this phase results in a different polarization. Linear 45° has 0° phase shift, while circular polarization has a phase different of 90°. A phase shift of 180° would create linear 135° polarization.

For the STAR mode it is assumed that horizontal and vertical polarization can be transmitted independently. This assumption can hardly be met in reality. There are several sources of coupling between horizontal and vertical polarization:

- antenna
- propagation path
- scatterer

Most antennas do not create purely the polarization desired. The polarization of the antenna pattern will change over azimuth and elevation even within the main beam. This can also be treated as a coupling between the polarizations. Furthermore, the radar pulse will be altered while traveling to the target. This distortion is dependent on the propagation media. While there are nearly no effects for C-Band in clear air and small raindrops - large raindrops, hail and melting particles can transform the radar pulse polarization. Higher frequencies are in general more affected. Many natural weather targets also produce depolarization upon scattering e.g. hail, snow and ice, which is useful for classification (parameter L_{DR}).

Measurements in the alternating H/V mode are not affected by this cross coupling as it can be explicitly determined. Hence, comparisons between STAR and alternating H/V mode can quantify the coupling effect. There are measurements concerning this effect, but the time difference between the scans was unfortunately always several minutes. This is due to the fact, that hardware modifications are necessary. As the weather situation (precipitation) is changing within this time, the comparison is of low significance. The fast switching capability of POLDIRAD allows measurements with nearly no time lag between the measurements. The signal processing involved was already detailed in Section 7.5.

There are several weather radar products which might be affected by the polarimetric cross coupling:

- ρ_{HV} - the correlation coefficient between S_{HH} and S_{VV}, which might be degenerated by the coupled terms
- Z_{DR} - the differential reflectivity, where the coupling might cause offsets
- ϕ_{DP} - the differential phase shift, which was found quiet robust.

No artefact were found for ϕ_{DP} in the analysed examples, which might be due to the minor phase error introduced by the small coupling term. The coupled power from the minor axis elements are always small compared to the major axis elements in the scattering matrix. The disturbance found for ρ_{HV} and Z_{DR} will be shown in more detail next.

8.1.2 Measurements of Copolar-Correlations-Coefficient

In Scott et al. (2001) a sphericity parameter

$$g = \frac{4\Re\langle \underline{S_{xx}}\,\underline{S_{yy}}^{*}\rangle}{\langle \left|\underline{S_{xx}} + \underline{S_{yy}}\right|^2\rangle} \tag{8.1}$$

is defined. From this parameter the correlation coefficient for different polarizations can be derived when scattering at randomly oriented particles occurs

$$\text{alternating H/V mode:} \qquad \rho_{HV} = \tfrac{1+g}{3-g} \tag{8.2}$$

$$\text{STAR mode 0° tx phase:} \qquad \rho_{HV|45,135} = \tfrac{1}{2-g} \tag{8.3}$$

$$\text{STAR mode 90° tx phase:} \qquad \rho_{HV|L,R} = \tfrac{g}{2-g} \tag{8.4}$$

Hence, the relation for ρ_{HV} with 0° and 90° transmit phase shift can be found:

$$\rho_{HV|45,135} = \frac{\rho_{HV|L,R} + 1}{2} \tag{8.5}$$

In Figure 8.1 both, the theoretical relation for random oriented particles as well as a measurement from 16/04/2012, 7:29 UTC are plotted. The data are from a weak stratiform event with reflectivity values mainly about 10 dBZ and never over 20 dBZ. The melting layer is nearly at the ground, therefore most of the ray is in the (random oriented) ice phase. The radar was alternating transmitting right hand circular and linear 45° polarization and receiving H and V. Both transmit trains were independently processing using the same STAR mode algorithms. The difference in the transmit phase can be verified by ϕ_{DP}. The antenna was pointing towards the target and 1024 pulses where averaged. There is a good agreement between predicted and measured values. The measured data were not filtered at all, which might be the reason for some of the departures. The particles observed may not be completely random oriented, which could be the reason for the slightly different slope.

Various Aspects of Measuring the Copolar-Correlation-Coefficient

In practice it was found that ρ_{HV} is very similar for linear 45° STAR and alternating H/V mode as long as the conversion from time lag one to lag zero is working well which is needed in alternating mode (see eq. (7.5)). This may fail for several reasons:

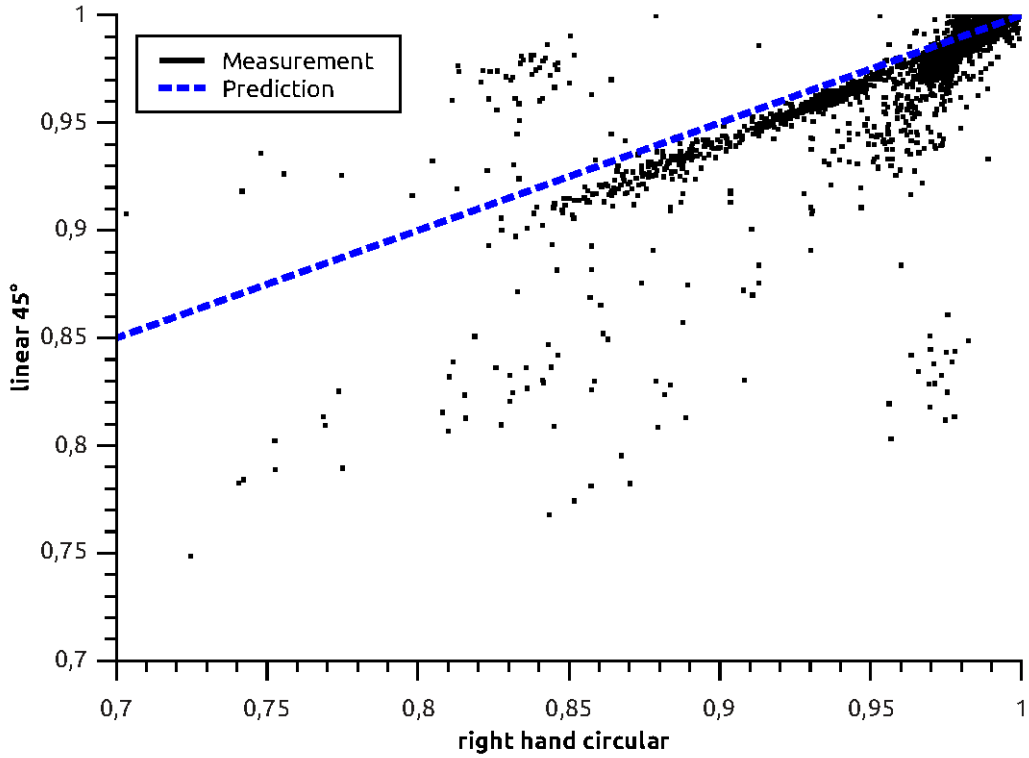

Figure 8.1: Measured Copolar-Correlation-Coefficient for 45° linear and right hand circular polarization and the theoretical prediction from Scott et al. (2001), eq. (8.5). Data from 16/04/2012, 7:29 UTC

- The Gaussian spectrum assumption fails, e.g. two peaks in the frequency spectra referring to two types of hydrometeors.
- The recorded samples are spaced too far in time and temporal decorrelation becomes too large for meaningful reconstruction, e.g. when using low PRFs (Tragl, 1990).
- Noise estimation is inaccurate for time lag zero correlations ($R(0)_H$ and $R(0)_V$), due to strong attenuation. Absorbing particles are always also emitting. This can be seen from the equation for the co-polar correlation coefficient to time lag 0 (8.6):

$$\rho_{HV}(0) = \frac{\left|\underline{R(0)_{HV}}\right|}{\sqrt{R(0)_{HH} \cdot R(0)_{VV}}} \tag{8.6}$$

The numerator is a cross correlation where the noise term vanishes. The

denominator consists of two autocorrelations where the noise term (or expected value) has to be removed. Often, the system noise is independently measured, which might lead to wrong estimations and causing $\rho_{HV}(0)$ to raise above 1. If a *2nd* trip echo is overlapping, this signal looks like noise for a random phase magnetron transmitter. This also leads to wrong noise estimation. These effects also affect the STAR mode.

8.1.3 Measurement of Differential Reflectivity

Figure 8.3 shows a range plot through a thunderstorm cell located about 30 km from the radar. The reflectivity goes up to nearly 50 dBZ and L_{DR} (right axis) is rising in this region as well as ϕ_{DP} (lower panel right axis). Three different Z_{DR} values are recorded: red - the alternating H/V mode, black - linear 45° STAR mode, green - right hand circular STAR mode. The different absolute values are due to system offsets (calibration offset) cause by the polarization network. All three Z_{DR} values are increasing to about 3 dB in the thunderstorm region and dropping to negative values behind it. This indicates a strong attenuation. The high L_{DR} values behind the cell are in a region where the ray hits the bright band. ϕ_{DP} is fluctuating there due to large particles causing Mie scattering. Even at the end of the ray the SNR is still high, as indicated by L_{DR}. It can be assumed, that with a L_{DR} of e.g. -25 dB (at 80 km) the SNR for the co-polar channel is also at least -25 dB.

There are differences in the Z_{DR} values along the range which is certainly due to propagation effects. Assuming the alternating H/V mode is least effected by cross coupling, it is used as the reference. While the offset between Z_{DR} from the alternating mode and the right hand circular (90° transmit phase) is approximately constant at 1 dB, the offset to the Z_{DR} from linear 45° STAR mode is changing. It is about 0.5 dB at the radar, increasing to 1 dB right after the thunderstorm cell and is further growing to 1.4 dB at 80 km.

This case shows a variation of Z_{DR} depending from the transmit phase of about 0.9 dB. Following Hubbert et al. (2010a) and Hubbert et al. (2010b) this effect is due to canted particles in the propagation path. The antenna is an unlikely source of depolarization as the calibration is good and the system L_{DR} limit is quite high (see Section 6.6).

It can be seen from this example, that the phase difference on transmit - respectively the transmit polarization - is important for the interpretation of Z_{DR}

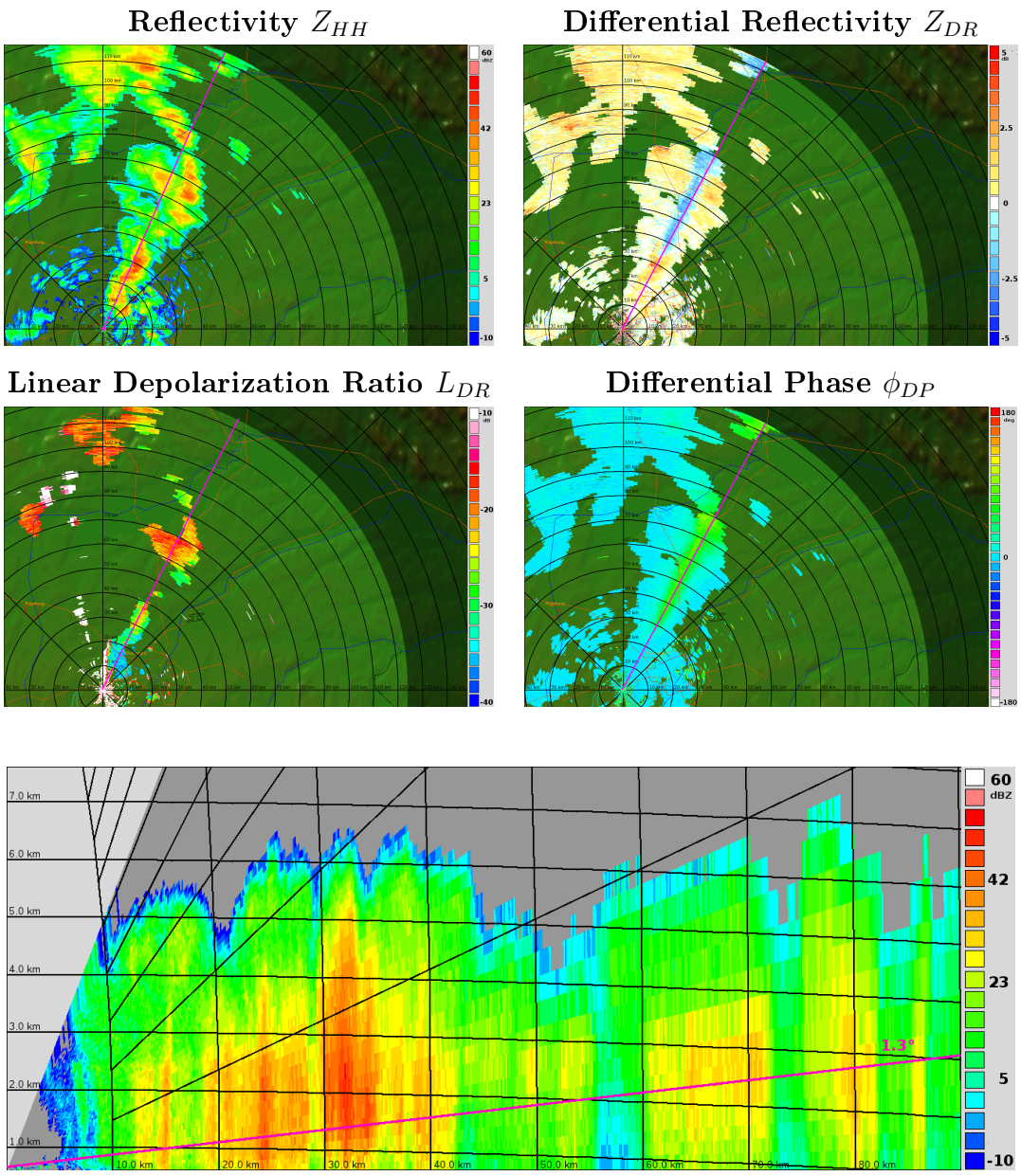

Figure 8.2: RHI through the thunderstorm (04/06/2012, 15:46 UTC). The ray indicated by the purple line is analysed in detail (Figure 8.3).

in attenuating regions when using the STAR mode. Unfortunately, the transmit polarization may change along the path as indicated by the differential phase shift (ϕ_{DP}). Hence, depending on the transmit phase shift and the differential phase shift accumulated, the propagation effect on Z_{DR} can change. On the other hand, this might give additional information about the hydrometeors involved in the scattering process.

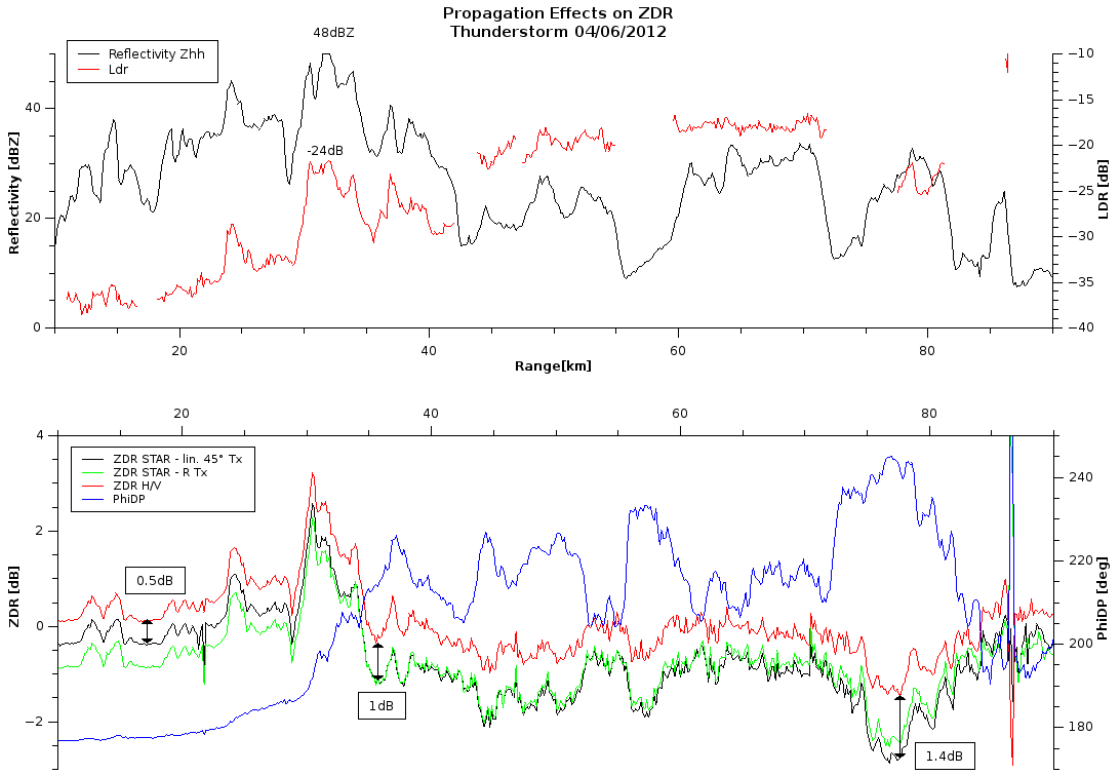

Figure 8.3: Offset in the Differential Reflectivity due to propagation effects through a thunderstorm (04/06/2012, 15:46 UTC). Elevation: 1.3°

8.2 Measurements of the Co-Cross-Correlation-Coefficient

Since the latest upgrade of POLDIRAD, it is capable to measure even the co-cross correlation coefficient $\underline{\rho_x}$ in magnitude and phase. Measurements of $\underline{\rho_x}$ will be shown for a Range Height Indicator (RHI) case from 30/05/2012, 12:58 UTC (Fig. 8.4). In the reflectivity field two strong thunderstorm cores can be seen, with values up to nearly 63 dBZ. The melting layer can be easily distinguished from the L_{DR} plots at a height of about 2.5 km. There are Z_{DR} values around zero above this layer indicating ice and slightly positive numbers below. At 10 km Z_{DR} is rising to $6dBZ$ which is a sign for large raindrops. Behind this region Z_{DR} goes negative due to differential attenuation, which can also be seen in ϕ_{DP}.

In the ice region L_{DR} is mainly very low (below 35 dB), but there one strips of higher L_{DR} behind the cell core in radial direction at about 20° elevation. These features have $L_{DR} \approx -30$ dB. The radial direction indicates a forward scattering

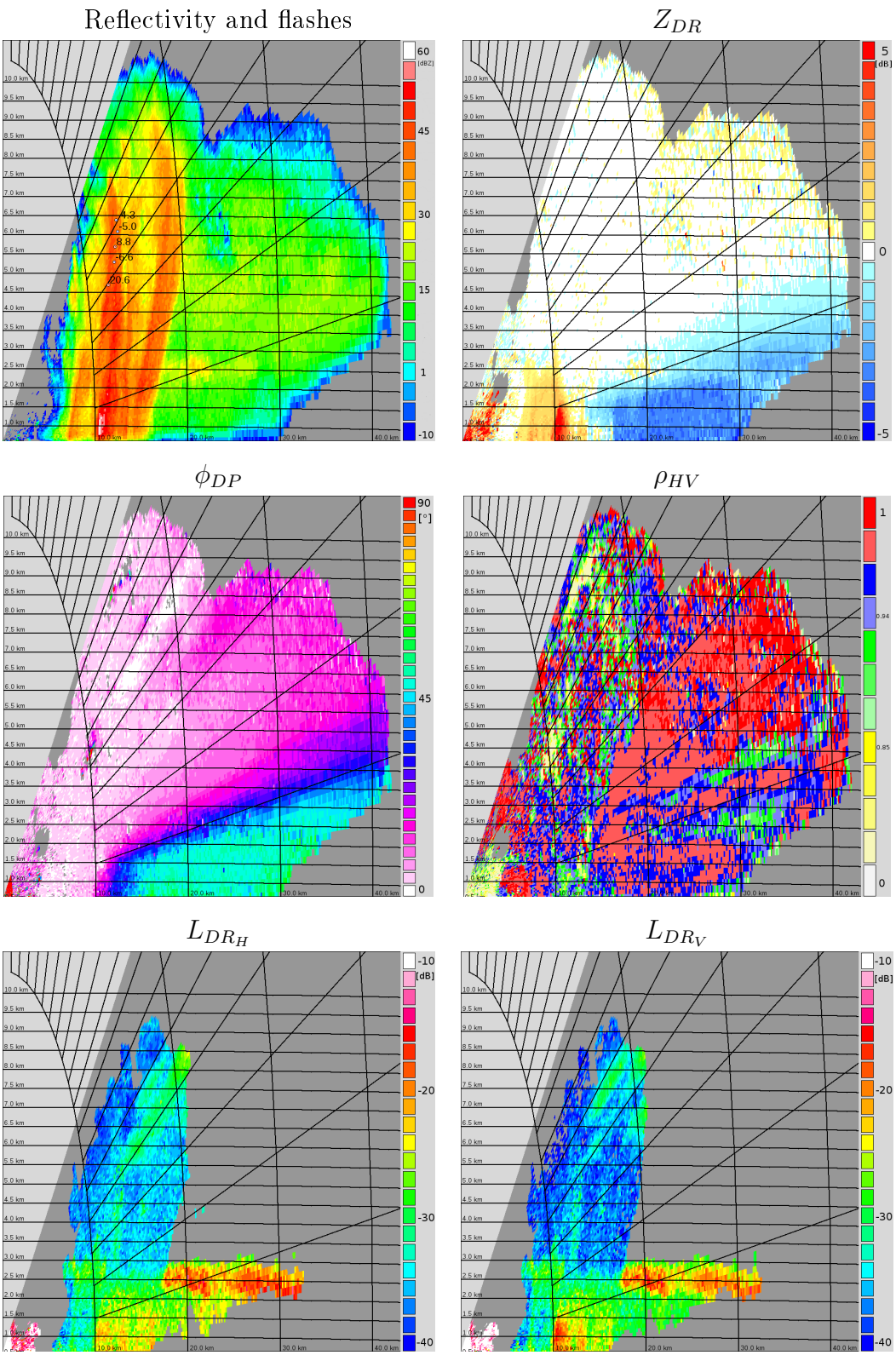

Figure 8.4: Vertical Scan data of a Thunderstorm from 30/05/2012, 12:58 UTC, elevation: 217°

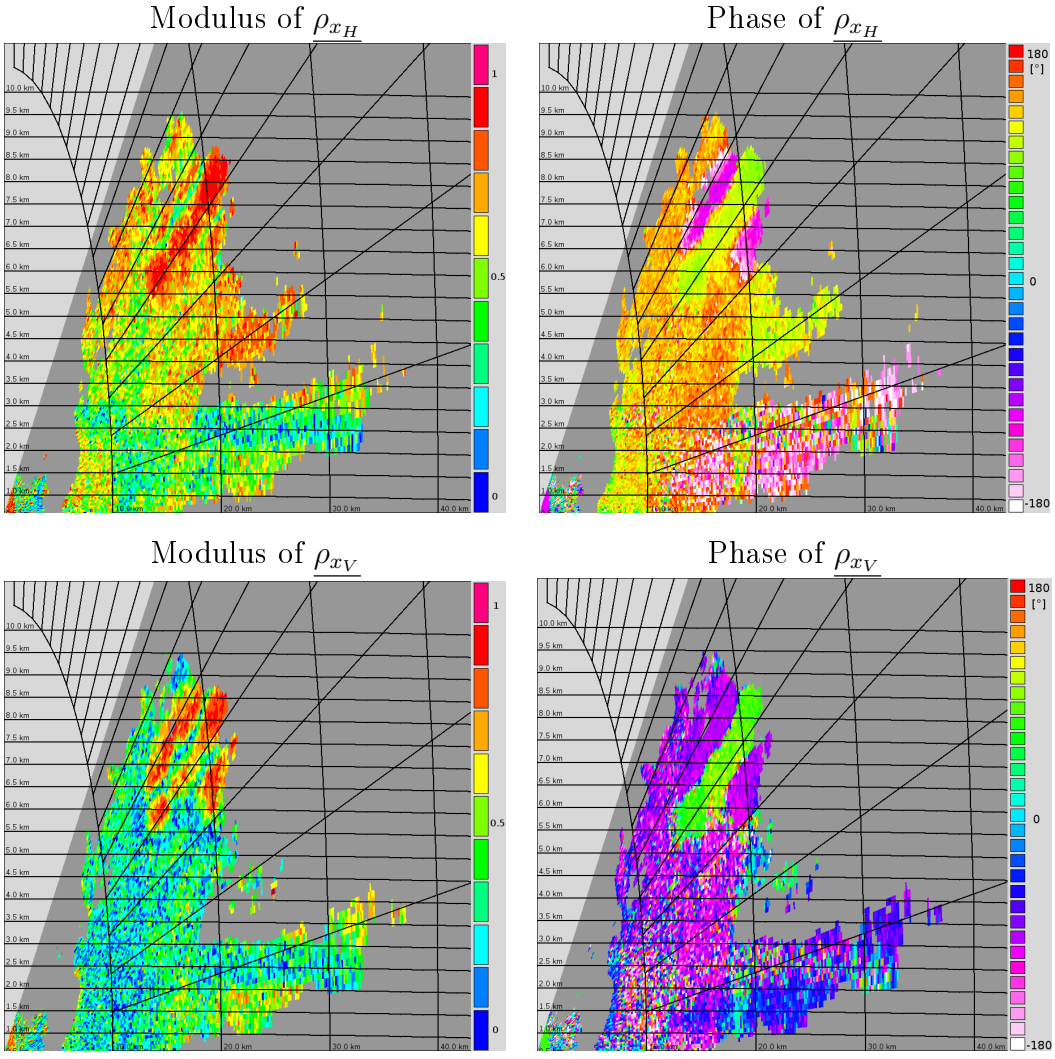

Figure 8.4 (Continued) : Vertical Scan data of a Thunderstorm from 30/05/2012, 12:58 UTC, azimuth: 217°

or propagation effect. The co-cross correlation coefficient $\underline{\rho_x}$ is high in this feature, which is probably not related to a higher SNR (low SNR reduce the correlation). This can be seen, when comparing the strips with a melting layer: Both features have high L_{DR} and therefore similar power difference between co-polar and cross-polar channel. The $\underline{\rho_x}$ values are low in the melting layer, but high in the strips.

It is proposed that the high L_{DR} values in the melting layer are due to depolarization on scattering, while the higher values in the strips are due to an altered polarization on propagation. This may be caused by aligned particles due to an electric field. Krehbiel et al. (1996) have shown that this electric field can be seen in a circular polarization basis. As all polarization bases contain equal information, similar result have to be seen in the H/V basis as well (Ryzhkov (2001)). Unfortunately, $\underline{\rho_x}$ was inaccessible for a long time. The hypothesis of an electric field is supported by the flashes seen in the same region. The argument of $\underline{\rho_x}$ may indicate (two times) the phase shift related to the complex depolarization process. The phase shift is not seen in ϕ_{DP}. It is to be noted that the phase difference between horizontal and vertical polarization was not yet calibrated to zero in this case. This means the absolute phase of $\underline{\rho_x}$ is probably incorrect, while the relative phase change is unaffected.

It should also be stressed that the modulus of the correlation coefficient is not equal for horizontal and vertical polarization ($\underline{\rho_{x_H}} \neq \underline{\rho_{x_V}}$) in this measurement. It can be summarized, that $\underline{\rho_x}$ adds additional information to L_{DR} and is low in the melting layer. Higher $\left|\underline{\rho_x}\right|$ and a jump in the phase of $\underline{\rho_x}$ may be related to electric field and therefore indicate lightning in that region. Furthermore, the phase of $\underline{\rho_x}$ contain information about the differential phase shift (precisely $\frac{1}{2}\phi_{DP}$) if there is no intense coupling between H and V (like in the electric field case).

Chapter 9

Conclusions

The presented work was aimed to perform measurements using several polarizations in one single radar scan. The polarization has to be changed for each radar pulse to gather the data within the decorrelation time of the target. These recordings were used to directly compare data from a hybrid polarization basis using the STAR mode with different transmit phases (or polarization) and data collected in the alternating H/V mode. It was found that ρ_{HV} is dependent on the transmit phase as proposed by Scott et al. (2001) and even Z_{DR} can suffer offsets after strong attenuating regions.

To perform these measurements several prerequisites had to be fulfilled first. The POLDIRAD radar has to be calibrated for several polarizations (horizontal, vertical, linear 45°, linear 135°, right and left hand circular) without using the reciprocity assumption. Several calibration techniques were analysed. The sun calibration was extended to work for higher elevation. It was shown how this source of unpolarized noise can be used for a rough receive polarization estimation.

Nevertheless, none of the techniques were sufficient for a complete calibration. Hence a polarimetric active radar calibration (PARC) was designed and built for POLDIRAD. This PARC device was designed for fast polarimetric measurements and can be used to record polarimetric antenna patterns, too.

It was also shown how to extend the real-time signal processing of weather radars to allow interleaved measurements using several polarimetric modes, like STAR mode, L_{DR} mode, alternating H/V and alternating R/L mode.

Chapter 10

Outlook

The presented work has shown how to use the fast switching capability of POLDIRAD to analyse cross coupling effects in STAR mode, which is used by the operation weather radars. This was done by transmitting several polarizations on a per pulse basis. This scheme could be extended to measure targets in completely different polarization bases. This is already possible on POLDIRAD using the covariance mode. Several polarimetric *views* might be used to separate propagation from back-scattering effect as more information is available. Knowing that the target scattering matrix is the same in each polarization basis any discrepancy might be related to propagation effects, multi-body scattering etcetera. Scott (1999) already proposed a technique to separate aligned and random orientated particles using linear 40° and circular transmit polarization and H/V receive.

The alternating modes are still to be extended: Modern techniques like second trip recovery and staggering are not yet implemented. The second trip recovery should be straightforward and would improve the quality - especially of L_{DR} - a lot. As the polarization is switching from one pulse to the next one, the polarimetric quantities are especially biased by the second trip echo. This is particularly annoying in summer with strong convective cells beyond the ambiguous radar range.

Staggering, especially staggered PRT might be more complicated because it interferes with the polarization switching. Therefore, new polarization switching schemes may be preferable like HVVH (or equally HHVV). This scheme would allow extracting the Doppler velocity for both polarization with time lag-0.5, but creates non-uniform sampled data for each polarization. Hence, a good algorithm for spectrum estimation of non-uniform samples is desirable. This would also allow even more

advanced measurement schemes.

In the future, this work might also be applicable to standard weather radar, if polarimetric phased array antennas would become reality. The functionality to control each antenna element in amplitude and phase could create a circuit similar to the POLDIRAD polarization network. The techniques developed for POLDIRAD would than become accessible to this kind of radar systems. A major problem of single polarization phase array antennas could be overcome: the increase cross-polarization for off axes beams could be compensated by a 180° phase shifted signal.

Another problem would still exist: Each beam of the phase array antenna needs to be individually calibrated. The PARC device developed for POLDIRAD might give the direction of research for the calibration devices needed. The fast polarimetric measurement capability of the PARC would be very useful for the characterization of a phase array systems.

Appendix A

PARC Specifications

A.1 Antenna

	H-Port H-Cut	H-Port E-Cut	V-Port H-Cut	V-Port E-Cut
Maximum	18.590 dBi 126.77°	18.588 dBi 127.00°	−14.530 dBi −122.82°	−16.963 dBi −118.52°
3dB Width	19.5445°	19.9374°	18.9391°	22.1709°
1st Sidelobe -	−75.7281° az −49.077 dBm	−77.5118° az −44.079 dBm	−37.0376° az −20.201 dBm	−36.8516° az −16.048 dBm
1st Sidelobe +	70.2883° az −49.475 dBm	71.6508° az −47.256 dBm	44.4247° az −28.292 dBm	27.7766° az −15.927 dBm

Table A.1: PARC antenna specification for horizontal polarization at 5.504 GHz

	V-Port H-Cut	V-Port E-Cut	H-Port H-Cut	H-Port E-Cut
Maximum	18.574 dBi −55.28°	18.569 dBi 126.63°	−2.5058 dBi −137.39°	−13.152 dBi 51.66°
3dB Width	19.5064°	19.9316°	19.7174°	20.4444°
1st Sidelobe -	−69.8399° az −53.884 dBm	−70.6227° az −47.195 dBm	−47.3858° az −24.719 dBm	−33.6418° az −24.995 dBm
1st Sidelobe +	70.6072° az −50.186 dBm	77.5775° az −47.044 dBm	34.8808° az −21.148 dBm	42.3293° az −23.466 dBm

Table A.2: PARC antenna specification for vertical polarization at 5.504 GHz

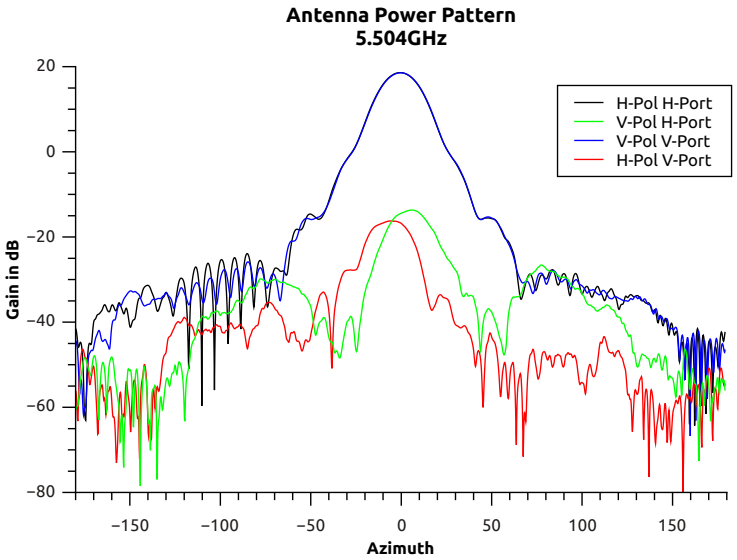

Figure A.1: PARC antenna power pattern

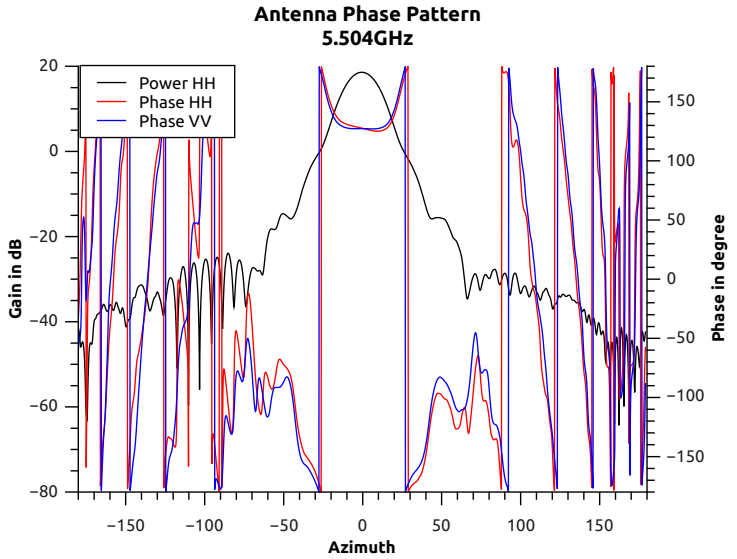

Figure A.2: PARC antenna phase pattern

A.2 PARC Circuits

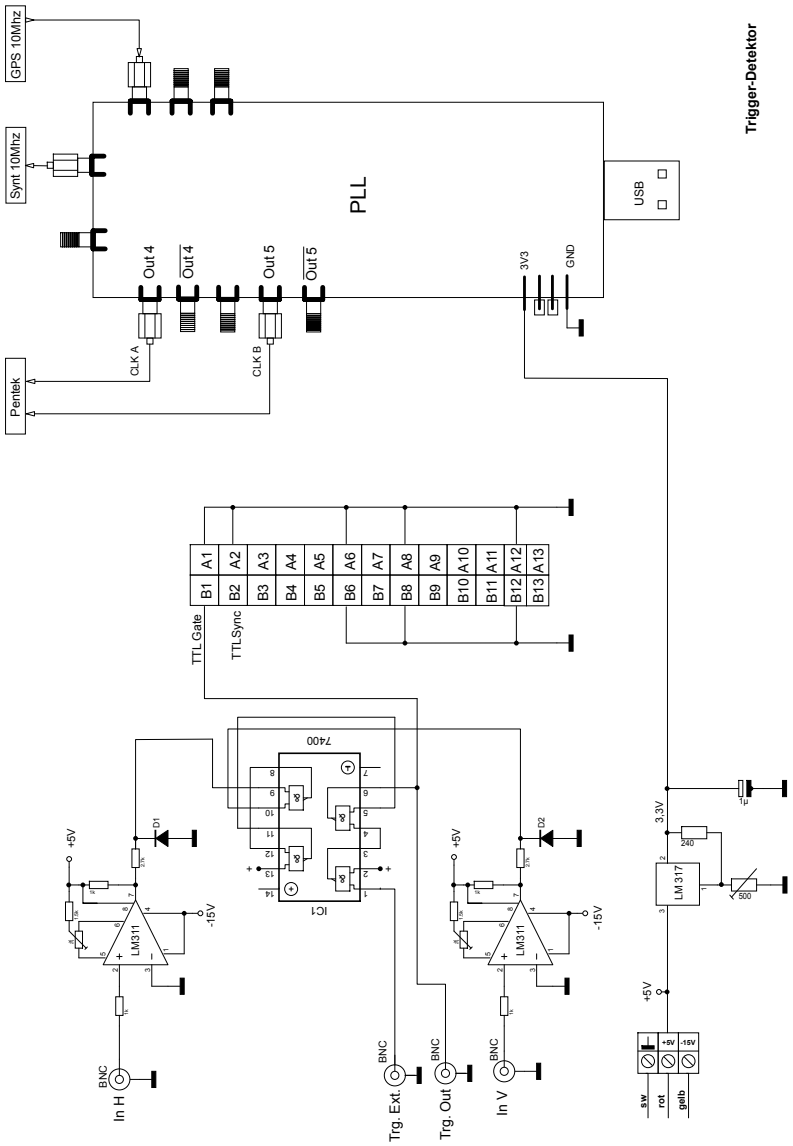

Figure A.3: PARC Trigger circuit: Frequency reference (PLL), pulse detection and signal generation

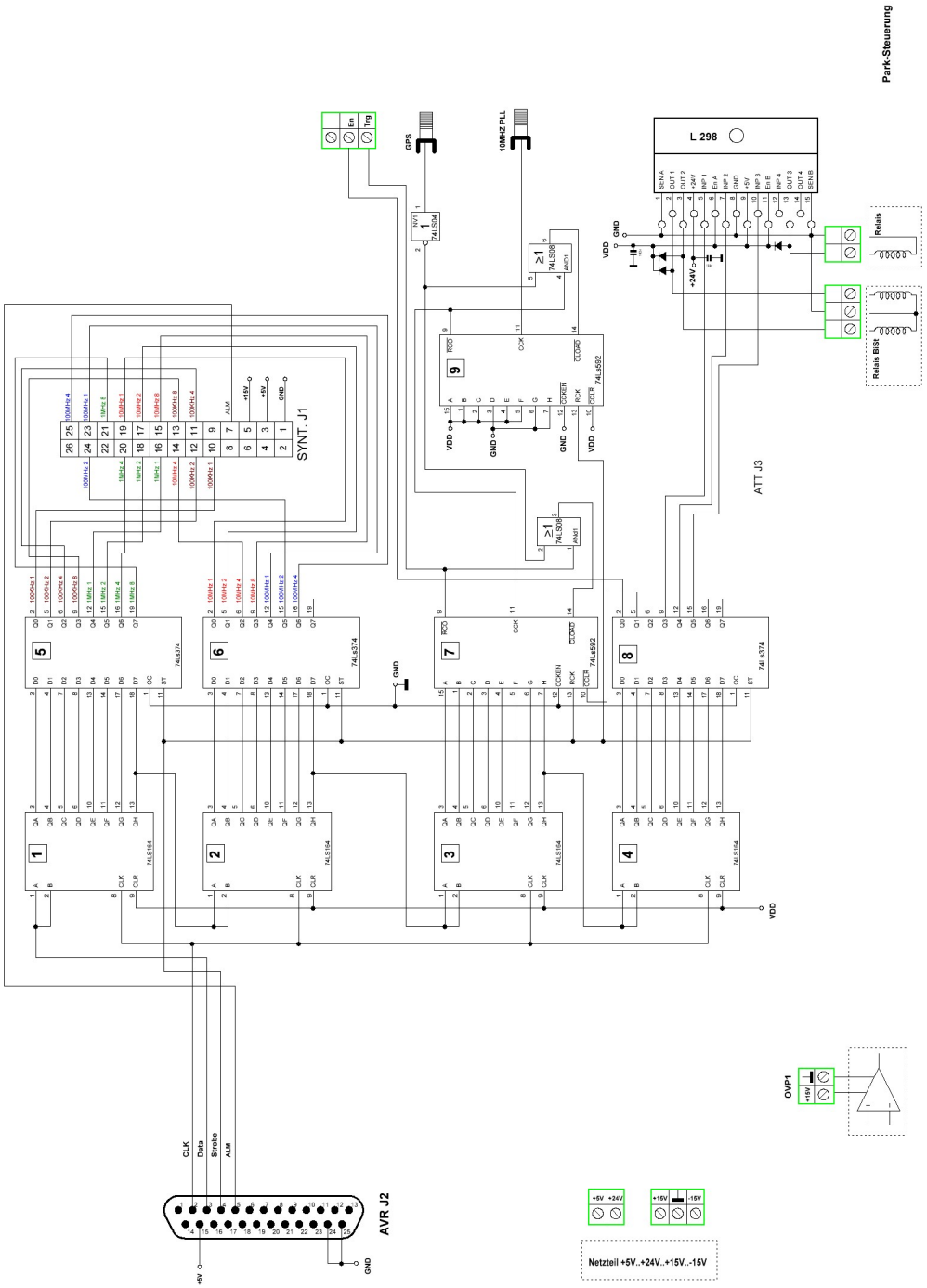

Figure A.4: PARC hardware control circuit: shift register for synthesizer, trigger frequency divider and switch control

Appendix B

Best Practice in Weather Radar Calibration

B.1 Introduction

Certainly, calibration is an important task in the maintenance of a weather radar. There are many approaches having their benefits and drawbacks. It has to be stated that a good calibration includes the usage of a range of techniques. No single tool will fit all demands. This chapter will give an overview of calibration techniques and will briefly describe its best usage.

B.2 Range

Range calibration includes finding the exact time the pulse travels within the system (on transmit and receive). Often this time is known well. If not, the range offset can be determined by ground echoes. Targets with a sharp range characteristic, like towers or high buildings, are to be preferred. High range oversampling should be used together with the antenna pointing towards the target to get best results. The measured distance is to be compared to the value from maps (e.g. the free maps from *OpenStreetMap*).

B.3 Antenna Pointing

While ground echoes from buildings can be used to check the azimuthal position, the elevation is hard to determine (as there are normally little objects creating a sharp elevation peak).

The sun has several benefits: It is an isolated target in the sky without any disturbances. It is present at any radar location and the position is known very precisely (about 0.01°). The disadvantage is the higher processing affords due to the movement of the target and the lower power received. A raster scan gives a map of the sun from with the pointing offset can be determined (see Section 4.5).

B.4 Receiver Offset

If the radar has several (polarimetric) channels, they have to behave similarly. This can be checked by comparing the power received from the sun, as this signal is unpolarized(details see also Section 4.5).

B.5 Absolute Power Calibration

Probably best RCS and absolute power calibration can be done using a metallic sphere with known diameter. The scattering matrix can be analytically calculated and is very precise (only uncertainties are diameter and conductivity). Unfortunately, the setup can become difficult: The sphere has to be the only object in the far field of the radar beam. This is often done by lifting the target with a balloon (while the balloon is outside the radar beam). Maybe some cheap unmanned aerial vehicle (like quadrocopters) can be used in the future. Calm wind is needed for good results anyway.

Signal generators and power meters attached to an antenna may also be used. However, this nearly always suffers from ground reflection/absorption (see Section 6.7).

The self-consistency check using polarimetric quantities as shown by G. Scarchilli and Dobaie (1996) may also be worth considering.

B.6 Polarimetric Calibration

Polarimetric calibration is probably the most challenging task. Often signal generators and power meters are to be used (see above). If some simplification are possible two targets with known scattering matrix are needed to determine the polarization errors (Sarabandi et al. (1990)). A metallic sphere as used for power calibration can be one. Is does not generate any depolarized echo for linear polarization. The polarization orientation angle needs to be determined by a second known target. If right/left hand circular polarization needs to be discriminated, a third target might be needed. For a non-reciprocal system (like POLDIRAD), the number of targets required is even higher.

Appendix C

Sun Scan Plots

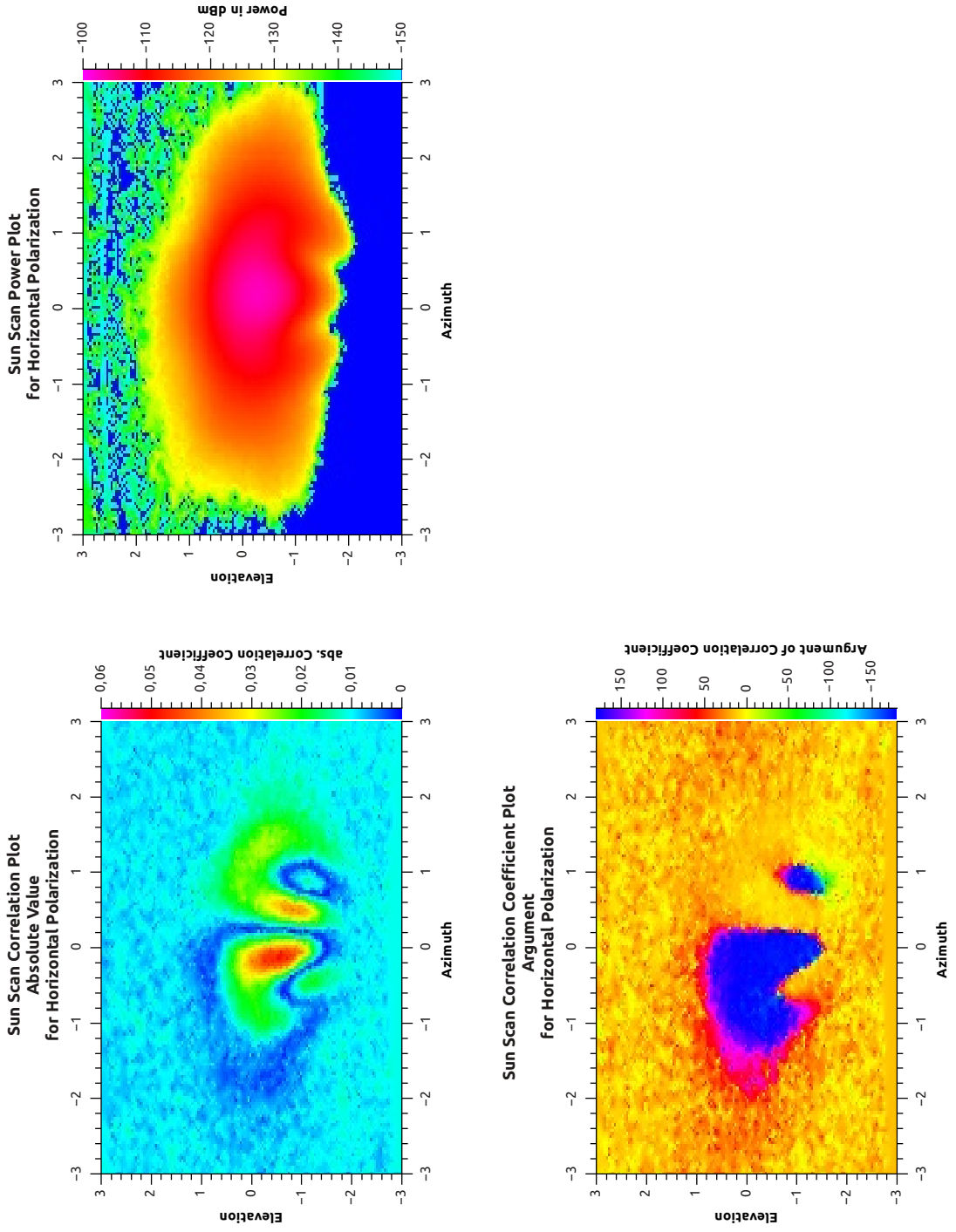

Figure C.1: Antenna pattern from sun for horizontal polarization

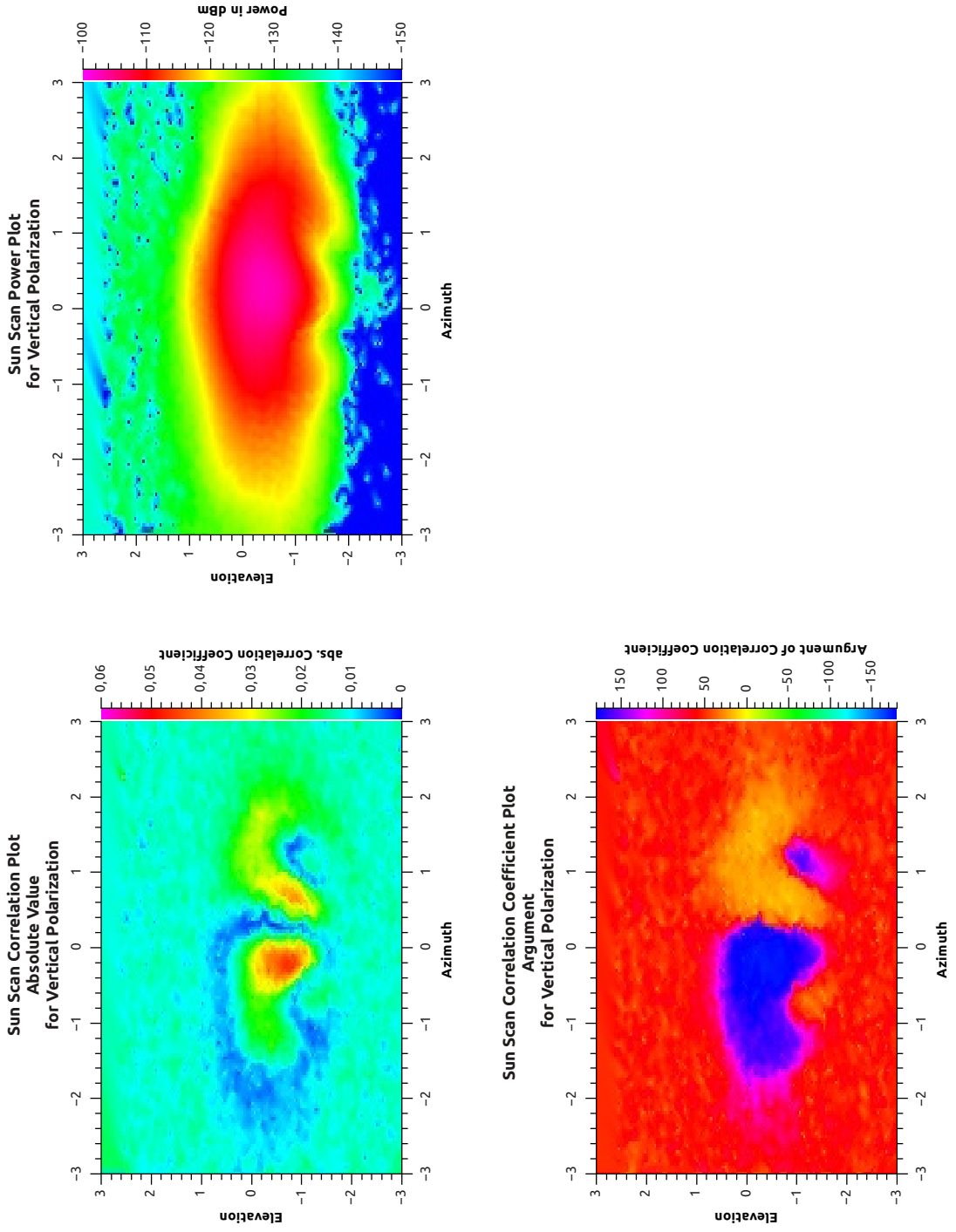

Figure C.2: Antenna pattern from sun for vertical polarization

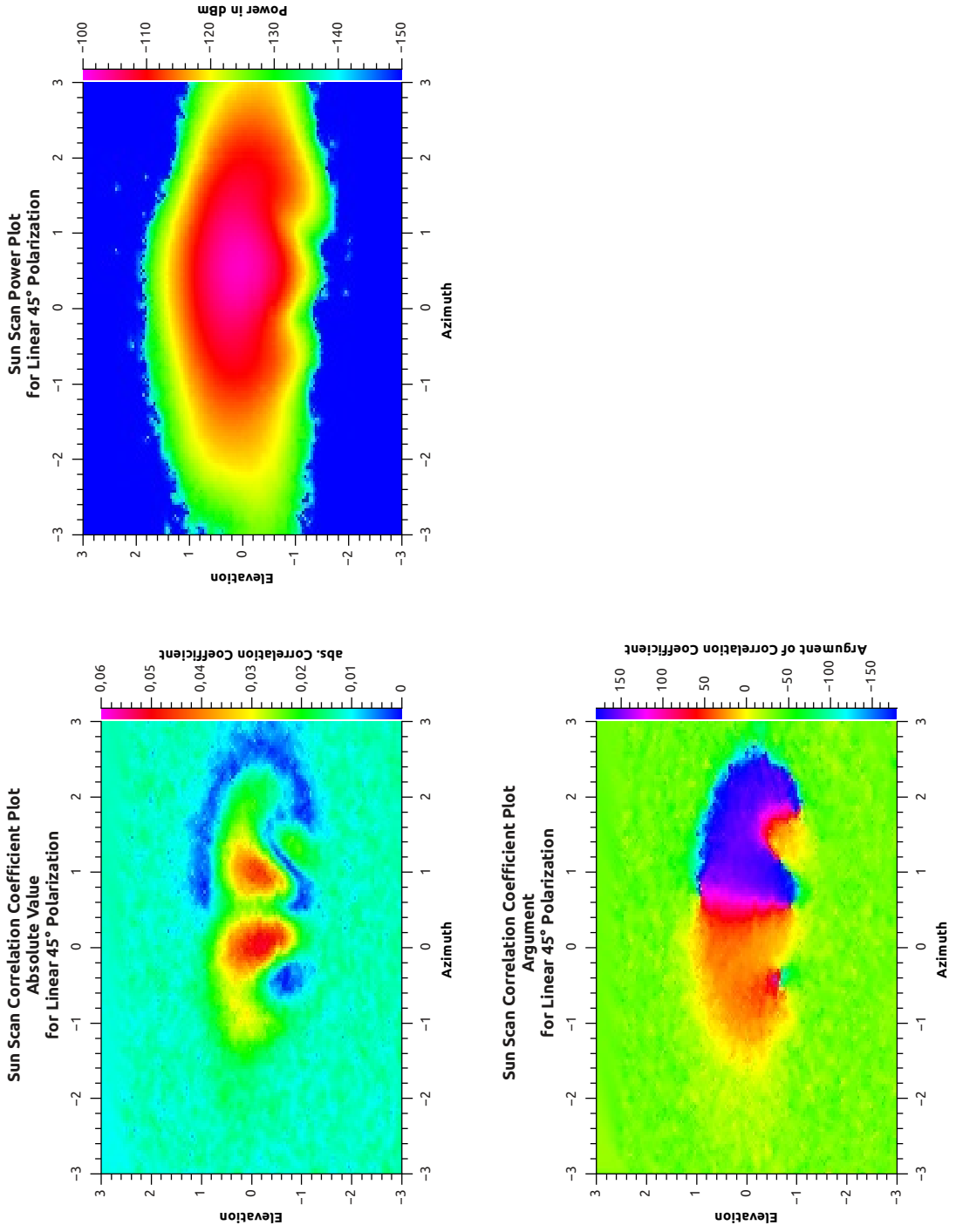

Figure C.3: Antenna pattern from sun for linear 45 ° polarization

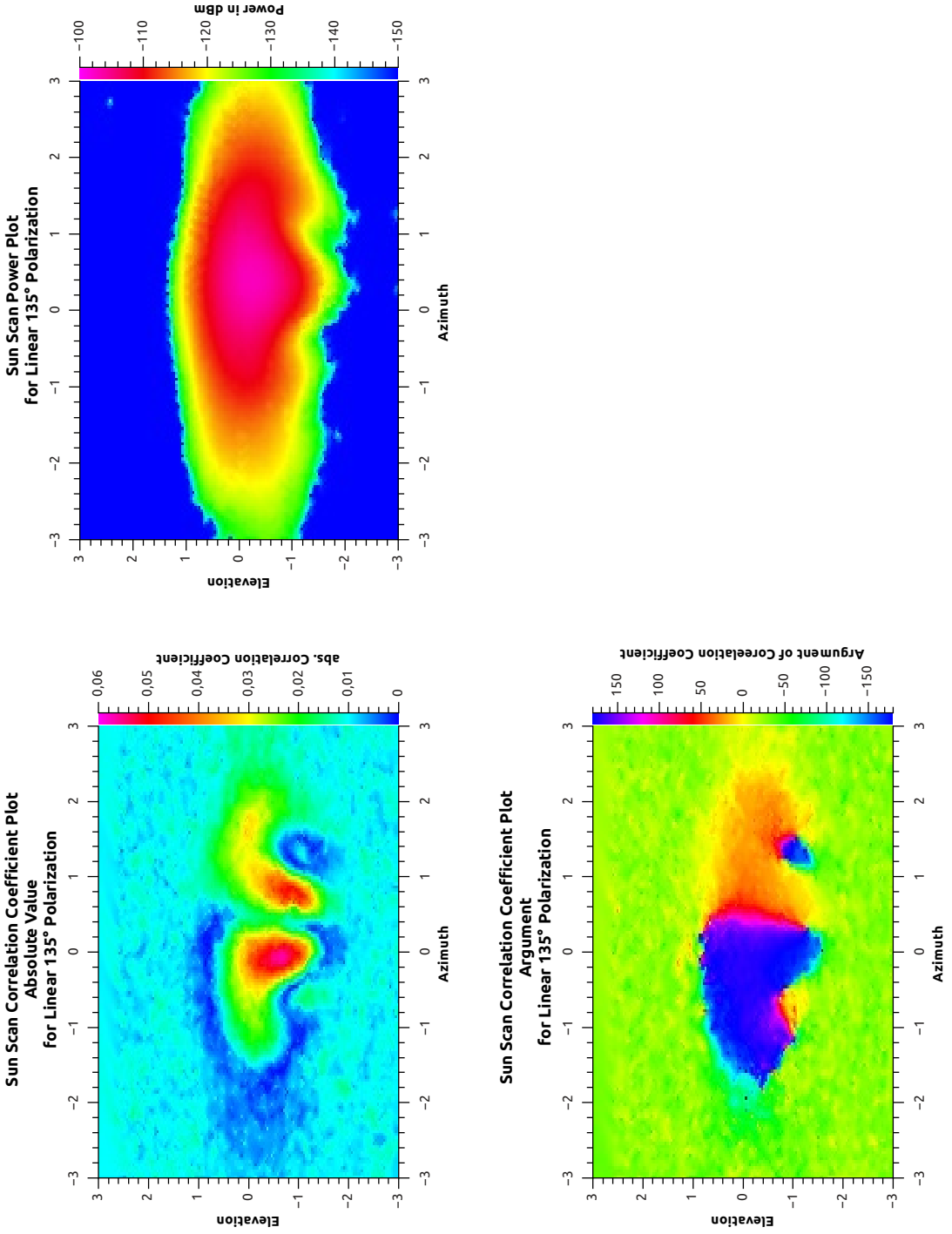

Figure C.4: Antenna pattern from sun for linear 135° polarization

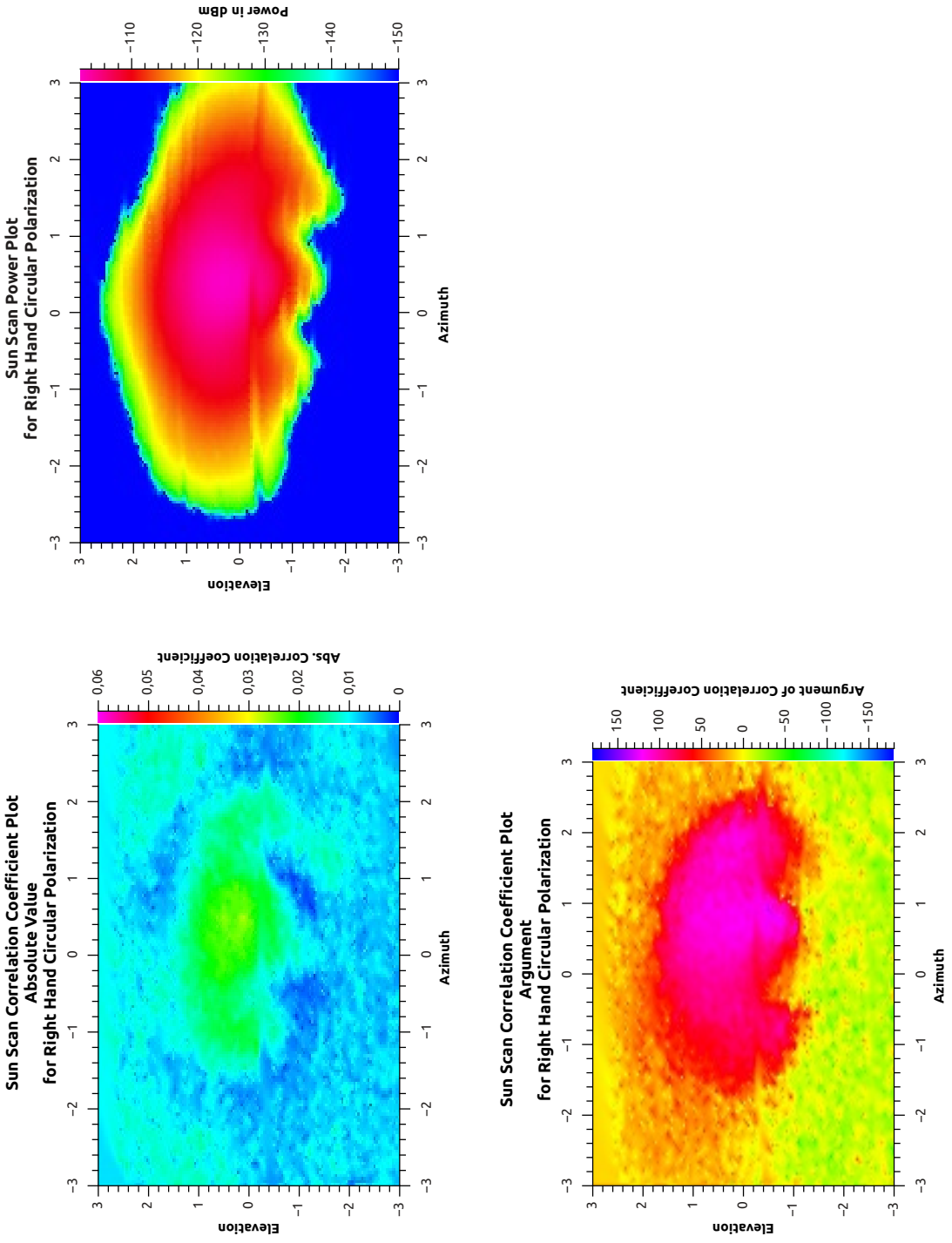

Figure C.5: Antenna pattern from sun for right hand circular polarization

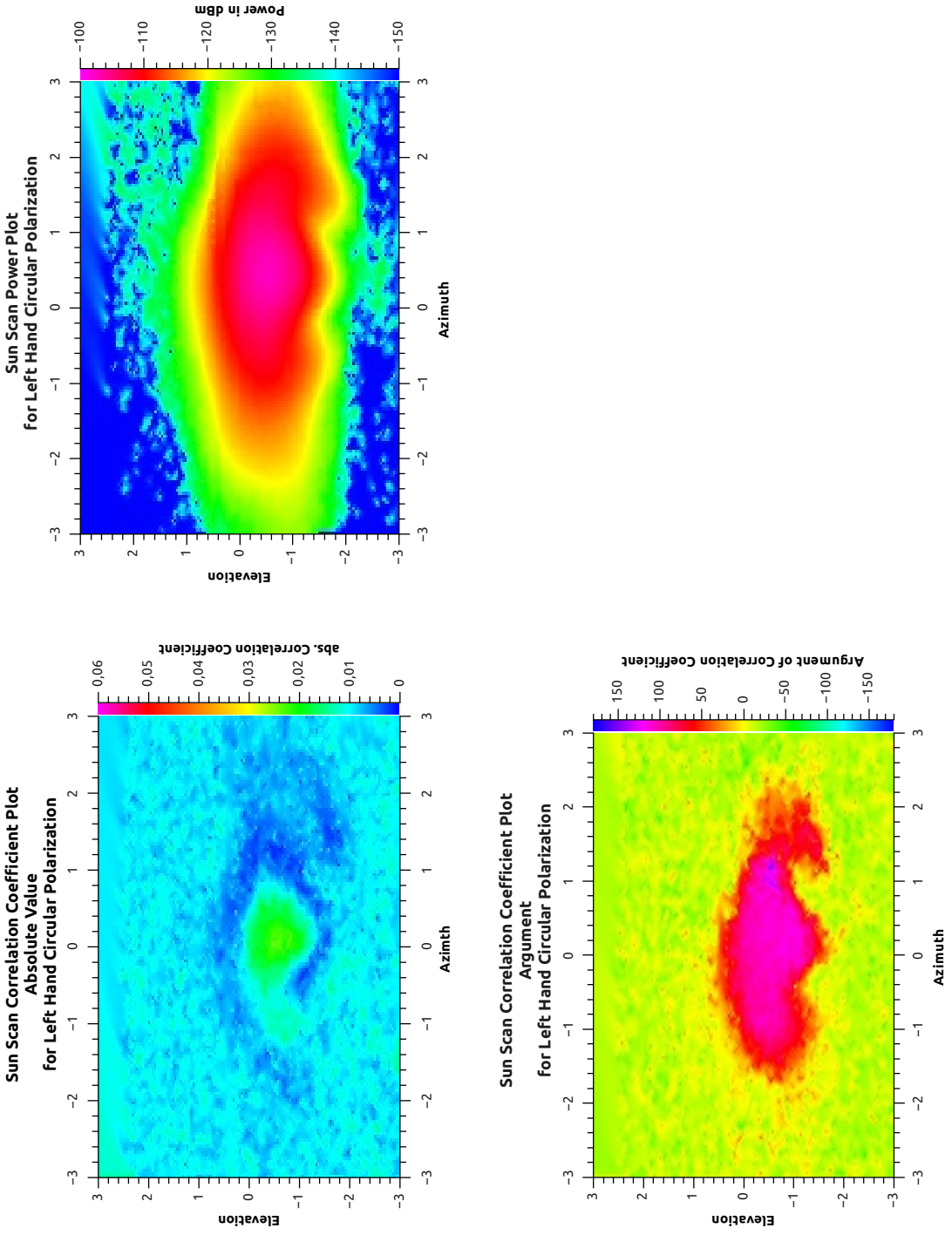

Figure C.6: Antenna pattern from sun for left hand circular polarization

Bibliography

Agrawal, A. P. and W. M. Boerner, 1989: Redevelopment of kennaugh's target characteristic polarization state theory using the polarization transformation ratio formalism for the coherent case. *IEEE Transactions on Geosciences and Remote Sensing*, **Vol. 2 (14)**, pg. 27.

Ahne, J. J., K. Sarabandi, and F. T. Ulaby, 1989: Design and implementation of a c-band single antenna polarimetric active radar calibrator. Tech. rep., Radiation Laboratory University of Michigan.

Baars, J. W. M., 1973: The measurement of large antennas with cosmic radio sources. *IEEE Transactions on Antennas and Propagation*, **Vol. Ap-21 (4)**, pg. 461.

Balanis, C. A., 2008: *Modern Antenna Handbook*. John Wiley and Sons.

Batton, L. J., 1973: *Radar Observation of the Atmosphere*. The University of Chicago Press.

Boerner, W.-M., 2011: *Basic Concepts in Radar Polarimetry*. UIC-ECE Communications, Sensing and Navigation Laboratory, polsarpro v3.0 - lecture notes ed.

Bringi, V. N. and V. Chandrasekar, 2001: *Polarimetric Doppler Weather Radar*. Cambridge University Press.

Böttcher, M., S. Weitz, and J. Borkes, 2011: Calibration certificate. Certificate, Antenna Test Laboratoy.

Ceccarelli, C., 2008: Analisi Meccanica Dell'Antenna Radar Polar 55. Tech. rep., C&C S.r.l.

Cerna, M. and A. F. Harvey, 2000: The fundamentals of fft-based signal analysis and measurement. *National Instruments Application Note 041*.

Chandrasekar, V. and R. J. Keeler, 1993: Antenna pattern analysis and measurement for multiparameter radars. *Journal of Atmospheric and Oceanic Technology*, **Vol. 10**, pg. 674–682.

Chu, T.-S. and R. H. Turrin, 1973: Depolarization properties of offset reflector antennas. *IEEE Transactions on Antennas and Propagation*, **Vol. AP-21 (3)**, pg. 339.

Cloude, S. R. and E. Pottier, 1996: A review of target decomposition theorems in radar polarimetry. *IEEE Transactions on Geoscience and Remote Sensing*, **Vol. 34 (2)**, pg. 498.

EMS, 2004: *EMS Tech Ferrite Deivce Reliability*. EMS Technology Inc.

Fasold, D., 2000: *Grundlagen von Reflektorantennen*. Antennen: Theoretische Grundlagen, Berechnungsmethoden, Ausführungsformen, Einsatzbereiche und Meßtechnik, Carl-Cranz-Gesellschaft e.V.

G. Scarchilli, V. C., E. Gorgucci and A. Dobaie, 1996: Self-consistency of polarization diversity measurement of rainfall. *IEEE Transactions on Geoscience and Remote Sensing*, **Vol. 34 (1)**, pg. 22.

Galletti, M., D. H. O. Bebbington, M. Chandra, and T. Börner, 2008: Measurement and characterization of entropy and degree of polarization of weather radar targets. *IEEE Transaction on Geoscience and Remote Sensing*, **Vol. 46 (10)**, pg. 3196.

Gekat, F., P. Gölz, and R. Hannesen, 2011: Weather radar calibration and testing using the moon as reference target. 35th Conference on Radar Meteorology - AMS.

Gekat, F., M. Hille, H. Niese, and M. Pool, 2010: Accuracy of the engineering calibration of weather radars. 2012 IEEE Int. Geoscience and Remote Sensing Symp. (IGARRS 2010).

Holleman, I. and H. Beekhuis, 2004: Weather radar monitoring using the sun. Tech. rep., KNMI.

Holleman, I., A. Huuskonen, R. Gill, and P. Tabary, 2010: Operational monitoring of radar differential reflectivity using the sun. *Journal of Atmospheric and Oceanic Technology*, **Vol. 27**, pg. 881.

Hubbert, J. C., 1994: A comparison of radar, optic, and spectral null polarization theories. *IEEE Transactions on Geoscience and Remote Sensing*, **Vol. 32 (3)**, pg. 658.

Hubbert, J. C. and V. N. Bringi, 1996: Spectral null polarization theory: Applications to radar meteorology. *IEEE Transactions on Geoscience and Remote Sensing*, **Vol. 34 (4)**, pg. 859.

Hubbert, J. C. and V. N. Bringi, 2003: Studies of the polarimetric covariance matrix. part ii: Modeling and polarization errors. *Journal of Atmospheric and Oceanic Technology*, **Vol. 20**, pg. 1011.

Hubbert, J. C., S. M. Ellis, M. Dixon, and G. Meymaris, 2010a: Modeling, error analysis, and evaluation of dual-polarization variables obtained from simultaneous horizontal and vertical polarization transmit radar. part i: Modeling and antenna errors. *Journal of Atmospheric and Oceanic Technology*, **Vol. 27**, pg. 1583.

Hubbert, J. C., S. M. Ellis, M. Dixon, and G. Meymaris, 2010b: Modeling, error analysis, and evaluation of dual-polarization variables obtained from simultaneous horizontal and vertical polarization transmit radar. part ii: Experimental data. *Journal of Atmospheric and Oceanic Technology*, **Vol. 27**, pg. 1500ff.

Huynen, J. R., 1970: Phenomenological theory of radar targets. Ph.D. thesis, Technical University of Delft.

IEEE, 1993: *IEEE Standard Definitons of Terms for Antennas (IEEE Std 145-1993)*. IEEE.

Ince, W. J. and E. Stern, 1967: Nonreciprocal remanence phase shifters in rectangular waveguide. *IEEE Transactions on Microwave Theory and Techniques*, **MTT-15 (2)**, pg. 87.

J. C. Hubbert, V. N. B. and D. Brunkow, 2003: Studies of the polarimetric covariance matrix. part i: Calibration methodology. *Journal of Atmospheric and Oceanic Technology*, **Vol. 20**, pg. 696.

Krehbiel, P., T. Chen, S. McCrary, W. Rison, G. Gray, and M. Brook, 1996: The use of dual channel circular-polarization radar observations for remotely sensing storm electrification. *Meteorology and Atmospheric Physics*, **Vol. 59**, pg. 65–82.

Krogager, E., 1990: New decomposition of the radar target scattering matrix. *IEEE Electronic Letters*, **Vol. 26 (18)**, pg. 1525–1527.

Liu, L., V. N. Bringi, V. Chandrasekar, E. A. Mueller, and A. Mudukutore, 1994: Analysis of the copolar correlation coefficient between horizontal and vertical polarization. *Journal of Atmospheric and Oceanic Technology*, **Vol. 11**, pg. 950–963.

Lüneburg, E., 2002: Aspects of radar polarimetry. *Turkish Journal of Electrical Engineering and Computer Sciences*, **Vol. 10 (2)**, pg. 219.

Lyakhovskii, A. F., Y. N. Chepurnyi, and V. A. Somov, 1996: Automated measurement of the polarization electromagnetic waves. *Radio and Communications Technology*, **Vol. 1 (8)**, pg. 92–95, transl. Radiotekhnika No. 8 pp. 84-87, 1996.

Mandelshtam, V. A. and H. S. Taylor, 1997: Harmonic inversion of time signals. *Journal of Chemical Physics*, **Vol. 17 (107)**, pg. 6756–6769, URL `http://ab-initio.mit.edu/wiki/index.php/Harminv,Dec.2012`.

Maxwell, J. C., 1865: A dynamical theory of the electromagnetic field. *Royal Society Transactions*, **(155)**, pg. 459–512.

McCormick, G. C. and A. Hendry, 1972: The anisotropy of precipitation media. *Nature*, **Vol. 238**, pg. 214.

Metcalf, J. I. and J. S. Ussailis, 1984: Radar system errors in polarization diversity measurements. *Journal of Atmospheric and Oceanic Technology*, **Vol. 1 (2)**, pg. 105.

Moisseev, D. N., C. M. H. Unal, H. W. J. Russchenberg, and L. P. Lighart, 2002: Improved polarimetric calibration for atmospheric radars. *Journal of Atmospheric and Oceanic Technology*, **Vol. 19**, pg. 1968.

Reda, I. and A. Andreas, 2008: Solar position algorithm for solar radiation applications. Tech. rep., National Renewable Energy Laboratory. URL `http://rredc.nrel.gov/solar/codesandalgorithms/spa,Dec.2012`.

Reimann, J., 2009: Erkennung und Filterung von Bodenechos in den Daten eines polarimetrischen Doppler-Wetterradars. Diplomarbeit, TU-Chemnitz, URL `http://elib.dlr.de/61766/,Dec.2012`.

Ryzhkov, A. and D. S. Zrnic, 2002: Polarimetric radar obserations and interpretation of co-cross-polar correlation coefficient. *Journal of Atmospheric and Oceanic Technology*, **Vol. 19**, pg. 340.

Ryzhkov, A. V., 2001: Interpretation of polarimetric radar covariance matrix for meteorological scatterers: Theoretical analysis. *Journal of Atmospheric and Oceanic Technology*, **Vol. 18**, pg. 315.

Sahler, H., E. Zocher, and R. Wohleben, 1968: Antennen für elliptisch polarisierte Wellen und ihre Meßtechnik. Forschungsbericht des Landes Nordrhein-Westfalen 1873, Institut für Technische Elektronik der Rhein.-Westf. Techn. Hochschule Aachen.

Sarabandi, K., F. T. Ulaby, and M. A. Tassoudji, 1990: Calibration of polarimetric radar systems with good polarization isolation. *IEEE Transaction on Geoscience and Remote Sensing*, **Vol. 28 (1)**, pg. 70–75.

Saxon, D. S., 1955: Tensor scattering matrix for the electromagnetic field. *Physical Review*, **Vol. 100 (6)**, pg. 1771.

Scarchilli, G., E. Gorgucci, D. Guili, L. Baldini, L. Facheris, and E. Palmisano, 1995: Weather radar calibration by means of the metallic sphere and multiparameter radar measurements. *Il Nuovo Cimento*, **Vol. 18 (1)**, pg. 57.

Schroth, A. C., M. Chandra, and P. F. Meischner, 1988: A c-band coherent polarimetric radar for propagation and cloud physics research. *Journal of Atmospheric and Oceanic Technology*, **Vol. 5**, pg. 803–822.

Scott, R. D., 1999: Dual-polarization radar meteorology: A geometrical approach. Ph.D. thesis, New Mexico Institute of Mining and Technology.

Scott, R. D., P. R. Krehbiel, and W. Rison, 2001: The use of simultaneous horizontal and vertical transmissions for dual-polarization radar meteorological observations. *Journal of Atmospheric and Oceanic Technology*, **Vol. 18**, pg. 629.

Selex Sistemi Integrati, G., 2010: Site acceptance test (sat) low noise frontend dynamic range measurements, unpublished.

Selex, 2009: *GDRX Digital Receiver User Manual.*

Sharon, T. E. and R. G. Roberts, 1984: Patent: Method and apparatus for fast-switching dual-toroid microwave phase shifter. Tech. rep., Electromagnetic Sciences Inc.

Sigmet, 2003: *RVP7 Users's Manual.* SIGMET Inc., URL `ftp://ftp.sigmet.com/outgoing/manuals/rvp7user/,Dec.2012`.

Tracksdorf, P., 2010: Poldirad polarisation switch vector network analyser measurement. Tech. rep., DLR e.V.

Tragl, K., 1990: Polarimetrische Radarbeobachtung von zeitveränderlichen Zufallszielen. Thesis, Universität Kaiserslautern, URL `http://elib.dlr.de/32553/,Dec.2012`.

U.S. Dept. of Commerce, 2012: *Solar Radio Data.* U.S. Dept. of Commerce, NOAA, Space Weather Prediction Center, URL `www.swpc.noaa.gov/ftpdir/lists/radio/,Dec.2012`.

Walker, W. H., 2009: Patent: Variable ratio power divider for a dual polarization radar system with automatic built-in test equipment and calibration. Tech. rep., Baron Services, Inc.

Wallis, D. W., J. R. Ashworth, and C. G. Wier, 1992: Simplified driver for controlled flux ferrite phase shifter. Tech. rep., Electromagnetic Sciences Inc.

Wang, Y. and V. Chandrasekar, 2006: Polarization isolation requirements for linear dual-polarization weather radar in simultaneous transmission mode of operation. *IEEE Transactions on Geoscience and Remote Sensing*, **Vol. 44 (8)**, pg. 2019.

Wanninger, H., 1994: Aufbau einer Kalibrierstation für ein Wolkenradarsystem bei 5.5GHz. Diplomarbeit, Fachbereich Nachrichtentechnik, Fachhochschule München.

Xi, A.-Q. and W.-M. Boerner, 1992: Determination of the characteristic polarization states of the radar target scattering matrix[s(ab)] for the coherent monostatic

and reciprocal propagation space by using the complex polarization ratio rho transformation formulation. *Optical Society of America*, **Vol. 9 (3)**, pg. 437.

Ziegler, V. and E. Clemens, 1993: Patent: Verfahren zur Kalibrierung von beliebig elliptischen, orthonormalen Polarisationsbasen. Tech. rep., DLR e.V.

Zrnić, D., R. Doviak, G. Zhang, and A. Ryzhkov, 2010: Bias in differential reflectivity due to cross coupling through the radiation pattern of polarimetric weather radar. *Journal of Atmospheric and Oceanic Technology*, **Vol. 27**, pg. 1624.

List of Figures

2.1 Polarization ellipse 28
2.2 Illustration of the Poincaré sphere 29
2.3 Simplified scheme of a monostatic polarimetric pulse radar 31

3.1 Schematic of the polarization network of POLDIRAD 37
3.2 Drawing of a phase-shifter as used in the polarization network (from EMS (2004)) 38
3.3 Picture of the polarization network. The dimensions are 208 × 203 × 1012 mm (height × depth × width) and the weight is approx. 32 kg . 39
3.4 Polarization optimized offset antenna of POLDIRAD 40
3.5 Simplified POLDIRAD Scheme 42

4.1 Simplified radar scheme for calibration as already shown in Fig. 2.3 . 45
4.2 Sphere calibration performed in the 1990'th at POLDIRAD 47
4.3 Sketch of the orthogonal coordinate system on the sphere. 51
4.4 Illustration of the coordinate system transformation. 52
4.5 Mounting of the spirit level on the antenna, picture from Ceccarelli (2008) 53
4.6 Antenna tilt measurement 53
4.7 Modelled antenna pattern (not to scale) 55
4.8 Antenna pattern for different polarization. Enlarged versions are found in Appendix C 57

5.1 First approach measurement range (distance approx. 2 km) 61
5.2 Second approach measurement range (distance approx. 227 m) 61

6.1 PARC schematics 70
6.2 Display for the raw radar pulse 83

6.3 Frontend showing the averaged radar pulse parameters as received by the PARC . . . 83
6.4 Window to setup PARC transmit signal . . . 84
6.5 Dialog for radar receive signal measurement . . . 84
6.6 Calibration dialog for radar receive polarization . . . 85
6.7 Calibration dialog for radar transmit polarization . . . 86
6.8 Plotted power as received from the PARC . . . 87
6.9 Phase difference between different polarization bases . . . 87
6.10 Measurement setup for calibration (the POLDIRAD antenna is the white, most left one) . . . 88
6.11 Configuration of the polarization network for better performance . . . 89
6.12 Measured Linear Depolarization Ratio in rain . . . 90
6.13 Two dimensional antenna radiation pattern of POLDIRAD . . . 91
6.14 POLDIRAD antenna radiation pattern azimuth cut at 0° . . . 91
6.15 POLDIRAD antenna radiation pattern elevation cut at 0° . . . 91
6.16 Reference points for POLDIRAD calibration. Losses for duplexer, polarization network and antenna were estimated from manufacture data . . . 92

7.1 Alternating H/V Mode processing chain . . . 99
7.2 Polarization splitting regime: $P1 \ldots P5$ name the pulses with polarization $1 \ldots 5$. They are split into three chains, which are independently processed. There is a new PRF (polarization PRF, PPRF) between the pulses of same polarization . . . 107

8.1 Measured Copolar-Correlation-Coefficient for 45° linear and right hand circular polarization and the theoretical prediction from Scott et al. (2001), eq. (8.5). Data from 16/04/2012, 7:29 UTC . . . 116
8.2 RHI through the thunderstorm (04/06/2012, 15:46 UTC). The ray indicated by the purple line is analysed in detail (Figure 8.3). . . . 118
8.3 Offset in the Differential Reflectivity due to propagation effects through a thunderstorm (04/06/2012, 15:46 UTC). Elevation: 1.3° . . . 119
8.4 Vertical Scan data of a Thunderstorm from 30/05/2012, 12:58 UTC, elevation: 217° . . . 120

8.4 Vertical Scan data of a Thunderstorm from 30/05/2012, 12:58 UTC, azimuth: 217° 121

A.1 PARC antenna power pattern 128
A.2 PARC antenna phase pattern 128
A.3 PARC Trigger circuit: Frequency reference (PLL), pulse detection and signal generation 129
A.4 PARC hardware control circuit: shift register for synthesizer, trigger frequency divider and switch control 130

C.1 Antenna pattern from sun for horizontal polarization 136
C.2 Antenna pattern from sun for vertical polarization 137
C.3 Antenna pattern from sun for linear 45° polarization 138
C.4 Antenna pattern from sun for linear 135° polarization 139
C.5 Antenna pattern from sun for right hand circular polarization 140
C.6 Antenna pattern from sun for left hand circular polarization 141

List of Tables

2.1 Commonly used abbreviations for polarization states 27

3.1 System characteristic of POLDIRAD, 2012 36

4.1 Scan parameters for sun-calibration at POLDIRAD 49

6.1 Differential power and phase recorded at the radar for H and V illumination (14/06/2012). 81

7.1 List of calculated covariances 98
7.2 Available processing modes on POLDIRAD 107
7.3 Huynen fork parameters calculated for a thunderstorm from 30/05/2012, 12:58 UTC, azimuth: 217°. 109
7.4 Standard and alternative Differential Reflectivity data for a thunderstorm from 30/05/2012, 12:58 UTC, azimuth: 217°. 111
7.5 Degree of Polarization for a thunderstorm from 30/05/2012, 12:58 UTC, azimuth: 217°. 112

A.1 PARC antenna specification for horizontal polarization at 5.504 GHz . 127
A.2 PARC antenna specification for vertical polarization at 5.504 GHz . . 127

Versicherung

Hiermit versichere ich, dass ich die vorliegende Arbeit ohne unzulässige Hilfe Dritter und ohne Benutzung anderer als der angegebenen Hilfsmittel angefertigt habe; die aus fremden Quellen direkt oder indirekt übernommenen Gedanken sind als solche kenntlich gemacht.

Bei der Auswahl und Auswertung des Materials sowie bei der Herstellung des Manuskripts habe ich Unterschützungsleistungen von folgenden Personen erhalten:

keine.

Weitere Personen waren an der Abfassung der vorliegenden Arbeit nicht beteiligt. Die Hilfe eines Promotionsberaters habe ich nicht in Anspruch genommen. Weitere Personen haben von mir keine geldwerten Leistungen für Arbeiten erhalten, die im Zusammenhang mit dem Inhalt der vorliegenden Dissertation stehen.

Die Arbeit wurde bisher weder im Inland noch im Ausland in gleicher oder ähnlicher Form einer anderen Prüfungsbehörde vorgelegt.

Chemnitz, den 14. Januar 2013

Propositions

1. The difficulties in calibration of non-reciprocal radar systems can be overcome by splitting transmit and receive calibration and treating it as a communication system.

2. A fast measurement of the polarization in far field is feasible and allows a quick optimization of the polarization settings of a radar.

3. A proper coordinate system transformation is needed for sun scans at higher elevations for undistorted data.

4. The modulus of the polarimetric cross-correlation-coefficient measured from the sun is a figure of merit for the cross-polar isolation of the antenna.

5. Polarization estimation using the sun is feasible when employing polarization dependent antennas (e.g. offset parabolic reflectors) even due to the fact that it is a unpolarized source.

6. Doppler velocity can be estimated from time lag 1 data in alternating polarization transmit mode and is only limited by the a rough estimation of the Differential Phase Shift ϕ_{DP}.

7. A radar able to transmit and receive in different polarimetric operation modes, can be used for a more details analysis of weather phenomena.

8. The proposed dependence of the polarimetric co-polar correlation coefficient ρ_{HV} on the phase between horizontal and vertical polarization component on transmit in simultaneous transmit and receive mode can be measured.

9. The Differential Reflectivity Z_{DR} is dependent on the transmit phase in simultaneous transmit and receive mode, probably due to cross coupling.

10. The polarimetric Co-Cross-Correlation $\underline{\rho_x}$ might be an indicator for electric fields in clouds, causing an alignment of hydrometeors (e.g. ice crystals). The modulus of Co-Cross-Correlation $\underline{\rho_x}$ is found to be low in the melting layer and contains additional information to the Linear Depolarization Ratio.

Curriculum Vitae

Personal Details

Name	Jens Reimann
Date of Birth	June 25, 1984
Place of Birth	Lichtenstein
Nationality	German

Education

since 10/2009	Ph.D. Student, German Aerospace Center (DLR e.V.), Germany
3/2009-9/2009	Research Assistant 'Implementation of a new radar control system for POLDIRAD', German Aerospace Center (DLR e.V.), Germany
5/2008-2/2009	Diploma thesis 'Detection and mitigation of ground clutter using data from a polarimetric weather radar', German Aerospace Center (DLR e.V.), Germany
9/2007-1/2008	Internship 'RF Cavity Filter Design for Space Application', Tesat-Spacecom GmbH & Co. KG, Germany
3/2007-6/2007	Student Research Project 'Design and Construction of a microwave amplifier', Irkutsk State Technical University, Russia
9/2006-10/2006	Internship 'FPGA Design', Moscow Aviation Institute, Russia
10/2003-2/2009	Studies of 'Information and Communication Technology', Technical University of Chemnitz, Germany

Chemnitz, den 14. Januar 2013